FIBRE OPTIC APPLICATIONS FOR DISSOLVED CARBON DIOXIDE MONITORING OF MARINE GEOLOGIC SEQUESTRATION SITES

by

Sonja Bhatia

Submitted in partial fulfillment of the requirements
for the degree of Doctor of Philosophy

at

Dalhousie University
Halifax, Nova Scotia
December 2015

To Robby, Mum, Dad, and dear friends and neighbours who made sure I was fed and there was always a cold beer in the fridge.

Table of Contents

List of Tables

List of Figures

Abstract

Marine-based Carbon Capture, Utilisation, and Storage (CCUS) has the potential to reduce the rate at which CO_2 is added to the atmosphere thereby contributing to the mitigation potential for anthropogenic climate change. There has, however, been public and regulatory resistance to the technology due to the the possibility of leakage, which could occur within a 5 km radius of the injection site. The risks of marine CCUS could be better characterised using distributed sensor networks to monitor possible leakage areas.

Laboratories at the Universities of Toronto and Victoria demonstrated that Long Period Grating Fibre Optic Sensors (LPGs) can detect CO_2 in laboratory conditions. These sensors have the potential for cost-effective, distributed seafloor deployment in sensor networks, but certain *in situ* deployment challenges must be overcome to move beyond the laboratory testing stage. *In situ*, LPGs will be susceptible to interference from non-target species and to biofouling. As such, sensor signal may not be uniquely responsive to CO_2, and other substances or factors could contribute to noise, or could even mimic a seep or leak. Furthermore, sediment dynamic and pore-water water column exchange of total alkalinity and DIC may influence both background variability and signal in the marine context.

The key research contributions of this thesis are as follows: (1) a characterisation of the effect of biofouling on the response of LPGs for both single and multi-species biofilms,(2) a defined set of concentrations of carbonate and non-carbonate species in application environments of interest and an estimate of the likelihood of interference with LPG signal as sensitivity improves, (3) a characterization of the impact in background variability in the key parameters of the carbonate system, (4) a discussion of the signal-to-noise ratio (SNR) for LPGs used in monitoring seafloor geologic sequestration sites, and (5) an evaluation of the technology readiness level of LPGs. Both laboratory experiments and field studies were conducted to ascertain the effect of biofilm growth on sensor response. These studies showed that biofouling would likely contribute increase the central wavelength of the attenuation band within the first 30 h of LPG immersion in seawater. Hydrochemical modelling work using *Phreeqc 2.18* revealed that carbonate species and non-carbonate species were likely to be present in concentrations below the detection limits of off-the-shelf LPGs. Finally, the contribution of these hydrochemical and biological variables to noise was calculated, and the type of signal escaping CO_2 would generate was used to estimate SNR under different seepage and leakage scenarios. The estimated SNRs showed significant variability for seeps and leaks of the same scale under various pressure and temperature conditions. More work is needed to test LPGs under temperature and pressure conditions likely to be experienced in seafloor environments, and also in settings where hydrate coatings may form films that prevent the LPG from contacting the fluid to be measured.

List of Abbreviations and Symbols Used

CCUS	Carbon Capture, Utilisation, and Storage: The capture of CO_2 from an industrial source and its subsequent utilisation or storage.
Coupling	Transfer of light energy from the core mode to a cladding mode in an optical fibre.
$\boldsymbol{dCO_2}$	Only the dissolved CO_2 component of dissolved inorganic carbon.
DIC	Dissolved Inorganic Carbon: the sum of the dissolved CO_2, carbonate and bicarbonate species present in solution.
Evanescent Field	Most of the light travels through the core of an optical fibre, but a small portion travels through the less refractive cladding. The amplitude of the light's electromagnetic field decays exponentially normal to the core-cladding interface. If the cladding is removed, the evanescent field forms in the surrounding medium.
LPG	Long Period Grating Fibre Optic Sensor.
Mode	Electromagnetic waves that propagate energy through the fibre. A guided mode is a function of the optical source wavelengths, along with the fibre parameters, such as the diameters and refractive indices of the core and the cladding.
MMV	Monitoring, Mitigation, and Verification: ongoing monitoring of the area surrounding the CO_2 injection and sequestration site, mitigation strategies, should a leak occur, and verification for future carbon credit trading schemes.
NDIR	Non-Dispersive Infrared Spectroscopy.
$\boldsymbol{pCO_2}$	Partial pressure of CO_2.
SNR	Signal-to-Noise Ratio.
Wavelength Shift	The shift in central wavelength of the attenuation band in the transmitted spectrum of an LPG that occurs in response to a shift in the refractive index of the surrounding medium.

Acknowledgements

Thank you to my supervisor, Dr. David Risk who challenged me to always do better and grow as an academic, whose flexible approach allowed me to pursue the questions that interested me, and who fostered a community in the lab that encouraged sharing of ideas and expertise between peers. Thank you also to the other members of my supervisory committee, Drs. Shannon Sterling and Peter Wild, who were always available to provide feedback and advice about my research whenever I needed, and who readily loaned equipment, provided laboratory space, and included me in their laboratory communities. I also received incredible amount of help from a number of friends and project partners without whom I could not have completed this very interdisciplinary work: Geoff Burton and Luis Melo from Dr. Peter Wild's lab for their help with the engineering side of things; Flux lab folks (especially Chelsie, Jocelyn, Sara, Chris, Matt, and Laura) who were always there to help with programming problems, carpooling, with a place to stay, when I forgot my wallet and/or keys, and lug equipment back and forth between Halifax and Antigonish; Drs. Truis Smith-Palmer and Amanda Pustam for their assistance with the bacterial side of things; Dr. Helmuth Thomas for his guidance on the marine carbonate system; and Drs. Don Lawton, Bernhard Mayer, and Ernie Perkins for their guidance with hydrochemical modelling work. This research would not have been possible without support from the National Science and Engineering Research Council of Canada, Carbon Management Canada, and the Offshore Energy Research Association of Nova Scotia.

Chapter 1

Introduction

Geologic sequestration of CO_2 beneath the seafloor is becoming more prevalent because of its potential to mitigate the effects of anthropogenic CO_2 on climate. Leakage can occur within a five kilometre radius of the initial injection site (Metz et al., 2005); distributed sensor networks are needed to monitor these sites. No examples exist in the literature where distributed CO_2 sensors have been economically deployed for distributed seafloor monitoring of CO_2 geologic sequestration sites, though some potential exists for non-dispersive infrared spectroscopy.

Poof-of-concept for Long Period Grating Fibre Optic sensors (LPGs) as CO_2 sensors has been achieved (Melo et al., 2014; Bao et al., 2013), demonstrating that LPGs can detect CO_2 in a binary solution or mixture. Long period grating sensors detect CO_2 through a CO_2-induced shift of the refractive index of the surrounding medium. The LPG signal is not uniquely influenced by CO_2; other substances that alter the refractive index of the surrounding solution could therefore contribute to signal drift, noise, and in a worst-case scenario, mimic a CO_2 seep or leak.

The goal of this thesis is to move the project beyond the bench testing stage by advancing understanding of the effect of biological (Chapters 2, 3, and 4) and hydrochemical variables (Chapters 5, 6, and 7) that could interfere with sensor response. Consideration is given to the effect of these parameters on background variability and signal-to-noise ratio (SNR; Chapter 8), the principal factor needed to ascertain a sensor's Monitoring, Mitigation, and Verification potential. This thesis presents the results from these studies.

1.1 Background

1.1.1 Carbon Capture, Utilisation, and Storage

Anthropogenic CO_2 emissions are expected to increase mean global surface temperatures and contribute to ocean acidification (Orr et al., 2005; Watson et al., 2009). These environmental and climatic changes are expected to reduce the breadth and scale of ecosystem services provided by natural marine and terrestrial systems (Bellard et al., 2012; Kurz et al., 2008; Parmesan and Yohe, 2003). Carbon Capture, Utilisation, and Storage (CCUS) refers to the capture of CO_2 from large industrial or power plant emissions, its subsequent transport, and commonly, its injection into a confined geologic formation (Metz et al., 2005). An important mitigation tool for global environmental change, CCUS is a strategy included in most climate mitigation scenarios developed by the Intergovernmental Panel on Climate Change (Pachouli and Meyer, 2014). Injection of CO_2 into the subsurface can serve two goals: (1) Long-term geologic sequestration of CO_2 purely for climate mitigation purposes, or (2) utilisation for enhanced oil or natural gas recovery, where injected CO_2 is used to extract hydrocarbons that could not be recovered through traditional methods (Metz et al., 2005). In the latter scenario, geologic sequestration of the CO_2 occurs only as a byproduct of the industrial utilisation. Life cycle analysis demonstrated that both scenarios resulted in a net reduction in anthropogenic CO_2 emissions (Zapp et al., 2012).

Despite its potential to reduce anthropogenic CO_2 emissions to the atmosphere, public and regulatory resistance to CCUS is prevalent. This resistance is primarily due to the potential health, safety, and environmental risks posed by large-scale CO_2 leakage or seepage from geologic sequestration sites into the surrounding environment. Land-based leakage could result in local-scale asphyxiation of neighbouring animal and human populations. At marine injection sites, large-scale release of CO_2 could cause localised acidification of the marine environment and negatively impact marine life in the area (Blackford et al., 2009). At a global scale, escaping CO_2 from all site types may re-enter the atmosphere and undermine the mitigation potential of a CCUS operation (Metz et al., 2005; Markusson et al., 2012). There are 19 commercial-scale CCUS sites currently under operation. Some examples of CCUS sites are the

Sleipner project in the North Sea (Arts et al., 2004) and the Weyburn project in Saskatchewan (Riding and Rochelle, 2005). Increasingly, CCUS project planners are looking to the sub-seafloor environment as the geologic storage reservoir because the human (though not ecological) risk is less than for land-based operations (Themann et al., 2009). Given the likelihood of more projects of this type, these marine sites will be the focus of this work.

1.1.2 Monitoring, Mitigation, and Verification

Carbon dioxide Monitoring, Mitigation, and Verification (MMV) programs are expected to perform three functions:
(1) monitor for CO_2 plume migration beneath the surface, as well as leaks and seeps to the surface;
(2) quantify localised concentration of CO_2 at a seepage or leakage site and mitigate the effect of a leak or seep accordingly; and
(3) verify the amount of injected CO_2 that is sequestered in the formation, should that be needed (Metz et al., 2005).
A comprehensive MMV program (along with appropriate site selection) is essential to mitigate environmental, health and safety risks (Metz et al., 2005); however, even if sensors can perform just one of these functions, particularly, if sensors can perform an alarm function, they should be considered for an MMV program. Appropriate monitoring of background variability (Themann et al., 2009), along with ongoing monitoring once injection occurs can also be used to demonstrate conformance with the operator's model of expected plume evolution and to attribute the source of a leak or seep (Metz et al., 2005).

Any MMV program should take place until there is a reasonable expectation that leakage or seepage will not occur. There was some debate over the required duration of MMV to meet this objective. Some authors suggested that a monitoring project should continue 1,000 years (White et al., 2003), until CO_2 is fully dissolved in the subsurface solution; however, this extremely long-term approach is financially and politically impractical. Other studies suggested that monitoring activities should be ceased when it can be demonstrated that the injected CO_2 plume is no longer migrating beneath the seafloor (Chow, J., Watson, J., Herzon, A., Benson, S., Hidy,

G., Gunter, W., Penkala, S., and White, 2003; White et al., 2003); the idea is that monitoring will provide little new information once the plume is stabilised (Metz et al., 2005). Regulators in most jurisdictions have chosen the more practical approach. The US EPA requires operators sequestering CO_2 in the subsurface to monitor for 50 years or until they have demonstrated non-endangerment (US EPA, 2013). Other jurisdictions require the operator to demonstrate conformity with pre-injection plume modeling projections. For example, in Alberta, post-closure liability is transferred to the provincial government after a closure certificate is issued. Closure criteria have not yet been defined by the Alberta Government, but, presumably, closure will be granted once the CCUS operator has demonstrated conformity. Once the government takes over post-closure liability, monitoring, and maintenance; there is no required minimum monitoring period (ABERCB, 2012; Government of Alberta, 2012).

1.1.3 Marine Monitoring, Mitigation, and Verification Challenges and Sensing Requirements

Long-term, continuous monitoring of CO_2 in marine environments is particularly challenging because monitoring sites are often inaccessible, salinity can be harmful to equipment, and the scale of leakage or seepage can be difficult to determine because of the likely dispersed nature of the escaped CO_2 plume. Sensors that are long-lived, require minimal maintenance, and have no electronics at the measurement site are logistically and economically appealing since access for deployment, maintenance, and repair may be limited. In seafloor environments, the escaped CO_2 plume may be diffuse and carried rapidly by changing ocean currents (Blackford et al., 2009; Dewar et al., 2013). Direct, instantaneous measurement that can quickly detect leakage prior to diffusion is therefore preferable. Since rapid dispersion of escaping CO_2 is likely, and sub-seafloor migration of the plume prior to escape is possible, targeted seafloor monitoring over an area greater than 100 km^2 (the estimated scale of the average sub-surface plume) is needed (Metz et al., 2005). Seafloor monitoring instruments that are able to form distributed networks and transmit signals over long distances without significant signal loss are ideal for targeted monitoring of this large area. Experience in monitoring subsurface sites for activities other than CO_2 storage is extensive, so effective monitoring technologies are available, but more work is needed

to develop standard MMV protocols and techniques for CCUS specifically (Benson and Surles, 2006). Current, commercially available techniques are discussed below (Section 1.1.4)

1.1.4 Current Monitoring Options

Five detection techniques currently exist for MMV of CO_2 injection sites in a marine environment: (1) time-lapse seismic surveys, (2) flare imaging, (3) plume monitoring, (4) monitoring of water chemistry, and (5) fibre optic structural health monitoring (Table 1; Themann et al., 2009). While these techniques are sufficient to detect a leak, none are able to make long-term, real-time, distributed, direct measurement of CO_2 along the seafloor (Table 1).

1.1.5 Fibre Optic Sensing for Monitoring, Mitigation, and Verification

Optical fibres are able to transmit signals over long distances with minimal loss because they are made up of a high refractive index silica core, and low refractive index silica cladding. The ratio of refractive indices of these two components of the cable cause total internal reflection at the core-cladding interface. This property allows for long distance signal transmission because almost no signal is lost to the surrounding environment. In addition to this transmission efficiency, optical fibres require no electronics at the measurement site, and are capable of distributed sensing, making them ideal for MMV. Temperature and strain sensors have been used successfully in the oil and gas sector for pipeline structural health monitoring and leakage detection (Niklès et al., 2004). Fibre optic sensors also exist for CO_2 in the gas phase. These sensors typically do not sense CO_2 directly, but employ materials that detect changes in pH (e.g., Vurek, G.G., Feustel, P., Severinghaus, 1984).

A new generation of fibre optic sensors capable of directly sensing CO_2 is under development (Bao et al., 2013; Melo et al., 2014; Burton et al., 2014). Two such sensors have been tested and/or manufactured: SintonLab at University of Toronto achieved initial laboratory success in detecting supercritical CO_2 in brine at high pressure (above 72 atm) using an LPG (Bao et al., 2013); and (2) in an atmospheric pressure environment, Dr. Peter Wild's laboratory at University of Victoria developed a polymer-coated LPG that was able to distinguish between $N_{2(g)}$ and $CO_{2(g)}$.

Though not the focus of the application tests conducted for this thesis, recent success was also achieved using a fibre tip refractometer to detect CH_4 and CO_2 bubbles in high pressure laboratory tests conducted at 95 atm (Burton et al., 2014) also at the University of Victoria. While these achievements show promise, challenges pertaining to *in situ* deployment must also be overcome to move beyond the laboratory benchmarking stage.

1.1.6 Long Period Grating Sensors–Principle of Operation

The LPGs used to achieve proof-of-concept by Bao et al. (2013); Melo et al. (2014), are manufactured using ultraviolet irradiance to inscribe gratings on the core of an optical fibre (James and Tatam, 2003). These gratings induce a permanent periodic modulation of the core, altering the refractive index of the core at the point of inscription. Light traveling through an optical fibre has a three dimensional electromagnetic field propagating through the core ('core mode') and cladding (there are multiple, discrete 'cladding modes'). The LPG causes some of the light from the core mode to be transferred to certain discrete cladding modes (termed 'coupling'), in the forward propagating direction (James and Tatam, 2003). Cladding modes attenuate more readily than the core mode, so the transmission spectrum of an LPG is comprised of a series of attenuation bands at discrete wavelengths, meaning the intensity of central wavelength of these bands is damped in the transmitted spectrum. The attenuation bands vary with the refractive index of the surrounding medium, the spacing of the gratings, and the optical properties of the fibre on which the gratings are inscribed. Long period gratings sensors are able to detect dissolved CO_2 by the small refractive index change contributed by the dissolved gas, and the resulting shift in central wavelength of the attenuation band in the transmitted spectrum of the LPG (James and Tatam, 2003).

1.1.7 Development Challenges for Long Period Grating Sensors

1.1.7.1 Noise and Interference

In the context of MMV for CCUS, noise would be a combination of instrument error and the effect of background variability on sensor response, with the latter likely to be

the dominant driver of noise (Nickerson and Risk, 2013). For LPGs, a given change in the refractive index of the surrounding medium may not be uniquely driven by CO_2. As a result, certain variables that are likely to alter refractive index *in situ* are likely to be the key components of the noise signal. In the marine context, biofouling and temperature are likely to be the dominant drivers of 'noise'. As sensor development matures background variability in both dissolved ion concentration (Bhatia and Risk, 2015) and the carbonate system are likely to contribute to noise. These factors may simply increase background variability in the sensor response, or may in fact generate a refractive index shift in the surrounding seawater solution that mimics the refractive index shift of escaping CO_2. In short, a given refractive index shift may not be uniquely generated by CO_2. In this thesis, I focus specifically on the biological and hydrochemical parameters that may interfere with sensor response.

1.1.7.2 Biofouling

Biofilms form quickly on surfaces immersed in aquatic environments as a result of successional colonisation in four dominant phases:
(1) Lag Phase, dominated primarily by molecular deposition;
(2) Exponential Growth Phase, characterised by colonisation of a substrate and an exponentially increasing number of bacteria;
(3) Stationary Phase, where the bacterial growth rate becomes zero (Zwietering et al., 1990); and
(4) Cell Death or Decline Phase, characterised by a negative growth rate because cells die if no new nutrients are available and/or waste is not removed (Fletcher, 1977; Monod, 1949).
In the marine environment, secondary colonisation by diatoms, algae and small organisms generally occurs. *In situ*, therefore, biofilms often exist as complex, highly structured communities (Stoodley et al., 2002).

Pure biofilm (a bacterial film made up of a single species of bacteria) has a refractive index that is approximately 0.15 % higher than that of deionised water (Philip-Chandy et al., 2000) and is estimated to be 1.336 (Wong et al., 2003). Given that this refractive index is lower than that of seawater, it is possible that biofilm growth will

drive the central wavelength of the attenuation band to shift (wavelength shift) upward due to the inverse relationship between the refractive index of the bulk medium and the central wavelength of the attenuation bands (James and Tatam, 2003). The actual influence of biofilm growth on wavelength shift may be different than expected for two reasons: (1) the effect of a film on wavelength shift may be different than that of bulk media of the same refractive index, and (2) the complex refractive index of bacteria may have a different effect on wavelength shift than the simple refractive index of, for example, a saline solution (James and Tatam, 2003).

1.1.7.3 Hydrochemical Interference and Influence on Sensor Response

As sensor development matures and sensitivity of LPGs improves, hydrochemistry may create challenges for sensor developers in three ways: (1) escaping dissolved CO_2 may speciate, forming HCO_3^- or CO_3^{2-}, which means a sensor calibrated to uniquely detect dissolved CO_2, may not detect a seep or leak where the dominant species is not dissolved CO_2; (2) escaping dissolved CO_2 may acidify the water column, shifting background DIC to dissolved CO_2, amplifying the scale of a seep or leak; and (3) variation in the background concentration of non-target carbonate or non-carbonate species may vary, mimicking a seep or leak. Hydrochemical studies report only the dominant dissolved ions present in solution (e.g., Mg^{2+}, Ca^{2+}), pH, and buffering capacity, without providing detail on carbonate speciation (e.g., Abu-Jaber and Wafa, 1996; Birkle and Aragon, 2002; Bruland and Lohan, 2006). Estimates of carbonate speciation are not discussed in sufficient detail in the literature to ascertain the expected influence of carbonate species on sensor response. Nor are non-carbonate species that may interfere with sensor response identified in a comprehensive way. This knowledge gap needs to be filled to advance development of LPGs for MMV applications.

In general terms carbonate dissolution in aqueous environments is well understood. Duration of contact with the rock, rock-type, pH, buffering capacity, salinity, temperature, and pressure all influence the dominant carbonate species (Appelo and Postma, 2005). In the marine context, specifically, carbonate dissolution, mineralization in the sediments and the water column (Friis et al., 2003), and anaerobic

degradation (Thomas et al., 2009) in the sediments are the dominant drivers of buffering capacity. Understanding the reactions that control carbonate dissolution provides some insight into the type of carbonate species that is likely to dominate in an application environment (Equations 1.1, 1.2, 1.3, and 1.4; Appelo and Postma, 2005); however, these equations do not account for the presence of other ions like Mg^{2+} and Ca^{2+} that can bond with bicarbonate or carbonate ions. So, if the reaction path suggests $CO_3{}^{2-}$ will dominate, it is possible that the dominant carbonate species may in fact be $MgCO_3$. The controlling reactions for carbonate dissolution are (Appelo and Postma, 2005):

$$H_2O \leftrightarrow H^+ + OH^- K_W = [H^+][OH^-] = 10^{-14.0}\, mol^2\, kg^{-2} \tag{1.1}$$

$$CO_{2(g)} + H_2O \leftrightarrow H_2CO_3^* K_H = [H_2CO_3^*]/[pCO_2] = 10^{-1.5}\, M\, atm^{-1} \tag{1.2}$$

$$H_2CO_3^* \leftrightarrow H^+ + HCO_3^- K_1 = [H^+][HCO_3^-]/[H_2CO_3^*] = 10^{-6.3}\, mol\, kg^{-1} \tag{1.3}$$

$$HCO_3^- \leftrightarrow H^+ + CO_3^{2-} K_2 = [H^+][CO_3^{2-}]/[HCO_3^-] = 10^{-10.3}\, mol\, kg^{-1} \tag{1.4}$$

Where * indicates that H_2CO_3 is shifting between carbonic acid and CO_2, and K represents equilibrium constants. K_H predicts the dissolution of CO_2 in water. K_1 predicts that at pH 6.3, the effective concentrations of CO_2 and $HCO_3{}^-$ will be equal. K_2 predicts that at pH 10.3, the effective concentrations of bicarbonate ion and carbonate ion will be equal. The carbonate system consists of six interconnected parameters: (1) Dissolved Inorganic Carbon (DIC), (2) Total Alkalinity (buffering capacity), (3) pCO_2, (4) $HCO_3{}^-$, (5) $CO_3{}^2-$, and (6) pH. Variations in anyone of these parameters can affect the others. The dominant species of DIC is influenced by pH, but there is a feedback mechanism: in higher pH environments, DIC shifts towards $HCO_3{}^-$ and $CO_3{}^2-$ (the components of DIC which contribute to buffering capacity, which act to buffer the pH shift with the addition of an acid to solution (Appelo and Postma, 2005). Upon dissolution a small part of pCO_2 forms carbonic acid, so increased uptake of atmospheric CO_2 or CO_2 release from geologic sequestration sites may alter pH, if the escaping CO_2 is sufficiently concentrated, but in higher pH environments, the dissolving pCO_2 may rapidly speciate to $HCO_3{}^-$ or $CO_3{}^2-$, which may alter the ionic composition of the ions that contribute to buffering capacity, but

does not alter net buffering capacity (Blackford and Gilbert, 2007).

Geochemical modeling work using these well-understood speciation mechanisms and the hydrochemical data available in the literature can estimate the likely concentration of carbonate and non-carbonate species present in a given application environment (Appelo and Postma, 2005). These data can then be used to assess the effect of these species on sensor response. Furthermore discussion of the seafloor processes that influence the six interconnected parameters of the carbonate system is essential, since these processes may influence background variability and ultimately contribute to noise sensors deployed near the seafloor.

1.1.7.4 Characterising Seepage and Leakage Signal

In terms of sensor response to a seep or leak, sensor signal would be determined by the nature of the seepage or leakage event. This signal component becomes more complicated in the marine environment for refractive index-based sensors because a seepage or leakage signal can be in different phases, and therefore generate very different shifts in refractive index. Escaping CO_2 may take many forms, including gas, liquid, or gas bubbles or liquid droplets with hydrate coatings (Dewar et al., 2013). The refractive index shift induced by this leakage or seepage may be different depending on the *in situ* pressure and temperature conditions, which will drive the phase of escaping CO_2 (Dewar et al., 2013), even for leaks of the same scale. Even more complicated, escaping CO_2 could acidify the surrounding environment, shifting background DIC towards dissolved CO_2, thus magnifying the scale of the seep or leak by increasing the concentration of dissolved CO_2 beyond the amount of CO_2 that is actually escaping. Lastly, leakage and seepage can be diffuse, so the sensor may only be able to detect a small portion of the escaped plume. Careful analysis and modelling work is required to estimate the SNR under various seepage and leakage scenarios.

1.2 Statement of Research Problem

Long period grating sensors for MMV of marine-based CCUS sites are under development. Sensitivity to refractive index, the effect of thin films, temperature sensitivity (James and Tatam, 2003), and salinity (Possetti et al., 2009) have all been

characterised for silica-based LPGs. Furthermore, two partner laboratories achieved proof-of-concept for LPGs as carbon dioxide sensors in binary solution and mixture (Melo et al., 2014; Bao et al., 2013). Since CO_2 induces a non-unique response in LPGs, other substances that alter refractive index could interfere with LPG response. Biological and hydrochemical variables are of particular concern. The effect of many of these variables, like variability in carbonate speciation and biofilm growth have not been investigated for LPGs in particular, though several studies publish results from testing of a declad plastic optical fibre (Wong et al., 2003; Philip-Chandy et al., 2000) and a tapered silica fibre (Zibaii et al., 2010) exposed to biofilm growth. Signal-to-noise ratio is the most important factor when considering the suitability of sensors for monitoring of CCUS sites (Nickerson and Risk, 2013). No studies have estimated SNR for LPGs in this context. To characterise the application challenges laid out in the problem statement, the following research questions must be addressed:
(RQ 1) What will be the effect of biofouling on LPG response? Addressed in Chapters 2-4, and 8.
(RQ 2) What is the expected concentration of carbonate species present in aqueous environments? Addressed in Chapter 5.
(RQ 3) What species are present that may interfere with sensor response *in situ*? Addressed in Chapter 5.
(RQ 4) Will the sensor be sensitive to carbonate speciation *in situ*? Addressed in Chapter 6.
(RQ 5) What effect will seafloor dynamics have on leakage and seepage signal? Addressed in Chapter 7.
(RQ 6) What is the expected SNR for MMV applications? Addressed in Chapter 8.
(RQ 7) In consideration of the answers to the above questions: what is the state of development for LPGs as CO_2 sensors for MMV? Addressed in Chapter 8.

1.3 Objectives

The overarching objective of this thesis is to advance development of LPG CO_2 sensors beyond bench testing stage by meeting the following sub-objectives: (O1) To test the effect of biofouling in laboratory and seawater conditions. This objective is

addressed in Chapters 4, 5 and 6 and answers RQ 4. These three chapters examine the effect of biofouling on LPGs in depth and also present the possibility of using LPGs as biofouling sensors.

(O2) To characterise selected application environments in terms of carbonate speciation and species that could interfere with sensor response *in situ*. This objective is addressed in Chapter 2 and answers RQ 1 and 2.

(O3) To test the effect of carbonate speciation on sensor response. This objective is addressed in Chapter 3 and answers RQ 3.

(O4) To consider the challenges of detecting small-scale seeps or leaks. This objective is addressed in Chapter 7 and answers RQ 5.

(O4) To determine the expected SNR for MMV in seafloor environments under plausible seepage and leakage scenarios. This objective is discussed as a review discussed in Chapter 8 to answer RQ 5 and 6.

(O5) To assess the state of technology for LPGs as CO_2 sensors. Chapter 8 also addresses this objective and answers RQ 7.

1.4 Outline and Interrelationship of Chapters

There are seven chapters in this thesis apart from the Introduction and Conclusion chapters (Chapters 1 and 9). Each chapter addresses a challenge associated with deployment of LPGs as CO_2 sensors. Chapter descriptions, journal and publication details, and the manuscript authors are provide below. Contributions of the lead author are discussed in more detail in the Preamble to each chapter.

Chapter 2 *Biofouling of an All-Optical Sensor for Seafloor Monitoring of Marine Carbon Capture and Storage Sites.* This chapter introduces the effect of biofouling on LPGs. It forms the basis for a conference proceedings. The manuscript on which it is based, was published in October, 2014 issue of Energy Procedia (Bhatia et al., 2014). Only the abstract was peer reviewed. Lead author: Sonja Bhatia. Co-authors: David Risk (supervisor), Amanda Pustam (biofouling expertise), Truis Smith-Palmer (biofouling expertise), Geoff Burton (optical expertise), Luis Melo (optical expertise), Peter Wild (optical expertise).

Chapter 3 *An all-optical biofouling sensor for marine applications.* This chapter

examines the effect of biofilm growth on LPG response in a nutrient-dense synthetic seawater solution. It presents a method for using LPGs as automated biofilm sensors to reduce maintenance visits for other marine and aquatic sensors, or to trigger the controlled release of anti-fouling substances. The manuscript on which the chapter is based, was submitted to Limnology and Oceanography: Methods in June, 2015. Lead author: Sonja Bhatia. Co-authors: David Risk (supervisor), Amanda Pustam (biofouling expertise), Truis Smith-Palmer (biofouling expertise), Geoff Burton (optical expertise), Luis Melo (optical expertise), Peter Wild (optical expertise).

Chapter 4 *Biofouling Field Trial of an All-Optical Fibre Optic Sensor.* This chapter presents the results of field trials for LPGs using seawater pumped from a protected cove. The manuscript on which the chapter is based, was submitted to the Journal of Environmental Sciences: Processes and Impacts (formerly the Journal of Environmental Monitoring) July 20, 2015. Lead author: Sonja Bhatia. Co-author: David Risk (supervisor).

Chapter 5 *Hydrochemistry of Application Environments for Dissolved Carbon Dioxide Sensors.* This chapter takes a broad view of potential application environments for the LPGs under development as part of this thesis and the larger project. This chapter is based on a manuscript that is the first of its kind to characterise carbonate and non-carbonate speciation in a range of representative application environments (including surface, subsurface, freshwater, saline, and transitional environments). The geochemical modelling software, *Phreeqc 2.1* was used to conduct the modelling. This manuscript was published in the April, 2015 issue of the Journal of Water, Air and Soil Pollution (Bhatia and Risk, 2015). Lead author: Sonja Bhatia. Co-author: David Risk (supervisor).

Chapter 6 *Challenges with Carbonate Speciation Experiments at Atmospheric Pressure.* This chapter presents the challenges in acidifying a carbonate solution at atmospheric pressure using HCl and the resulting signal response of the LPG. Author: Sonja Bhatia.

Chapter 7 *Consideration of Sediment Dynamics and Biogeochemical Cycling on Future Deployment of Seafloor Sensors: A North Sea Case Study.* This chapter looks at pore water-water column exchange, using the North Sea as a Case Study. Lead author: Sonja Bhatia. Co-author: Helmuth Thomas.

Chapter 8 *Marine Carbon Dioxide Geologic Sequestration Sites: A Review of fibre Optic Sensor MMV Potential*. This chapter is a review of the potential of fibre optic CO_2 sensors to be used for MMV of sub-seafloor geologic sequestration sites for CO_2. The manuscript on which this chapter is based will be submitted to the International Journal for Greenhouse Gas Control July 20, 2015. Lead author: Sonja Bhatia. Co-author: David Risk (supervisor).

Table 1.1: Currently Available Technologies for MMV of CO_2 Injection Sites in the Marine Environment.

	Technology	Description	Advantages	Disadvantages
Physical	Flare Imaging	With specialised multi-beam systems. Mapping of areas above the storage site (Themann et al., 2009).	Can detect gas bubbles above the seafloor for reasonably intense gas escape (Dewar et al., 2013).	Requires modeling and an experienced individual to interpret the images accurately. Cannot be automated (Themann et al., 2009).
	Seismic Surveys	Time lapsed seismic data is used to monitor the initial injection (Themann et al., 2009).	Able to show plume evolution and distribution in the early stages of CO_2 injection. (Themann et al., 2009).	Accuracy declines with upward migration towards the seafloor. Would not be effective at detecting a post-injection leak. Not real-time (Themann et al., 2009).
	Indirect Fibre Optic Sensing	Uses distributed fibre optic temperature (Bourne, 2010) and strain sensors to monitor for well integrity.	Distributed, cost-effective sensing.	Indirect. Only detects seepage or leakage via proxy measurement.
Chemical	Plume Monitoring	Uses geochemical sniffers to detect hydrocarbon and CO_2 leaks (Themann et al., 2009).	Able to detect leaks in real time (Themann et al., 2009).	Not specific to CO_2. Sniffers are unable to quantify the amount of leakage (Themann et al., 2009).
	Monitoring of Water Chemistry	Measurement of pH or pCO_2 concentrations. Escaping CO_2 would rapidly acidify and show a detectable pH drop (Themann et al., 2009).	Provides high-resolution and pH can be measured in real-time (Themann et al., 2009).	pH is not a direct method of detection.

Chapter 2

Biofouling of an All-Optical Sensor for Seafloor Monitoring of Marine Carbon Capture and Storage Sites

2.1 Preamble

Sonja Bhatia, David Risk, Amanda Pustam, Truis Smith-Palmer, Geoff Burton, Luis Melo, and Peter Wild

This chapter forms the basis for a paper published in the Fall, 2014 issue of *Energy Procedia*. I hold the copyright for this manuscript. I was the lead author for this study and conducted all experiments. Dr. David Risk provided funding and additional input into experimental design and draft revision. Dr. Amanda Pustam provided guidance with respect to culturing bacteria, proper disposal of biohazardous waste, and experimental design. Dr. Truis Smith-Palmer provided input into experimental and flow-cell design and provided laboratory facilities, and Luis Melo, Geoff Burton, and Dr. Peter Wild helped with the fibre optic component of experimental design.

2.2 Abstract

Fibre optic sensors for dissolved CO_2 are an emergent technology for monitoring marine geologic CO_2 sequestration sites. Fibre optic sensing technology has been used successfully in the oil and gas sector and is advantageous because it is capable of cost-effective, instantaneous, distributed sensing. Fibre optic sensing is an improvement over current practice, which normally requires samples to be pumped to the surface for analysis. Biofouling of fibre-based sensors is a concern for the marine environment, as the biofouling can cause signal drift and also adversely impact the sensor's ability to detect dissolved CO_2 (dCO_2). The effect of biofouling on sensor response must therefore be characterised. Long Period Grating Fibre Optic Sensors (LPGs) were used for this study. *Pseudoalteromonas* sp. NCIMB 2021, a common

marine bacterium, was cultured and grown on sensing elements using nutrient-dense synthetic seawater. The biofilm experiments demonstrated that biofouling caused shifts in the baseline signal for LPGs. Post-fouling sensitivity of the sensor was also reduced relative to pre-fouling levels. Mechanical cleaning of the sensors restored sensor sensitivity to that seen prior to bacterial colonisation.

2.3 Introduction

Seafloor monitoring of geologic sequestration sites for CO_2 is necessary to ascertain safety and efficacy of sub-seafloor injection and storage of CO_2. A new generation of fibre optic dissolved gas sensors promises cost-effective, distributed, sensing of dissolved CO_2, facilitating seafloor and down-hole monitoring of marine geologic CO_2 sequestration sites (Bao et al., 2013). Long Period Grating Fibre Optic Sensors (LPGs) are capable of sensing CO_2-induced shift in refractive index, and are an improvement over commercially available fibre optic technology, which relies on proxy temperature and pressure measurement to detect leakage. More conventional non-fibre optic dissolved CO_2 sensing technology, like gas chromatography cannot be easily deployed in distributed fashion because it requires the sample to be pumped onboard a ship for analysis (Schuster et al., 2009).

2.3.1 Fibre Optic Dissolved Gas Sensing

Standard single mode optical fibres have a silica core and cladding of differing refractive indices. The ratio of the two refractive indices causes total internal reflection as the light is transmitted through the core of the fibre; however, a small portion of light propagates through the cladding, forming an evanescent field (Figure 2.1). Evanescent field sensors typically modify a portion of the optical fibre so that the evanescent field interacts with a portion of the surrounding medium. Long Period Grating sensors, like the one described by Bao et al. (2013) and Melo et al. (2014) respond to a change in the refractive index of the surrounding medium. These dissolved gas sensors have long period gratings inscribed onto an approximately 2.5 cm section of the fibre. These gratings cause coupling between the core mode and discrete cladding modes. The cladding modes attenuate more readily than the core mode causing attenuation bands at discrete wavelengths in the transmission spectrum of an LPG. The central

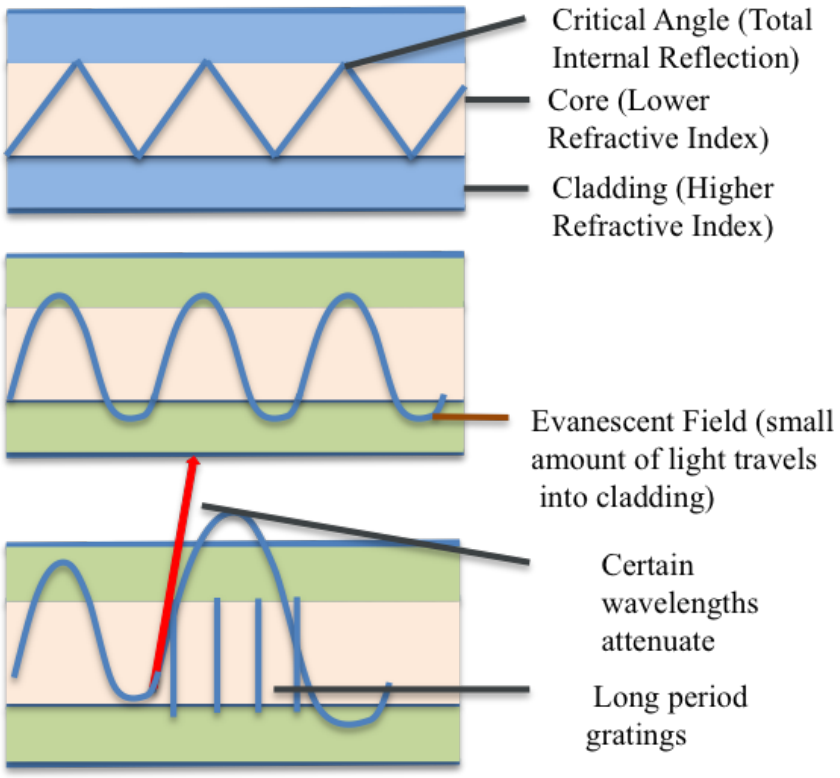

Figure 2.1: Basic operating principle for LPGs. A shows total internal reflection. B. Illustrates a small portion of light traveling through cladding, and C. Illustrates attenuation of select bands of light as they interact with the surrounding medium

wavelength of the attenuation band shifts inversely with the refractive index of the surrounding medium, referred to hereafter as 'wavelength shift' (Figure 2.2). For a more in-depth description of an LPG, please refer to Section 1.1.6.

2.3.2 Sensitivity of Long Period Gratings and Coatings

Long period grating sensors have maximal sensitivity (i.e., undergo the greatest wavelength shift per unit change in refractive index) when the refractive index of a surrounding bulk medium is just below the refractive index of the cladding (1.44-1.46; Rees et al., 2002; Patrick et al., 1998). Conversely, thin coatings of sub-wavelength thickness have been theoretically and experimentally shown to increase the sensitivity of long period grating sensors when the refractive index of the coating is equal to or greater than the refractive index of the cladding (Wang et al., 2005). The degree to

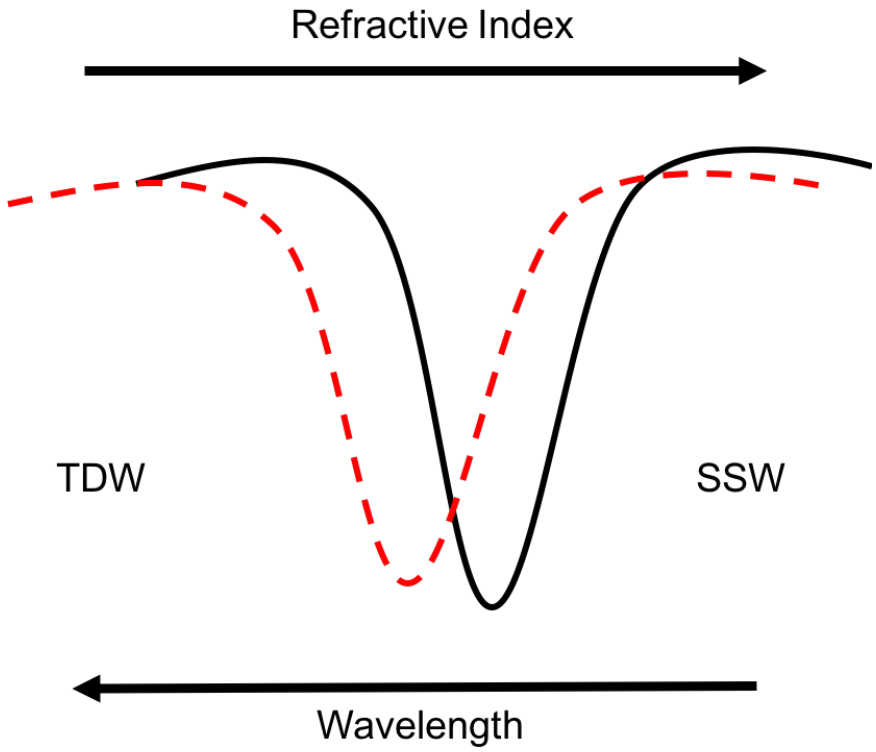

Figure 2.2: Shift in output signal with change in refractive index of the surrounding bulk media. Arrows point from lower values to higher values. Black line represents sample seawater output and dashed red line represents sample triply distilled water output.

which these higher refractive index coatings enhance sensitivity depends on a number of factors including coating thickness and refractive index of the coating relative to the refractive index of the cladding (Wang et al., 2005). For coatings of a refractive index lower than the cladding, sensitivity is likely to be reduced. In this refractive index range, film thickness itself does not have a significant impact on sensitivity (Rees et al., 2002). Little is known about coatings of refractive indices below the refractive index of the cladding, and whether these coatings are able to enhance the sensitivity of long period grating sensors.

2.3.3 Susceptibility to Biofouling

In marine, groundwater and other aquatic environments, it is expected that the transmitted spectrum from fibre optic dissolved gas sensors will be influenced by biofilm growth. The susceptibility of these sensors to biofouling is so great that several fibre optic sensors to measure biofilm growth have been tested in the laboratory (Wong et al., 2003; Philip-Chandy et al., 2000; Zibaii et al., 2010). Biofilm has a refractive index of approximately 1.336, which is close to that of freshwater (Wong et al., 2003), but below the refractive index of the cladding (Rees et al., 2002). The refractive index of the film is not in the range of optimal sensor sensitivity for bulk media (Rees et al., 2002), and films of this refractive index have not been shown to improve the sensitivity of long period grating sensors to refractive index shifts. It is unlikely therefore that biofilm growth will enhance sensor sensitivity and biofouling may in fact reduce sensor sensitivity to refractive index changes in the surrounding medium.

2.3.4 Objective

Prior to widespread implementation and commercialization of fiber-optic dissolved gas sensors, the influence of biofouling on wavelength shift needs to be understood. The objective of this study is to characterise the impact of biofilm growth on the sensitivity and baseline output signal of LPGs.

2.4 Methods

A series of laboratory experiments were conducted to ascertain the effect of biofilm growth on the response of LPGs. The experiment used nutrient-dense synthetic seawater, *Pseudoalteromonas* sp. NCIMB 2021 bacterial cultures, a peristaltic pump and a long period grating fibre optic sensor housed in a flow cell. Sterility was ensured by pumping 70 % ethanol solution into the experimental system and all fluids used in the experiment were autoclaved prior to injection into the flow cell.

The experiments were conducted as follows:

(1) Triply deionised water was pumped into the flow cell and the peak attenuated wavelength was measured.

(2) Synthetic seawater (0.05 g Na_2HPO_4, 5.00 g $NaNO_3$, 23.00 g NaCl, 0.75 g KCl, 1.47 g $CaCl_2.2H_2O$, 5.08 g $MgCl_2{\cdot}6H_2O$, 6.16 g $MgSO_4{\cdot}7H_2O$, 10 g of Sodium Pyruvate, and 1 L of triply distilled water) solution was then pumped into the flow cell and the peak attenuated wavelength was measured.

(3) NCIMB 2021 culture in synthetic seawater was pumped into the flow cell. The pump was stopped for one hour to allow bacteria to settle on surfaces in the flow cell.

(4) Synthetic seawater solution was pumped into the flow cell for up to 48 h and peak attenuated wavelength was measured twice per second.

(5) Triply deionised water was once again pumped into the flow cell and peak attenuated wavelength measured.

(6) The wavelength between synthetic seawater and triply deionised water was compared pre and post fouling.

2.5 Results and Discussion

2.5.1 Impact of Biofouling on Sensor Response

Wavelength shifted by 39-56 pm between triply distilled water and synthetic seawater solution (Table 2.1). The post-fouling percent reduction in sensitivity ranged from 37-66 % (Table 2.1). This reduction was expected since it was predicted that biofilm growth would inhibit the sensor's interaction with the surrounding medium; the relatively low refractive index of the film was not expected to act as a sensitivity

Table 2.1: Changes in Sensor Sensitivity Post-Fouling between Triply Distilled Water and Synthetic Seawater

Experiment No.	**Pre-Fouling Sensitivity TDW-SSW (pm)**	**Percent pm Post-Fouling Change Relative to Pre-fouling Sensitivity**
1	56	-37 ± 5 %
2	39	-63 ± 9%
3	45	-66 ± 8.5%

enhancing coating. Mechanical cleaning of the sensor returned sensitivity to normal levels.

2.5.2 Biofilm Growth and Baseline Signal

Twelve hours of bacterial growth induced an upward shift in baseline signal that was up to 60 % greater than the wavelength shift generated by switching the surrounding medium from synthetic seawater to triply deionised water (Figure 2.3). The upward trajectory in baseline due to biofilm growth could have occurred in part because biofilm is largely comprised of freshwater which has a lower refractive index than synthetic seawater (Wong et al., 2003); however, the wavelength shift seen in this experiment cannot be explained by the film's refractive index alone because the magnitude of the wavelength shift was greater than that expected for bulk media of the same refractive index. It seems possible that the film influenced sensor signal by acting like a coating around the sensing portion of the fibre, thus causing a higher wavelength shift than might have been the case in bulk media. Films with refractive indices below the refractive index of the cladding have been shown to reduce sensor sensitivity (James and Tatam, 2003).

2.6 Conclusion and Future Work

In these experiments, biofouling reduced sensor sensitivity by between 36 and 67 % and upwardly shifted the baseline wavelength in LPGs by 60 %. Biofouling growth can happen rapidly and may confound experiments conducted *in situ*, as well as in medium to long-term non-sterile laboratory conditions. More work is needed to

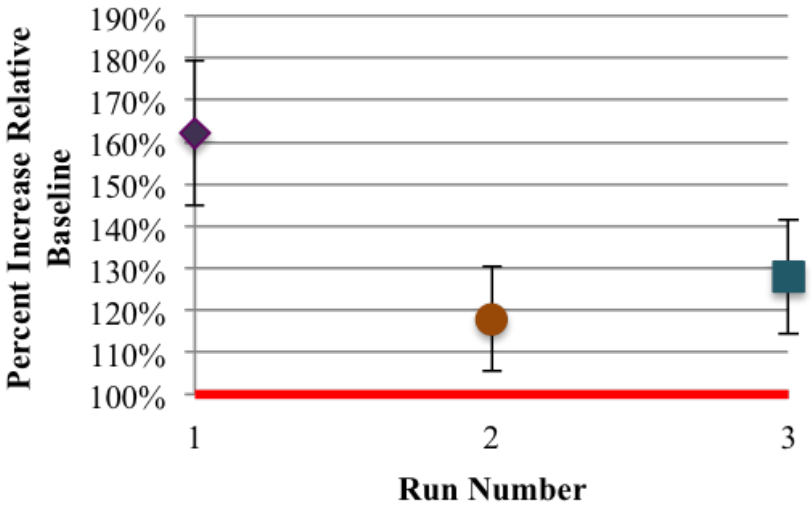

Figure 2.3: Percent shift in mean baseline peak wavelength as a function of sensor sensitivity. Red bolded line (100 %) indicates baseline at the start of the experiment. Error bars denote standard deviation.

ascertain the speed at which sensors can become fouled in experimental situations where bacteria are not being intensively grown. As a way to explore the possible mechanisms responsible for upward baseline shifts during biofilm growth, numerical modeling could provide useful insights into the theoretical influence of biofilms on sensor signal. *In situ* experiments are needed to understand the effect of multi species biofilms expected to grow in natural environments. Furthermore, the impact of fouling on protective coatings and membranes, along with methods to slow or prevent biofouling of optical fibres need to be studied.

2.7 Acknowledgements

Special thank you to funders who made this research possible. National Research Council of Canada CREATE, Carbon Management Canada, and Encana Education and Training and Research and Development Fund.

Chapter 3

An All-Optical Biofilm Sensor for Marine Applications

3.1 Preamble

Sonja Bhatia, David Risk, Amanda Pustam, Truis Smith-Palmer, Luis Melo, Geoff Burton, and Peter Wild

This chapter forms the basis for a methods paper submitted to Limnology and Oceanography: Methods on May 15, 2015. This paper was the result of work to test the potentially negative effect of biofilm growth on LPGs used for CO_2 sensing. In the process, we developed a method to use LPGs as biofilm sensors. This journal is methods-focused and requires an 'recipe book' style description of the methods; the journal also has specific requirements for section headings. These headings are unconventional, but were reproduced here to reflect the submitted manuscript. I was the lead author for this study and conducted all experiments. Dr. David Risk provided funding and additional input into experimental design and draft revision. Dr. Amanda Pustam provided guidance with respect to culturing bacteria, proper disposal of biohazardous waste, and experimental design. Dr. Truis Smith-Palmer provided input into experimental and flow-cell design and provided laboratory facilities, and Luis Melo, Geoff Burton, and Dr. Peter Wild helped with the fibre optic component of experimental design.

3.2 Acknowledgements

Carbon Management Canada, Encana Research and Educational Fund, CREATE NSERC, and Dr. Shannon Sterling.

3.3 Abstract

Biofouling may decrease the longevity of marine and freshwater sensors. The Long Period Grating Fibre Optic Sensor (LPG) discussed in this work is able to detect changes in the refractive index of the surrounding environment because bands of light traveling through the fibre are attenuated. The wavelength of these attenuation bands varies inversely with the refractive index of the surrounding medium and the magnitude of the intensity of attenuation bands will also vary in response to changes in the surrounding environment. Biofilm growth alters the refractive index surrounding the sensor. The LPG therefore has the potential to directly monitor biofilm growth in aquatic environments and could reduce site visits for equipment maintenance, thus saving time and reducing the cost of data collection in these environments. Temperature sensitivity, response to salinity, and wavelength shift relative to the refractive index of the surrounding medium have all been characterised for LPGs. Though the effect of biofouling on other refractive index-based fibre optic sensors has been tested, little is known about the effect of biofilm growth on LPGs. Laboratory tests were conducted where marine bacteria *Pseudoalteromonas* sp. NCIMB 2021 were grown on an LPG immersed in synthetic seawater. An upward shift in attenuated wavelength was seen in all three laboratory experiments. The consistency in response demonstrated that the LPG is capable of directly detecting bacterial growth. This response can be automatically recorded via peak detection computer software. Intensity of attenuation decreased in two out of three trials. A reduction in sensor sensitivity was observed post-fouling; however, mechanical cleaning restored sensor sensitivity to pre-fouling levels. The consistent, upward wavelength shift that occurred in response to biofilm growth, demonstrates the potential of LPGs as biofouling sensors. The intensity output is still too unreliable to quantify biofilm growth rate, but this is not a significant impediment to sensor efficacy. *In situ* testing with multi-species marine biofilms is required to understand the correlation between laboratory results and *in situ* environments.

3.4 Introduction

Biofouling decreases the lifetime of aquatic sensors and increases their operating and maintenance costs (Whelan and Regan, 2006). Often, changes in the quality of output signal provide an indication that biofilm growth is interfering with sensor operation. In some sensing systems, however, biofouling can also cause long-term signal drift and noise that may not be easily distinguished from other interferences. For example, acoustic receivers are susceptible to biofouling-induced noise, as well as to noise caused by vessel movement and other acoustic disturbances (Heupel et al., 2008). Currently, distinguishing between the causes of the noise can only be accomplished through a site visit.

3.4.1 Biofouling and Biofilm Formation

Bacterial biofilms quickly foul surfaces immersed in aquatic environments as a result of successional colonisation in four dominant phases: (1) Lag Phase, dominated primarily by molecular deposition; (2) Exponential Growth Phase, characterised by colonisation of a substrate and an exponentially increasing number of bacteria; (3) Stationary Phase, where the bacterial growth rate becomes zero (Zwietering et al., 1990); and (4) Cell Death or Decline Phase, characterised by a negative growth rate because cells die if no new nutrients are available and/or waste is not removed (Fletcher, 1977; Monod, 1949). In ocean, lake, and river environments, secondary colonisation by diatoms, algae and small organisms generally occurs. *In situ*, therefore, biofilms often exist as complex, highly structured communities (Stoodley et al., 2002).

3.4.2 Existing Methods of Biofouling Prevention

Various methods to prevent or reduce biofouling of aquatic sensing equipment are discussed in the literature. Protective equipment, like UV-based inhibitors (e.g., Woods Hole Oceanographic Institute, 2014), copper-based coatings or enclosures, wipers (e.g., Campbell Scientific Inc., 2013), and other mitigation techniques such as controlled release of toxic substances, and monitoring and cleaning of equipment (Chavez et al., 2000; Davis et al., 1997; Manov et al., 2004) are often used to remove or reduce biofilm growth on sensing equipment. The copper-based enclosures are not

practical for all types of sensors, and wipers may damage or break fragile sensors. Controlled release of toxic substance and monitoring and cleaning of equipment both need to be timed appropriately. Without an automated mechanism of biofouling detection, it is possible that there could be unnecessary release of toxic substances and/or site visits may also be conducted prematurely, adding to maintenance costs. Premature site visits, where a scheduled maintenance occurs sooner than is necessary, may be especially problematic for sensors deployed in less accessible locations, such as offshore marine environments.

3.4.3 A Need for Biosensors

Equipment deployed in hard-to-access environments could benefit from a sensor that indicates when controlled release and/or maintenance and cleaning of such equipment may be needed. A biofouling sensor that can detect biofilm growth in real-time and transmit signals easily to on-shore receivers could prove to be a solution to this problem. A biofouling sensor would also allow operators to separate biofouling noise from other acoustic disturbances, better identifying when maintenance is required without having to remove equipment for inspection.

3.4.4 Conventional Biosensors

There are conventional indirect methods that are used to monitor biofouling in industrial systems (e.g., water cooling towers and heat exchangers). These methods monitor reductions in heat transfer or frictional flow resistance in the plumbing caused by biofilm build-up in the lines (Philip-Chandy et al., 2000). *In situ* biosensors are also used in bioprocess monitoring to measure growth of suspended cells (not biofilm), where cells are being cultured. Capacitance sensors can directly sense cell growth (Vojinović et al., 2006); however, most other conventional biosensors used in cell-growth monitoring typically rely on proxy measures, like pH, the partial pressure of CO_2, or temperature, rather than direct sensing of biofilm growth (Vojinović et al., 2006). The sensitivity of capacitance sensors is typically low compared with other technologies (Vojinović et al., 2006). Using proxy-type sensors could prove challenging in a marine environment, where the influence of bacterial growth on the partial pressure of CO_2 and temperature would be dwarfed by the stronger background variability of

these parameters.

3.4.5 Evanescent Field Fibre Optic Sensors

The new generation of fibre optic sensors, called evanescent field fibre optic sensors, offers opportunities in sensing for a variety of applications. In evanescent field fibre optic sensors, a section of the fibre is modified so that a portion of the light passing through the fibre also propagates into the surrounding medium. A change in the refractive index of the surrounding medium therefore causes a perturbation in the evanescent field which can be detected in the transmitted signal (e.g., Gaston et al., 2003). Optical fibres can transmit signals over long distances with minimal loss because they are composed of a lower refractive index core and a higher refractive index cladding, causing forward propagation of light by total internal reflection. Evanescent field fibre optic sensors can take advantage of this transmission efficiency.

Two custom-fabricated fibre optic evanescent field sensors that can directly measure biofilm growth have been tested in laboratory and *in situ* conditions: a tapered fibre (Zibaii et al., 2010) and a stripped plastic fibre (Philip-Chandy et al., 2000; Wong et al., 2003). The tapered fibre was developed by drawing a heated fibre to narrow down a region of the fibre and allow propagation of light into the surrounding medium adjacent to the narrow portion (Zibaii et al., 2010). The target application for the sensor was the biomedical or food industries (Zibaii et al., 2010). To test the sensor, *Escherichia coli* bacteria were grown on the tapered portion of the fibre (Zibaii et al., 2010). The authors reported a decrease in transmitted intensity particularly during the exponential growth phase (Zibaii et al., 2010). A detection limit of 60 *E. Coli* mm^{-2} was observed (Zibaii et al., 2010).

For the plastic optical sensor, the cladding of a large-diameter, plastic, multi-mode fibre was removed over a 5 cm portion of the fibre (Philip-Chandy et al., 2000; Wong et al., 2003). The declad portion of the fibre promoted interaction of the evanescent field with the surrounding medium (Wong et al., 2003). Both *in situ* and laboratory experiments with the plastic optical fibre demonstrated a decrease in intensity of light at the core-cladding interface with bacterial growth (Philip-Chandy et al., 2000; Wong et al., 2003). Introduction of a cleaning solution allowed the transmitted intensity to return to pre-biofouling levels, demonstrating that the sensor could be re-used (Wong

et al., 2003). The plastic optical fibre was able to detect biofilm growth up to 1 mm in thickness (Philip-Chandy et al., 2000).

As proof of concept, experiments with both the plastic optical fibre (Philip-Chandy et al., 2000; Wong et al., 2003) and the tapered fibre (Zibaii et al., 2010) demonstrated that variations in transmitted light intensity could be used to measure biofilm growth. The metrics each author used to gauge sensor sensitivity were different; therefore, a direct comparison of this performance parameter is difficult. Nonetheless, the type of fibre on which the sensor was manufactured and the relative cost of the fibre would also influence the target applications for each sensor. Plastic optical fibre is a cheaper alternative to silica fibres, with improved ease of handling over silica, but plastic fibres cannot transmit signals as well as silica-based fibres if the transmission distance exceeds 100 m (Wong et al., 2003). The silica-based tapered fibres can transmit signals with less loss than a plastic optical fibre at distances greater than 100 m; however, the tapered portion of the fibre is quite brittle so durability is a concern. Of note, wavelength data, another parameter that could be used to measure biofilm growth optically, was not published by either Wong et al. (2003) or Zibaii et al. (2010), though (Wong et al., 2003) noted that a wavelength shift was observed. Using both intensity and wavelength, rather than just a single parameter, could provide redundancy of measurement, or assurance that the sensor is behaving as expected.

3.5 Long Period Grating Fibre Optic Sensors

Like the tapered and plastic optical sensors described above, Long Period Grating sensors (LPGs), an alternative fibre optic evanescent field sensor, are suited to sensing biofilm growth. Unlike the plastic optical fibre described above, LPGs do not require etching (removal of the cladding) to be sensitive to the refractive index of the surrounding medium. Moreover, LPGs are less brittle than tapered fibres. The sensing portion is written on a silica fibre, a fibre type that is more suited to long distance signal transmission than plastic optical fibre.

An LPG consists of a permanent localised change of the refractive index of the core of an optical fibre (Figure 3.1). This change has a specific spatial period (Figure 3.1). Long period grating sensors are typically inscribed by ultraviolet irradiation with

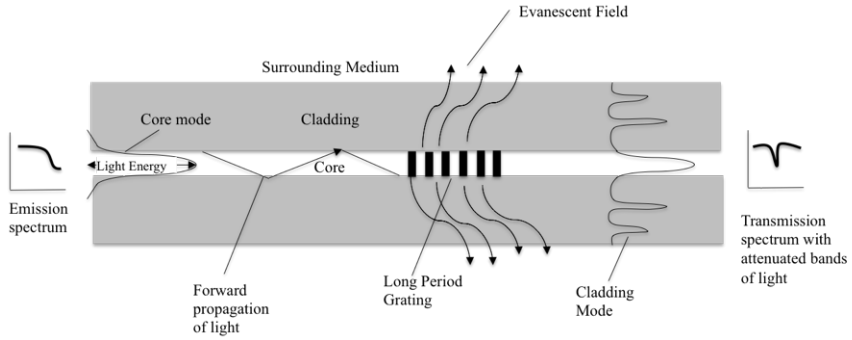

Figure 3.1: Conceptual drawing of a LPG sensor. Guided light modes are shown as they travel through the single mode fibre and then pass through the LPG. Emission and transmission spectra conceptually illustrates wavelength (x axis) and intensity (y axis) for core cladding modes that attenuated outward into the surrounding medium. Wavelength of attenuated bands varies with the refractive index of the surrounding medium, the spacing of the gratings, and the refractive index of the cladding.

periods ranging from tens to hundreds of micrometres (Figure 3.1; James and Tatam, 2003). An optical fibre has both a core mode and multiple cladding modes. A mode refers to a three-dimensional distribution of the electromagnetic field as it propagates through the fibre. This distribution is a strong function of the diameter and refractive index of both the core and the cladding. An LPG enables transfer of some of the light from the core mode to discrete cladding modes, in the forward propagating direction (Figure 3.1). The cladding modes have higher attenuation compared to the core modes. As a consequence, the transmission spectrum of an LPG consists of a series of attenuation bands at discrete wavelengths (Figure 3.1). The surrounding refractive index can be measured by monitoring the wavelength shift and change in intensity of the attenuation bands (James and Tatam, 2003). The wavelength shift has an inverse relationship to the refractive index of the surrounding medium (James and Tatam, 2003).

Long period grating sensors have achieved proof of concept for a number of applications, e.g., high and atmospheric pressure dissolved gas measurement (Bao et al., 2013; Melo et al., 2014). Long period grating sensors may be susceptible to interference from substances that alter refractive index in a way that is similar to the measurand (Bhatia and Risk, 2015); however, LPG sensors (without specialised coatings) are not directly sensitive to pCO_2 in environments at atmospheric pressure,

where the solubility of the gas is low (Melo et al., 2014). Therefore, these sensors are less likely to be susceptible to interference than are commercially available sensors that rely on indirect measurement parameters, like pCO_2.

3.5.1 Estimated Refractive Index of Biofilms

Pure biofilm (a bacterial film made up of a single species of bacteria) was measured using an Abbe refractometer and found to have a refractive index of 1.336, that is approximately 0.15 % higher than that of deionised water (Philip-Chandy et al., 2000). Given that this refractive index is lower than that of synthetic seawater, it is possible that biofilm growth will drive the wavelength shift upward due to the inverse relationship between the refractive index of the bulk medium and the central wavelength of the attenuation bands (James and Tatam, 2003). The relationship between biofilm growth and wavelength shift may be different than in bulk media, since a film has different optical properties than bulk media.

The refractive index of biofilm is also lower than the refractive index of the cladding (1.44; James and Tatam, 2003). Thin films with refractive indices lower than the cladding have been shown to reduce sensor sensitivity. Biofilm, however, has a complex structure, and therefore the refractive index and thickness of the film may vary. In addition, the relationship between the refractive index and sensitivity of the film has only been demonstrated in thin films (with diameters in the nanometre range; James and Tatam, 2003); biofilm would have a diameter in the micrometre range given that a single NCIMB 2021 cell is was measured to be 1 micron in diameter, and biofilms could form multiple layers, growing up to 200 microns in diameter.

3.6 Objectives

An LPG's wavelength shift response is induced by changes in the refractive index of the surrounding medium. Examples are available in the literature of the temperature response of LPGs, the wavelength shift in response to refractive index (James and Tatam, 2003), and the response of LPGs to salinity (Falciai et al., 2001), but little is known about how biofilm growth will affect LPGs. Other studies have demonstrated that refractive index-based sensors are able to detect biofilm growth (Philip-Chandy et al., 2000; Wong et al., 2003), so it is expected that LPGs will respond to biofilm

growth on the LPG. The aim of this study is to develop a method to detect biofilm growth in an automated way and to measure and interpret the effect of biofilm growth on the wavelength shift on an LPG. To achieve this objective, the following research questions must be answered:

(1) How does biofilm growth affect LPG sensitivity?

(2) What effect does biofouling have on baseline wavelength?

(3) Will intensity also be a reliable measurement parameter?

(4) Will mechanical cleaning restore sensor sensitivity?

3.7 Materials and Procedures

To evaluate the ability of LPGs to measure biofilm growth, three laboratory experiments were conducted: Trial 1 conducted for 12 h; and Trials 2 and 3 conducted for 48 h. The same LPG was used for Trial 2 and 3, but a different LPG was used for Trial 1. Pure bacterial biofilm comprised of *Pseudoalteromonas* sp. NCIMB 2021, a marine, rod shaped bacteria,, measured to be approximately 1 μm X 1.7 μm in diameter was grown on the fibre in a flow cell containing nutrient-dense synthetic seawater. The following sections detail the expendable and non-expendable materials that were required and the procedures used to conduct the experiments.

3.7.1 Expendable materials

The following expendable materials were used for each trial:

a. Synthetic seawater dense nutrient solution (made up of: 0.05 g Na_2HPO_4, 5.00 g $NaNO_3$, 23.00 g NaCl, 0.75g KCl, 1.47 g $CaCl_2{\cdot}2H_2O$, 5.08 g $MgCl_2{\cdot}6H_2O$, 6.16 g $MgSO_4{\cdot}7H_2O$, 10 g of sodium pyruvate, and 1 L of triply distilled water) was used to culture bacteria and grow the biofilm on the fibre (modified from Yakimov et al. (1998)). See procedures section for preparation of synthetic seawater;

b. Seventy percent ethanol solution for sterilization of the system;

c. Bacteria grown on the LPG was *Pseudoalteromonas* sp. NCIMB 2021; and

d. Triply distilled water.

3.7.2 Non-Expendable Materials

The following non-expendable materials were used for this study:

a. Off-the-shelf LPG optical fibres inscribed on a single mode 28e fibre from Technica SA. Central wavelength was 1550 nm ± 10 nm, with a 10 mm LPG length, a period of 450 m transmission loss was greater than 90 %, and full wave half maximum bandwidth was greater than 10 nm. The LPG was not recoated. Breakage did occur during mechanical cleaning, so a different sensor was used for the first trial than for subsequent trials;

b. fibre strippers, cleaver and a core-alignment splicer (Figure 3.2A-C);

c. Custom designed flow cell (Figure 3.2D);

d. Septa to grip fibre (Figure 3.2E);

e. Hypodermic needle to load septa onto fibre;

f. FC/APC Adaptors to connect two male pigtail ends (Figure 3.2F);

g. Optical circulators (Figure 3.2G);

h. A temperature controlled bath contained the flow cell, temperature sensors, and solutions to be pumped through the flow cell (Figure 3.3);

i. Insulated box to insulate the water bucket and its contents;

j. Micron Optics SM125 Interrogator (Figure 3.3H);

k. Thermocouple temperature sensors;

l. Any windows computer able to run the Micron Optics Enlight Software Package;

m. Campbell Scientific CR1000 data logger;

n. A Cole-Parmer Masterflex pump, with a flow rate between 1 and 5 mL/minute. If the flow rate is too low, tubing could become clogged, if the flow-rate is too high, nutrient solution will be wasted unnecessarily. Flow-rate also determines the rate of biofilm growth;

o. Tubing with the appropriate diameter for the peristaltic pump and connection for the flow cell;

p. Enlight Software Settings (Figure 3.4); and

q. Campbell Scientific Loggernet software to record temperature data at 2 Hz.

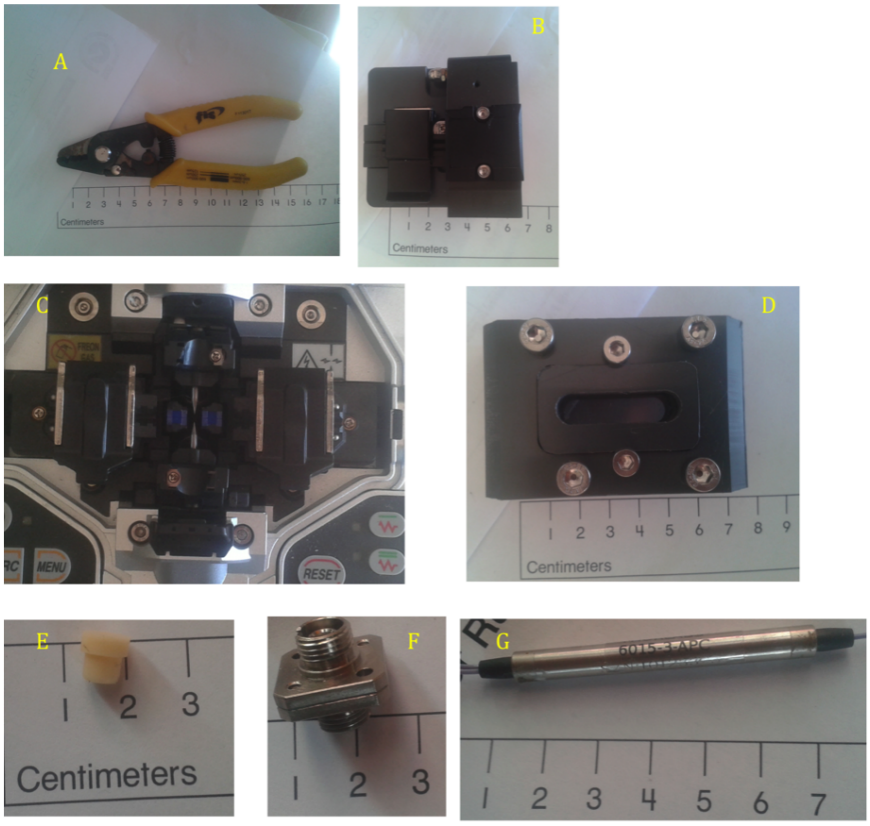

Figure 3.2: A: fibre strippers. B: fibre cleavers. C: Core alignment splicer. D: Custom fabricated flow cell. E: Septa. F: FC/APC adaptors. G: Circulator (ensures unidirectional movement of light).

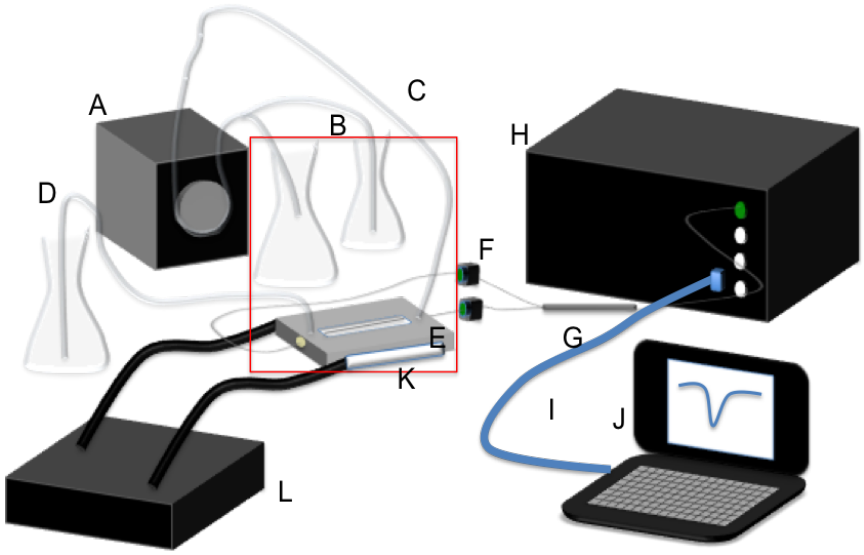

Figure 3.3: Setup for biofouling laboratory experiments. A: Peristaltic pump used to pump synthetic seawater and distilled water into the flow cell and to inject NCIMB 2021 into the flow cell. B: Distilled water and synthetic seawater flasks (autoclaved). C: In-flow tubing. D: Waste flask housing outflow tubing. E: Aluminum flow cell. F: Pigtails and FC/APC adaptors. G: Circulator (ensures unidirectional movement of light). H: Micron Optics SM125 interrogator with integrated swept LASER technology. I: LAN connection between interrogator and computer. J: Computer with Enlight software. K: Thermistors (attached to each side of flow cell). An additional thermistor (not shown) was used to make reference air temperature measurements. L: Campbell Scientific data logger. Red box indicates all components that were immersed in a bucket of water and insulated box to prevent temperature fluctuations. Note: All flasks were covered to prevent contamination.

3.7.3 Procedures

3.7.3.1 Fibre Preparation

A non-erasable marker was used to mark just outside the sensing portion of the fibre. The fibres connected to the LPGs were clipped at approximately 45 cm from the sensing portion to allow the septa to be loaded on each side of the LPG using the hypodermic needle. The larger-diameter end of the septa was loaded onto the hypodermic needle. The fibre end was then threaded through the tip of the needle. The needle was then threaded along the fibre until it was within one centimetre of the sensing portion of the fibre. The septa was pulled off the needle and threaded onto the fibre. This was repeated for fibre on the other side of the LPG. The LPG was then secured in the flow cell as described in the next section.

Once the LPG was secured, the fibre ends were stripped of their protective polymer coating, cleaned with an acetone-soaked non-residue wipe and placed in the cleaver. The cleaver was used to cut the fibre-ends cleanly for splicing. Two pigtails were then prepared for splicing onto the fibre in the same way, using the stripping and cleaving process. Once complete, one of the fibre ends connected to the LPG was placed inside the splicer along with one of fibre ends connected to the pigtails. The splicer automatically aligned the two fibre ends and fused the fibres together. It was important that this spliced section of fibre be protected because it is more delicate than an un-spliced section of fibre, so each splice was taped to a piece of cardboard to prevent flexure.

3.7.3.2 Loading the Flow Cell and Laboratory Setup

A flow cell (Figure 3.2D) was custom fabricated using a computer-controlled milling machine. The flow cell was rectangular in shape with almost identical top and bottom halves (Figure 3.4). The two halves could be screwed together with four screws (one on each corner). When the two halves were taken apart, the LPG could be easily loaded in the flow cell (Figure 3.4). Each half of the flow cell had a viewing pane carved into the centre (Figure 3.2D; Figure 3.4F). The top half also had two small nozzles on the outside surface. The nozzles were inlet and outlet valves to which inflow and outflow tubing could be connected (Figure 3.3E). On the inside panels,

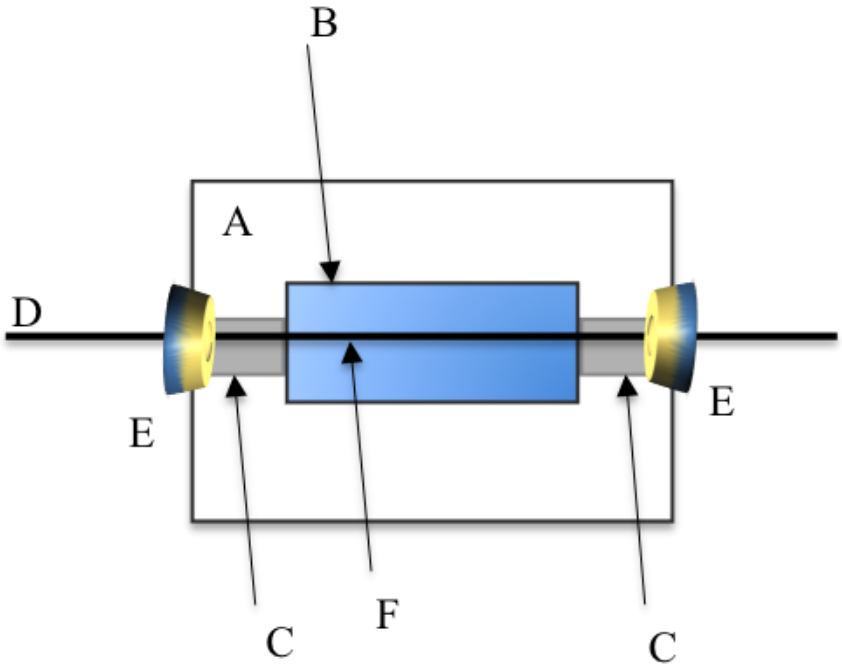

Figure 3.4: Inside view of the bottom half (A) of the flow cell with viewing pane (B) and semi-cylindrical slots (C) to allow room for the fibre and also to allow transfer of liquids through the flow cell. The fibre (D) is threaded through the septa (E), which are inserted on either end of the cylindrical slots. The long period grating sensor (F) is centred in the viewing window. The inside view of the top half is identical.

each half of the flow cell contained a narrow semi-cylindrical slot for the fibre to be housed and to allow for flow of liquids through the cell (Figure 3.4C). The LPG with pre-threaded septa was placed inside the flow cell (Figure 3.4E) and the two halves of the cell were screwed shut. The septa acted to seal each end of the flow cell and to maintain tension on the LPG (Figure 3.4E).

Once the flow cell was screwed shut and tubing was connected to the inlet and outlet valves of the flow cell, the pigtails were screwed into to the FP/APC adapters (Figure 3.3F), which were connected to the circulators (Figure 3.3G) and then the free pigtail attached to the circulator was inserted to a port on the interrogator (Figure 3.3H). The interrogator was connected to the computer via a LAN connection (Figure 3.3H) and Enlight software was used in the 'detect valleys' mode to monitor and record the LPGs transmitted wavelength spectrum.

3.7.3.3 Checking for Leaks

Tubing was connected to the inlet and outlet nozzles. Inlet tubing was connected to the peristaltic pump and outflow tubing was inserted into an Erlenmeyer flask marked 'waste'. Distilled water was pumped through the flow cell while the flow cell was sitting in air using the peristaltic pump to check for leakage.

3.7.3.4 Temperature Measurement and Calibration

Campbell Scientific 107 temperature sensors with 0.01 ^{o}C accuracy were used to measure temperature (Campbell Scientific Inc., 2014). Data was collected at 2 Hz using a Campbell Scientific CR1000 data logger and Loggernet software. The two temperature sensors were connected to the flow cell with plastic ties, and the flow cell was immersed in a temperature controlled water bath (in the same configuration as Figure 3.3) filled with hot tap water. Distilled water was pumped into the flow cell. The bath and flow cell were left overnight to cool with the cover off. Attenuated wavelength data and intensity of attenuation data were collected via the interrogator and the Enlight Software package. Once temperature data were collected, a regression analysis was performed using Excel^{TM} to characterise the relationship between peak attenuated wavelength and temperature. This relationship was used to remove temperature effects from the experimental data.

3.7.3.5 Temperature Control

Despite the temperature calibration, every effort was made to limit temperature variation during the experiment. Air temperature in the laboratory was held constant to within 2^{o}C. The flow cells, temperature sensors, and solutions that were pumped into the flow cell were all placed inside an insulated water bath.

3.7.3.6 Sterilization

Prior to pumping through any nutrient solutions or bacteria cultures, 70 % ethanol was circulated through the tubing for one hour followed by a one hour rinse with autoclaved triply deionised water (Sandt et al., 2009). All liquids were autoclaved prior to injection into the system.

3.7.3.7 Preparation of Synthetic Seawater

A 1 L solution of synthetic seawater was mixed using a recipe modified from Yakimov et al. (1998). Four one-liter Erlenmeyer flasks were each filled with 250 mL of triply deionised water. In the first flask, 0.05 g Na_2HPO_4 and 5.00 g $NaNO_3$ were added. In the second flask, 23.00g NaCl, 0.75 g KCl, and 1.47 g $CaCl_2{\cdot}2H_2O$ were added. The third flask contained 5.08 g $MgCl_2{\cdot}6H_2O$ and 6.16 g $MgSO_4{\cdot}7H_2O$ were added. The fourth flask contained only the triply deionised water. Each solution was autoclaved and, upon cooling, the contents of all four flasks were mixed together in one flask. To ensure minimal bacterial growth prior the experimentation, the nutrient, sodium pyruvate, was withheld until just prior to use.

3.7.3.8 Sensitivity Test

Flasks filled with distilled water and synthetic seawater were placed inside the temperature controlled water bath along with the flow cell and temperature sensors (Figure 3.3). Triply deionised water was pumped through the flow cell for up to one hour, followed by synthetic seawater. The attenuated peak wavelength was recorded during that time. The value for the refractive index of triply deionised water of 1.334 was taken from the literature (Wong et al., 2003) and the refractive index of synthetic seawater was measured using an Abbe refractometer and found to be 1.3405. The mean wavelength shift was divided by the difference between the refractive indices of the two substances to calculate a value for sensitivity. The same sensitivity test was conducted after biofilm growth had stabilised.

3.7.3.9 Bacterial Culture Preparation and Injection

An inoculum of NCIMB 2021 was cultured in 100 mL of synthetic seawater with 0.1 g sodium pyruvate for 24-48 h with shaking on an orbital shaker tray. After about 24 h, the bacteria had grown and the nutrient solution was cloudy, indicating that it was ready to be injected into the flow cell. Prior to injection any surfaces that may have come into contact with the flask containing the bacteria, were sterilised with 70 % ethanol solution. The mouth of the flask was heated with a flame and a gloved hand was used to remove the cotton and tinfoil covering of the flask. A sterile tubing was

inserted into the culture and the culture pumped into the previously sterilised flow cell containing the LPG, where it was allowed to sit for one hour to allow colonisation of the fibre.

3.7.3.10 Growing Biofilm

After bacterial culture was allowed to sit for one hour in the flow cell, sterile synthetic seawater was pumped through the flow cell at a rate of up to 0.5 mL m^{-}. This was continued for up to 48 h after the initial injection of bacteria.

3.7.3.11 Post Fouling Cleanup

All bacterial waste was collected in silica containers and autoclaved. Seventy percent ethanol solution and/or an enzymatic cleaner was pumped through the system and allowed to sit for one hour before rinsing with distilled water. The sensor was then cleaned mechanically using 70 % ethanol and a low residue wipe.

3.8 Assessment

The above procedure was repeated three times using NCIMB 2021 to ascertain the efficacy of LPGs to sense the rates of biofilm growth. It was determined that biofilm sensors were able to detect the rate of growth of biofilm because this growth could be measured by changes in the wavelength of the attenuation band. Shifts were greatest early in the experiments, during the exponential growth phase of bacterial growth (Figure 5a and b). There was a subsequent stabilisation in signal for the two 48 h trials, when bacterial growth slowed and/or sensor sensitivity may have declined due to increasing biofilm thickness (Figure 3.5a and b). In total, upward wavelength shift ranged from 50 pm to 80 pm (Figure 3.5a).

As a point of comparison, wavelength with triply deionised water as surrounding bulk media increased by 23 ± 5 pm to 71±14 pm between pre- and post-fouling (Figure 3.6). Sensor sensitivity was also reduced between pre and post biofilm growth by between 37 % and 67 % (Figure 3.6). This is a smaller reduction than was expected. It is possible that the biofilm absorbed some of the bulk media, causing a change in refractive index of the film itself. It is also possible that since only two

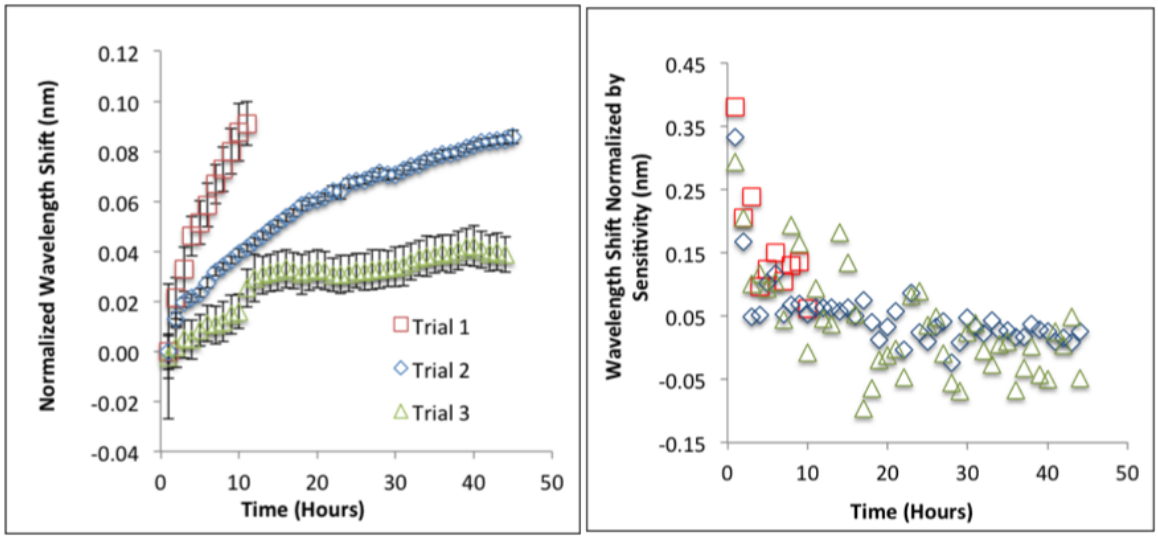

Figure 3.5: LPG response to biofouling from *Pseudoalteromonas* NCIMB 2021.](a) Delta wavelength shift in mean peak attenuated wavelength over time. Error bars denote standard deviation for hourly means. (b) Presents delta wavelength shift over the course of the biofilm growth divided by the wavelength shift between synthetic seawater and triply deionised water. Squares represent Trial 1, diamonds represent Trial 2, and triangles represent Trial 3.

media (synthetic seawater and triply deionised water) of similar refractive index were used to calculate sensor sensitivity, that both pre-and post-fouling sensitivity may have been different had substances with a broader range of refractive indices been used to calculated sensitivity.

It was hoped that redundancy of measurement would be present; i.e., that both intensity and wavelength of the peak attenuated wavelength would vary with bacterial growth. This did occur during two out of three experimental runs, but intensity measurement in the first run was too noisy to detect any type of shift in intensity. Wavelength therefore seems to be the most reliable indicator of biofilm growth. In cases where intensity measurements had less noise, the magnitude of the intensity decreased with biofilm growth.

Of key importance in biofilm measurement, and sensing in general, is sensor resilience; a return of sensor sensitivity to pre-fouling levels after biofilm growth has been removed. Although sensor sensitivity returned after mechanical cleaning, standard deviation increased upon re-use (Figure 3.7). Mechanical cleaning provided

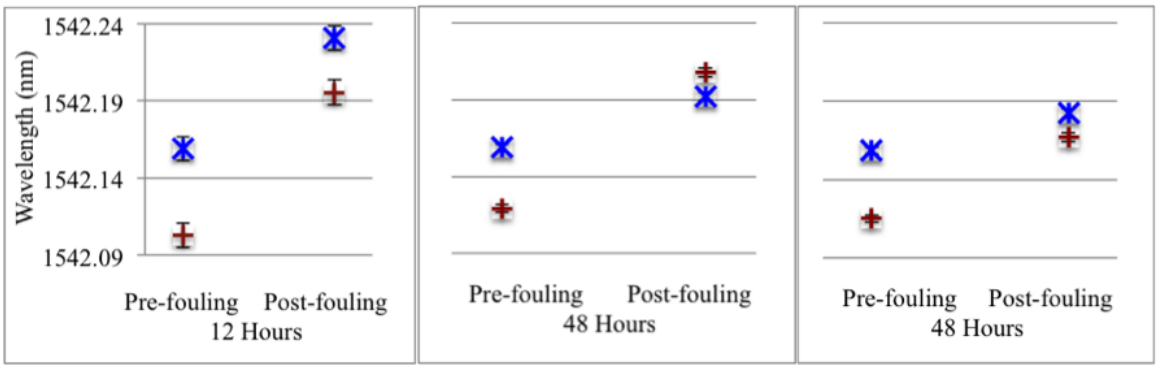

Figure 3.6: Pre- and post-fouling wavelength shift for triply deionised water (blue 'x') and synthetic seawater (red cross). For Trials 1, 2, and 3

proof-of-concept that with additional research, automated cleaning may restore sensor sensitivity and allow for sensor reuse. In some cases, mechanical cleaning led to breakage of the sensor since the sensing portion of the fibre lacked a polymer coating and was therefore brittle (though not as brittle as tapered fibres).

3.9 Discussion

This fibre optic biofilm sensing method provides a tool to measure rates of biofouling in aquatic environments to limit the need for costly excursions to check instruments. The laboratory experiments conducted as part of the development of this method demonstrate that such a sensor would be feasible because the LPG used in this experiment responded consistently to biofilm growth; however, more development is needed to protect the sensor from damage, to automate parts of the process, including mechanical cleaning, and to develop redundancy of measurement. Secondly, there is a need for the sensor to be able to distinguish biofouling from other types of noise for instruments like acoustic receivers. The biofouling curve (Figure 3.5a) does show a unique pattern, with greater rate of wavelength shift in the first 12 h, followed by a period of increasing stability as the experiments approach the 48 h mark. It is therefore possible that computer algorithms could be used to distinguish a unique biofouling fingerprint from other *in situ* variability.

Experiments conducted during development of this method demonstrated that

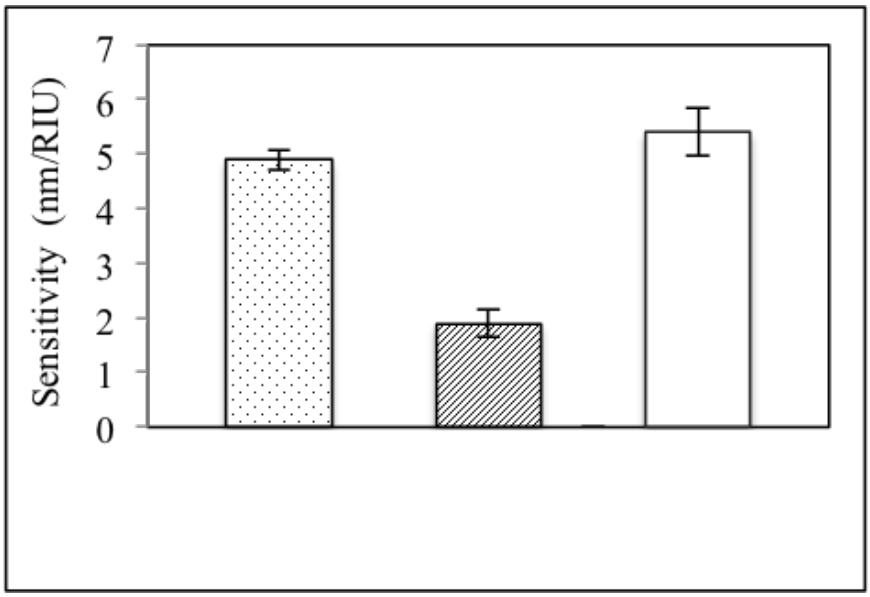

Figure 3.7: Shows mean peak wavelength shift between triply deionised water and synthetic seawater pre-fouling, post-fouling and post-mechanical cleaning of the sensing portion of the fibre. Changes in the sensitivity of the LPG pre and post fouling are likely due to instrument error.

LPGs are able to measure the rate of biofilm growth by the resulting shift in attenuated peak wavelength; however, the ability to use intensity measurements as a secondary measure of biofilm growth did not meet expectations since this measurement parameter only responded to biofilm growth in two out of three trials. Nonetheless, this redundancy may not be needed for optimal sensor performance, since wavelength shift on its own was demonstrated to be a reliable method to detect biofilm growth.

The potential for automatic recording and detection of biofilm growth was only partially demonstrated. The sensor was able to measure biofilm growth in real-time; however, additional interpretation of the signal is still required by the user at this time. Algorithms designed to interpret and identify signal changes due to biofouling could help with automation; however, for full automation, mechanical cleaning would also need to be automated to restore the sensor to its baseline condition.

Alternative applications of this method may have the potential to monitor for the nature of the growth (perhaps bacteria growing in chains will have an initial difference compared to bacteria growing in clumps or individually). There may also be the potential to identify secondary colonisation or how a given biofilm responds to

changes in temperature or light in an automated way without having to conduct cell counts. Existing published data does not need to be reinterpreted, but this method could complement or be used in conjunction with visual characterization of biofilm growth.

3.10 Comments and Recommendations

Improvements to LPGs and the design of the interrogation software are necessary for improved consistency of performance. Furthermore, adjustments to the flow cell design could increase the tension placed on the LPG and thus the sensor's performance. For example, in the experiments reported here, the septa apply a mechanical downward pressure to hold the fibre in place. Alternatively, locking devices that also pull outward on the fibre can provide increased tension. This additional tension may allow the sensor to produce a sharper peak and improve measurement precision.

To improve sensor resilience and robustness, more work is needed to consider mechanisms to house the sensor to protect it from breakage both during operation and mechanical cleaning of the device. Some type of flexible coating that still allows for biofilm growth may be of the greatest value. Hard mounting the sensor to a rigid protective device may improve longevity and robustness.

The consistency of LPGs needs to be improved at the point of manufacture. There is a great deal of inter-sensor variability with respect to sensitivity, the quality of the signal in terms of both peak wavelength output and intensity. As the technology evolves, manufacturers may be able to improve the reliability of their products and/or in-house fabrication techniques may mature, allowing for improved quality control. It is also not currently known how the sensor would respond to species that grow in different configurations, or to multi-species biofilms. Preliminary *in situ* testing suggests a similar pattern to laboratory results may occur early in the first few days of fouling, but the growth rate may be slower. In the longer term, factors other than biofouling may have a stronger influence on sensor signal. Experiments to consider the effect of flow rates, protective membranes, and multi-species biofilms on sensor response are also important prior to commercialization and *in situ* deployment.

3.11 Conclusion

The LPGs used in this work consistently underwent an upward wavelength shift in response to biofilm growth. Wavelength shifted upward in response to bacterial colonisation by as much as 80 pm. Sensor sensitivity was reduced post-fouling by as much as 67 % compared to pre-fouling levels, but mechanical cleaning restored sensor sensitivity. More work is needed to move towards automation, but these results show promise and for the first time, present a fibre optic sensing method where wavelength shift is the primary parameter used to detect biofilm growth.

Chapter 4

Biofouling of Fibre Optic Long Period Grating Sensors in Seawater

4.1 Preamble

Sonja Bhatia and David Risk

This chapter forms the basis for a paper submitted to Environmental Science: Processes and Impacts on August 15, 2015. I led the experimental design, site selection, and writeup with guidance and financial support from my supervisor, Dr. David Risk.

4.2 Abstract

A new generation of sensors, fibre optic long period grating sensors (LPGs), have the potential to advance environmental monitoring in the marine environment for a number of applications (e.g., monitoring subseafloor geologic sequestration sites, and biofilm sensing). Biofouling of LPGs is both a problem and an opportunity for sensor developers because LPGs can act as biofilm sensors in their own right, but biofouling can also cause signal drift when the film itself is not the intended measurand. Laboratory experiments with LPGs demonstrated that LPGs respond to biofilm growth, but little is known how multi-species biofilms likely to be present *in situ* will influence sensor response. Three 48 h field trials were conducted to ascertain the effect of biofilm growth in seawater. Seawater was pumped and filtered from a protected cove and run through a flow cell that contained the LPG. SEM images were taken of optical fibres immersed in seawater every 4 h for a 48 h period to visualise growth that was expected to be similar to biofilm growth on the LPG itself. LPGs are gratings inscribed on the core of an optical fibre, that cause interaction of a portion of the light traveling through the fibre to interact with the surrounding environment. Certain light modes traveling through the fibre exponentially decay (attenuate) and therefore

the intensity of the associated central wavelengths is damped in the transmitted spectrum. These attenuation bands have an inverse dependence on the refractive index of the surrounding medium, undergoing a 'wavelength shift' in response to changes in the refractive index of the surrounding medium. Biofilm has a lower refractive index than the surrounding seawater, therefore it is expected to cause an upward wavelength shift in sensor signal. In all three trials, an upward wavelength shift of between 20 and 40 $\pm$ 9.8 pm was observed. SEM images showed too much variability to confirm that increased coverage of the fibre with biofilm drove upward wavelength shift. It was hypothesised that thickness of the coating rather than fractional coverage of the fibre was actually driving the upward wavelength shift in sensor signal.

4.3 Introduction

A new generation of sensors currently under development for environmental monitoring applications Bao et al. (2013), Long Period Grating Fibre Optic Sensors (LPGs), have the potential to advance environmental monitoring in the marine environment. Long period gratings are able to transmit signals over long distances with minimal losses, are able to operate in both low and high pressure environments (Melo et al., 2014; Bao et al., 2013), and they require no electronics at the measurement site and therefore are not susceptible to electromagnetic interference, and have the potential for multi-parameter sensing (James and Tatam, 2003). These features mean that LPGs can be deployed in remote marine environments, allowing for sensing in the deep ocean and other hard-to-access sites that were previously inaccessible to most sensors without remote sensing capabilities.

These sensors are versatile and have the potential to be engineered to detect changes in a number of marine variables of interest. For example, LPGs are highly sensitive to temperature (James and Tatam, 2003), so the sensors could theoretically be used for long-term continuous measurement of seawater temperature in the deep ocean. Long period grating sensors could also be used to monitor salinity (Falciai et al., 2001). Long period grating sensors are also being considered to sense dissolved carbon dioxide (dCO_2) for seafloor monitoring of sub-seafloor marine geologic sequestration sites (Bhatia and Risk, 2015). In Chapter 5, laboratory results demonstrated

that LPGs could also be used to measure rates of biofilm growth (Chapter 5), providing an estimate of bacterial load in a given marine (or other aquatic environment). Sensor coatings can be used to enhance sensor sensitivity (Melo et al., 2014) and selectivity for a given application (e.g., molecular sieve ceramics Centeno and Fuertes, 2001), and to prevent biofouling (by using some type of sheathing coated in an antifouling substance, like a polymer membrane (Chambers et al., 2006), should that be required.

4.3.1 Biofilm Growth in the Marine Environment

Biofilms are dense, microbial films, formed by surface-association between individual bacteria of the same species and also inter-species associations (other non-bacterial microorganisms may also be present in biofilm communities; Costerton et al., 1999). These films create protective and nurturing environments for microorganisms to grow; mature biofilms are usually covered in a protective, extracellular polysaccharide coating (Pavlovsky et al., 2013). Quorum sensing refers to the ability of a bacterial colony to sense its own density by exchanging autoinducers (diffusable molecules). Production of autoinducers increases with density and can trigger production of extracellular polysaccharide coating, leading to colony shrinkage (Amin et al., 2012). Biofilm growth occurs in four distinct phases:

(1) Lag phase, where molecular molecular deposition occurs;

(2) Exponential growth phase, which for the purposes of this article includes the acceleration and retardation phases;

(3) Stationary phase, where the growth rate is zero; and

(4) Death phase, if nutrients are not added or waste not removed (Monod, 1949).

Multi-species biofilms form readily in the marine environment (Lee et al., 2008). Within seconds of immersion in seawater, molecular deposition of organic matter occurs on submerged surfaces (Qian et al., 2007). The composition of this deposition can influence the species of the primary coloniser, which is typically bacterial due to the abundance of bacteria in the marine environment (Qian et al., 2007). Secondary colonisation is determined by the attraction of additional species by the primary coloniser, or the secondary coloniser's ability to displace existing bacteria (Qian et al., 2007). Mature biofilm is not static; synergistic and competitive interactions shape

the biofilm community, and mature biofilms typically form highly structured, multi-species communities (Stoodley et al., 2002). In a study in coastal waters, significant variability in colonising species was noted between biofilm communities within 9 and 24 h of colonisation on various substrates, including glass (Lee et al., 2008). Non-bacterial species, such as diatoms can also settle at anytime during the colonisation process, though diatoms are typically only consistently associated with two bacterial phyla (Amin et al., 2012).

4.3.2 Long Period Grating and other Evanescent Field Biofilm Sensors

To manufacture evanescent field fibre optic sensors, a section of optical fibre is modified to allow a small portion of light guided through the fibre to interact with the surrounding medium. The attenuated wavelengths and transmitted intensity of these wavelengths is a function of the refractive index of the surrounding medium (Gaston et al., 2003). Three types of evanescent field biofilm sensors have been demonstrated to be able to detect biofilm growth. Two sensors detected biofilm growth through intensity modulation: a declad plastic optical fibre (Philip-Chandy et al., 2000; Wong et al., 2003) and a tapered silica fibre (Zibaii et al., 2010). When tested, both sensors showed a progressive decrease in transmitted intensity with biofilm growth (Philip-Chandy et al., 2000; Wong et al., 2003; Zibaii et al., 2010). A third type, Long Period Grating Fibre Optic Sensors (LPGs) were also tested in the laboratory conditions where a single-species biofilm was grown in synthetic seawater conditions. In this case, wavelength, and not intensity, was the most effective sensing parameter. Biofilm growth was shown to cause an upward wavelength shift of between 50 and 80 pm (Chapter 5).

4.3.3 Objectives

Long period gratings have already been tested in laboratory conditions with single-species biofilm grown in synthetic seawater (Chapter 5). The aim of this study is to isolate the effect of biofilm growth on LPGs in natural seawater conditions, where multi-species biofilms are likely to form. This will further development of an LPG biofilm sensor, but also characterise the drift caused by biofouling that could negatively impact LPGs intended for other applications in marine sensing. To meet this

research objective, the following questions will be addressed:
(1) How does the LPG respond to biofilm growth *in situ* and how does this response compare to laboratory results published in Chapter 5?
(2) Can fractional coverage be detected through wavelength shift?
It seems likely that biofilm growth *in situ* will also drive wavelength shift upward, but the magnitude of the shift may vary and may occur more slowly in the less bacteria- and nutrient- dense seawater as compared to laboratory conditions. Fractional coverage may not be the primary driver of LPG signal. It is possible that thickness of the biofilm growth will be a more important factor in the magnitude of the wavelength shift.

4.4 Instrumentation and Field Setup

4.4.1 Field Site and Setup

The study site was Fawson Cove, a protected cove on Canada's East Coast (44.4711 ^{0}N, 63.6533 ^{0}W; Figure 4.1), with freshwater input from adjacent Gray Lake through a small stream-estuary system. An established rural fishing community borders the cove and lake; lot sizes are small and septic systems poorly maintained. It is therefore likely that septic runoff is contaminating both the lake and cove, possibly increasing bacterial load in Fawson Cove. Fuel release from motorised vessels operating in the cove is also likely. Tide height varies, but is approximately 1.5 m.

Equipment was housed inside a protected building at the foot of Fawson Cove (Figure 4.2). Seawater was pumped with a peristaltic high volume pump (*Geopump 2*) from approximately 1 m depth below the low tide level to avoid freshwater stream runoff and also any contamination from fuel spills, both of which would float near the surface. Seawater was coarsely filtered through a bubbler to remove large sediment particles and release air bubbles prior to injection into equilibration buckets immersed in an insulated water bath to allow seawater temperature to equilibrate with the temperature of the experimental system. Once equilibrated, seawater was pumped using a miniature peristaltic pump (*Williamson Mini 100 series*) into a custom fabricated flow cell (approximately 1 cm high, 4 cm long, and 2.5 cm wide) that housed the LPG (See: Chapter 5 for illustration; Figure 4.3). Temperature sensors (*Campbell*

Figure 4.1: Map illustrating location and vegetative cover of Fawson Cove-Gray Lake system, NS, Canada (modified from Google Maps). Elevation above sea level between the lake and the ocean does not exceed 3 m.

Scientific 107 Thermistor Temperature Sensors) were secured on either side of the flow cell and wired to a data logger (*Campbell Scientific 1000*; Figure 4.3).

Three, 48 h long field trials were conducted with this setup. The first trial was completed in August, 2014, and the last two in May and June, 2015, respectively. The LPG was replaced between Trial 1 and Trial 2. Trials 2 and 3 used the same LPG. All LPGs, tubing and other equipment were cleaned mechanically and soaked with 70 % ethanol before each trial. Seawater was pumped continuously through the flow-cell during each trial using the miniature peristaltic pump. Wavelength shift and temperature were recorded at a rate of 2 Hz.

Figure 4.2: Photograph showing protected building at the foot of the cove and stream connecting the Gray Lake-Fawson Cove estuary system pictured to the right of the building. Elevation between the cove and the lake is approximately 5 m.

4.4.2 SEM Visualization of Biofilm Growth

Interrupting a field trial to visualise bacterial growth on the LPG would have interfered with data collection, therefore silica optical fibres (that would provide a similar substrate to the LPG) were inserted into the outflow container every four hours for the first 48 h of the experiment. It was expected that the last optical fibre inserted

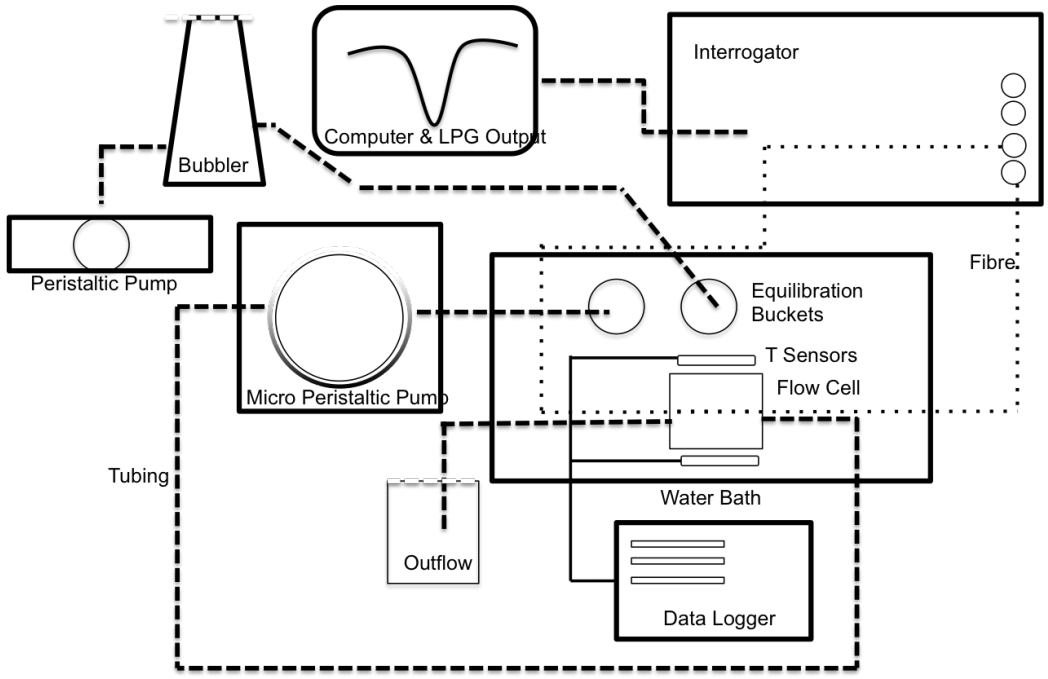

Figure 4.3: Illustration of experimental setup. A geopump used to pump seawater from cove, a bubbler to remove sediments and bubbles, containers to temperature equilibrate seawater with experimental system, contained in an insulated water bath. The flow cell was also immersed in the insulated water bath, where the micro peristaltic pump was used to pump water from the equilibration buckets to the flow cell which housed the LPG. Waste was pumped into a waste bucket. Temperature sensors (H) were attached on either end of the flow cell and wired to a data logger. LPG was connected to an interrogator (J) and the signal processed by a Windows operated computer. Thick dashed line represents tubing, thin dashed line represents optical fibre. Solid line indicates cable connecting temperature sensors and data logger. Overlap does not indicate interconnection.

would have undergone bacterial colonisation similar to the first four hours of the experiment. Upon completion of the experiment, the optical fibres were cut and placed in 100 % ethanol and dried in a critical point dryer. The fibres were then placed on stubs and gold coated for visualization under the SEM. Images of the fibre at the same resolution and magnification were taken at random (without selecting the most covered or least covered section), hereafter referred to as 'standard view'. Fractional coverage of the fibre was estimated using a 25X16 grid. The grid was placed over the image in a position where the majority of the squares covered the fibre. Squares with prominent features, or that appeared to have more than 50 % coverage, were counted as 'covered', and used to calculate the fractional coverage value. Higher magnification

SEM images of bacterial clumps growing on the fibre were also taken to provide more insight into the bacterial communities growing on the fibres.

4.4.3 Long Period Grating Sensors: Theory and Operation

Long period gratings are inscribed on a portion of the core of an optical fibre. These gratings cause the core mode to couple to certain discrete cladding modes. The cladding modes attenuate more readily than the core mode, causing certain discrete wavelengths to be attenuated in the transmission spectrum of the LPG. The attenuated wavelength shifts inversely with the refractive index of the surrounding medium. A substance that causes a shift in the refractive index of seawater within the sensitivity limits of an LPG could therefore be detected by this method. For a more complete description of the operating principle of an LPG, please refer to Section 1.1.6. Biofilm has a refractive index of approximately 1.336 (Wong et al., 2003), lower than that of seawater, which has a refractive index of between 1.337 and 1.343 (Austin and Halikas, 1976). It is therefore likely that biofilm growth will generate an upward wavelength shift relative to seawater. For a complete description of the manufacture and optical properties of LPGs please refer to James and Tatam (2003), and for an in-depth discussion of biofilm growth on LPGs, please refer to Chapter 5.

4.4.4 Calibration

Both a reduction in salinity and temperature could generate a wavelength shift that mimics the shift generated from biofouling. The seawater intake was deployed at a depth 1 m below the low tide minimum to attempt to minimise variations in salinity that would be likely in the surface layer, which would be susceptible to variation due to rainfall and riverine inputs. Salinity was also sampled synoptically in the months leading up to field trials and during the field trials themselves using a conductivity metre. The impact of any expected variation was calculated to ascertain the likely direction and magnitude of the wavelength shift it would induce.

A temperature calibration was also conducted prior to each field trial to ascertain the relationship between wavelength shift and temperature. Deionised water was injected into the flow cell and the temperature in the water bath was raised to 35 ^{o}C and allowed to cool to between 12 and 15 ^{o}C. A regression analysis was performed to

determine the relationship between temperature and wavelength shift, and the slope of the temperature-wavelength shift curve was then used to subtract the effect of temperature from wavelength shift during all three field trials. Beyond removal of temperature, every reasonable attempt was made to control temperature in the water bath. Temperature throughout each experiment only varied by a maximum of 2 ^{o}C.

4.5 Results and Discussion

4.5.1 SEM Visualization: Fractional Coverage and Qualitative Observations

SEM images revealed considerable variability in the colonisation pattern and fractional coverage with time (Figure 4.4), and size and shape of the colonising bacteria (Figure 4.5). No clear pattern between fractional coverage and immersion time was evident; some of the fibres that were immersed longer had lower fractional coverage than those that were immersed for shorter periods (Figure 4.6B). There are several plausible explanations for this. Firstly, because sections of fibre were chosen at random for the standard view, it is possible that other sections of the same fibre had more or less coverage than shown in the image. Secondly, patterns and rates of colonisation have been shown to vary considerably in the marine environment (Lee et al., 2008), with biofilm distribution and species composition being driven in large part by the primary coloniser. In addition, quorum sensing has been demonstrated in biofilm communities, so bacteria will often settle next to other symbiotic bacterial species (Qian et al., 2007), or individuals of the same species, making it likely that certain portions of the fibre would have well developed colonies before other portions of the fibre were even colonised by one individual.

Size and shape of the colonising bacteria also varied. All species present appeared to be bacterial in origin; no diatoms were noted. The absence of diatoms may have been a function of the colonising bacteria (Amin et al., 2012) or the smoothness of the fibre surface because diatoms have been shown to favour rougher substrates in some environments (Hutchinson et al., 2006). Higher magnification SEM images revealed a general trend, still with considerable variability, to increasing complexity, density, and species variability with immersion time. What appeared to be extracellular

polysaccharide coating began to appear, though not consistently, by the 8 h mark, with what appeared to be more extensive extracellular polysaccharide coating after 44 h of immersion. This is also in line with the literature which suggest that extracellular polysaccharide coating is typically present in more mature biofilms (Pavlovsky et al., 2013).

4.5.2 Biofouling and Wavelength Shift

All three field trials showed an upward wavelength shift of between 20 and 40 ± 9.8 pm within the first 30 h of the trial, followed by subsequent stabilisation of the signal, except in the last 3 h of Trial 3 (Figure 4.7). Temperature effects were removed using the relationship established through the earlier temperature and wavelength regression analyses that had R^2 values above 0.98 in all cases. Salinity values did not vary by more than 1 g/L, corresponding to less than a 5 pm wavelength shift, which was within the standard deviation of a sensor signal immersed in deionised water in a temperature controlled environment during calibration; i.e. 'noise'. The upward wavelength shift matched the direction of shift seen in laboratory experiments where biofilm was grown on LPGs in synthetic seawater (Chapter 5), where an upward wavelength shift of between 50 and 80 pm was seen.

In the laboratory, the upward wavelength shift began almost instantaneously upon injection of bacterial culture, and stabilised after about 48 h. The upward wavelength shift in the field is likely also due to biofilm growth, despite the slower and reduced response of the LPG; concentration of bacteria is likely to be lower in seawater than in ideal, nutrient-dense the laboratory conditions, so colonisation and subsequent growth phases would take longer *in situ* than in the laboratory setting. The smaller wavelength shift could be also be due to a possible smaller relative difference in refractive index between seawater and biofilm and synthetic seawater and biofilm. Seawater has a refractive index ranging from 1.337 and 1.343 (Austin and Halikas, 1976), and synthetic seawater has a refractive index of 1.3405; Chapter 5). The shape of the curve matches the known growth phases of biofilm colonies, with an initial stable signal that matches what would be expected in the lag phase, followed by upward wavelength shift, like what would be expected in exponential growth phase, and then stabilisation of the signal, as expected during stationary phase (Monod,

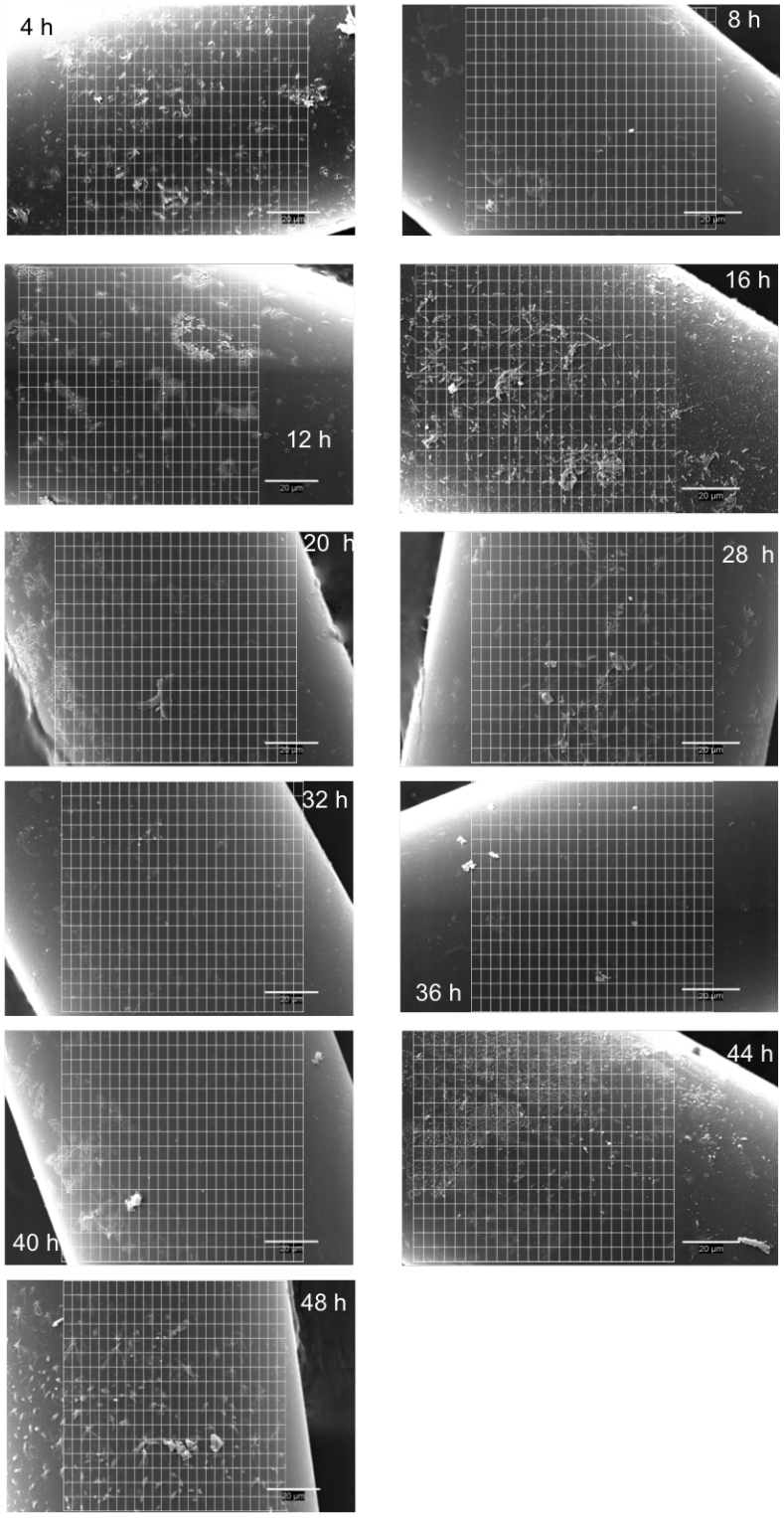

Figure 4.4: Images in four hour intervals of bacterial growth on silica fibres immersed in seawater. Images were taken so that whole sections of fibre could be viewed. Images were taken randomly, rather than specifically targeting a covered area to try to estimate fractional coverage. White grids were used to estimate fractional coverage. Scale bars show 20 μm. Hour 24 is missing.

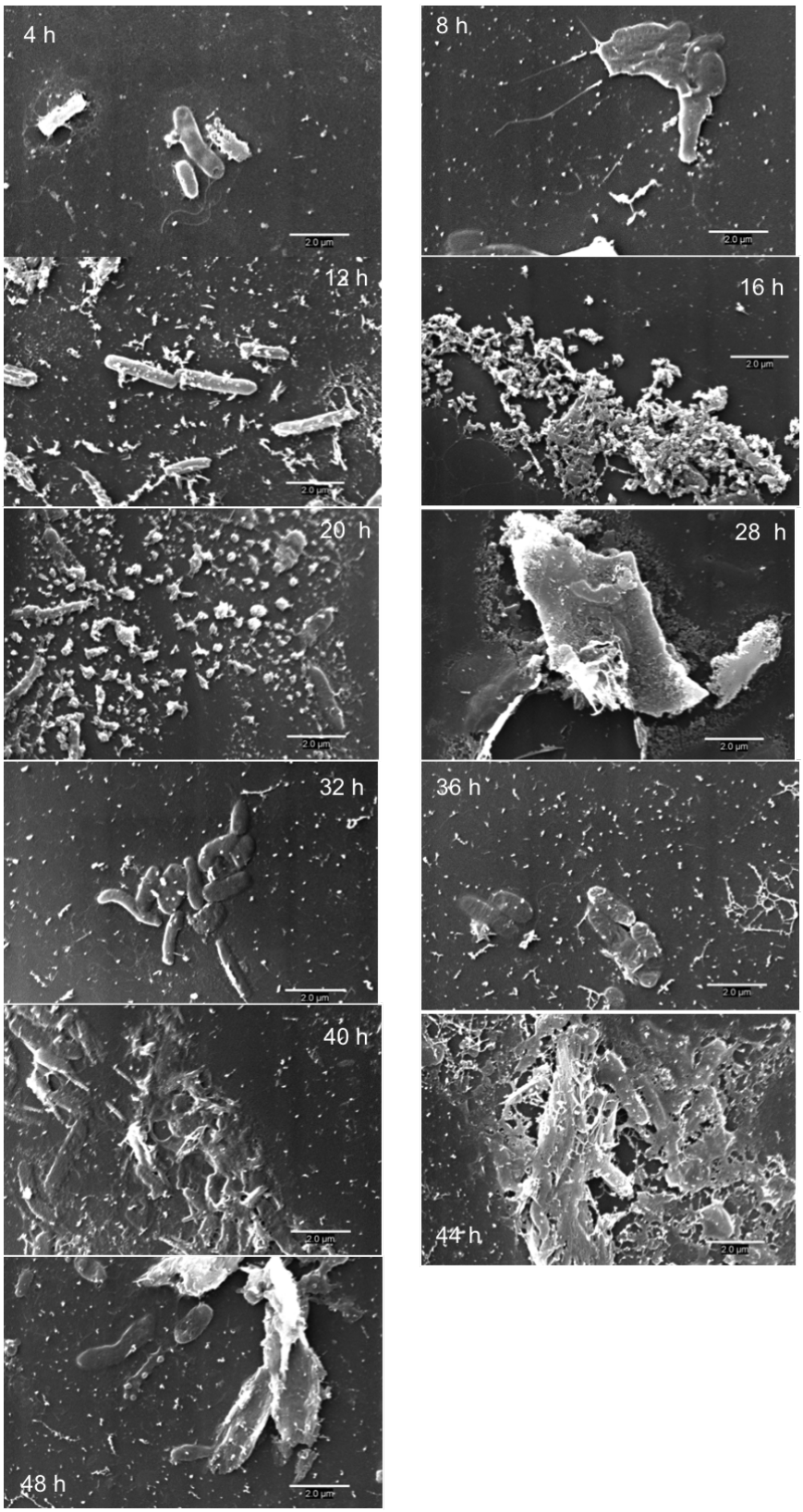

Figure 4.5: High magnification SEM images in four hour intervals of bacterial growth on silica fibres immersed in seawater. Scale bars indicate 2 μm. Hour 24 is missing.

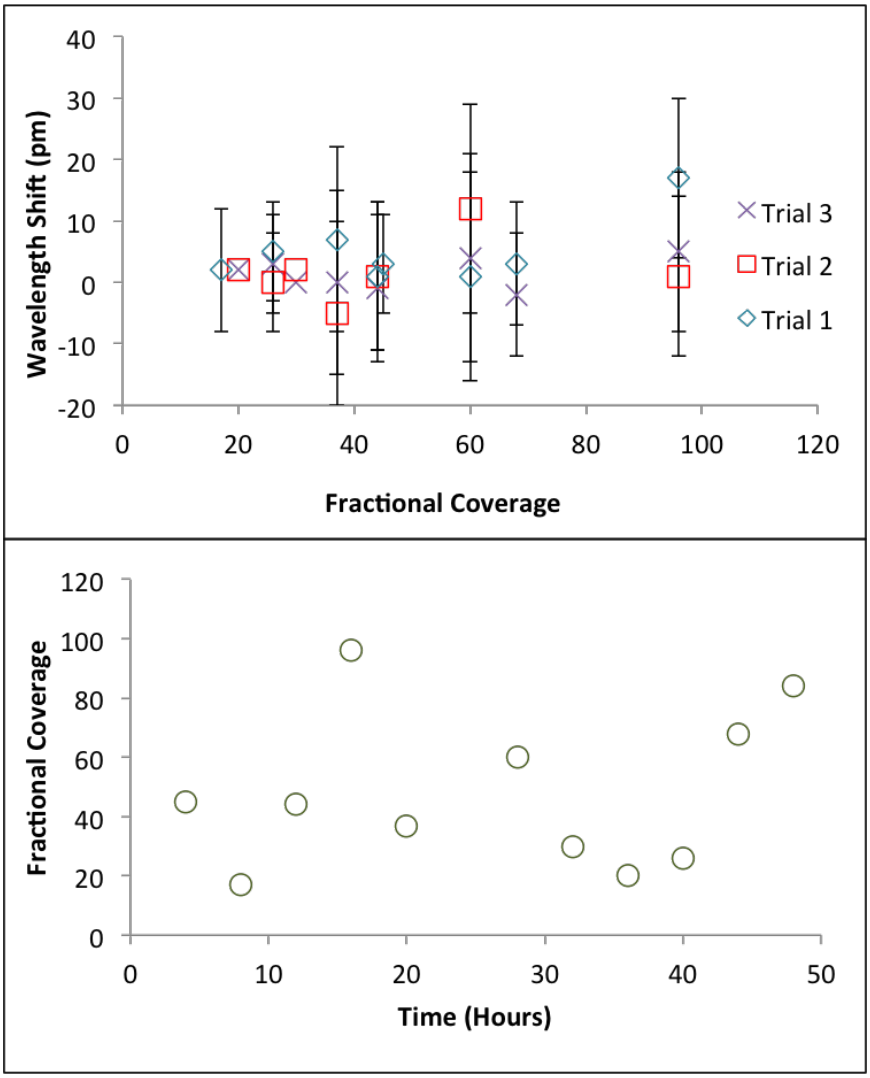

Figure 4.6: (A)Fractional coverage vs. wavelength shift every 4 h for Trials 1, 2 and 3. Error bars denote standard deviation and (B) Fractional coverage estimated using grids superimposed over SEM images vs. time. For both A and B, n= 7200.

1949, Figure 4.7).

Despite the upward wavelength shift common to all trials, timing and pattern of the wavelength shift showed strong inter-trial variability. In Trial 1, the wavelength shift was smooth and began at 14 h, stabilizing at the 21 h mark (Figure 4.7A). In Trial 2, the wavelength shift showed an initial drop in wavelength of 5 pm starting at the 22 h mark, with rapid upward growth beginning at 26 h. The initial drop may have been due to a rapid change in temperature, where temperature was not taken out effectively for this period (Figure 4.7B). Trial 3, shows a two phase shift in upward wavelength. There is no apparent temperature explanation for this pattern (Figure 4.7C). Also, in the last 3 h of Trial 3, wavelength does not remain stable, but drops significantly, unlike in the other two trials. There is no clear explanation for this downward wavelength shift. It is possible that cell death occurred, driving wavelength shift down.

Inter-trial variability in the scale, pattern, and timing of the upward wavelength shift that cannot be explained by rapid temperature variations is likely due to a number of factors. The most likely causes of the variability may be the initial location of colonisation relative to the gratings, the species of bacteria that colonised the fibre and its diameter, growth rate, and growth pattern. Bacterial load in the cove may also vary temporally, leading to variations in the rates of colonisation of the fibres. Sensors deployed at other marine sites may experience different rates of fouling, depending on the species and density of bacteria present in those environments. Indeed, considerable variability in biofilm colonies is expected in the marine environment (Lee et al., 2008).

4.5.3 Wavelength Shift and Comparison to SEM Images

Preliminary attempts were made to link wavelength shift to fractional coverage of the fibre by bacteria (Figure 4.6A). Unfortunately, given the variability in both LPG response and SEM images, it was not possible to draw a definitive link between these two variables. Biofilm thickness was not measured, but qualitatively, an examination of the higher magnification images revealed that fibres that were immersed longer had larger clumps of bacteria, rather than simply a few colonising bacteria as in the 4 h photo of Figure 4.5, and were also covered in what appeared to be extracellular

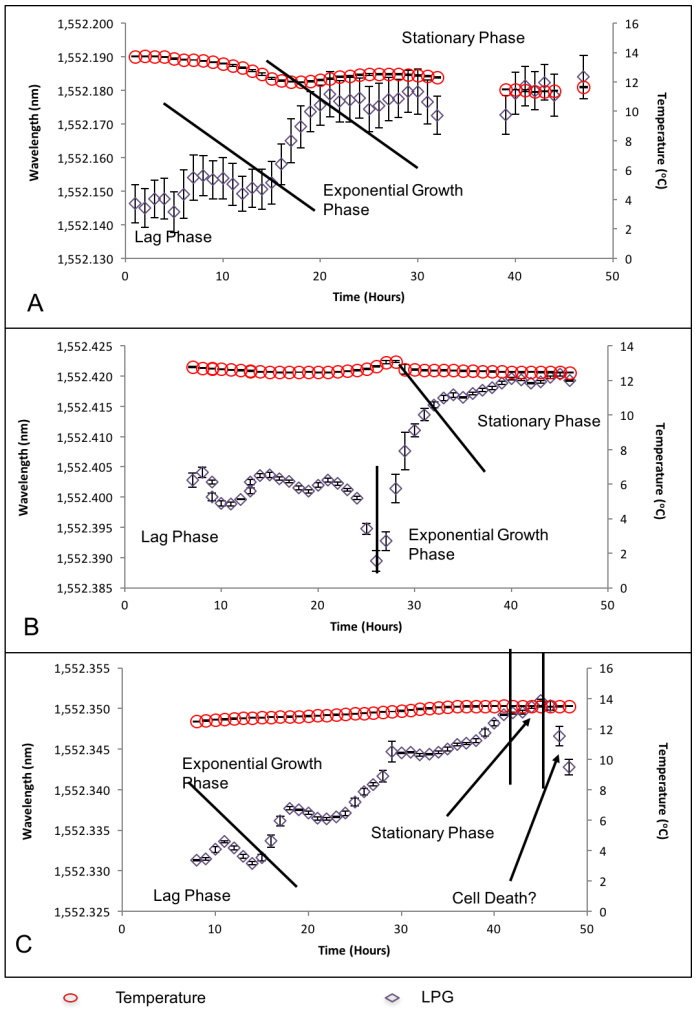

Figure 4.7: First 48 h of data for 3 trials (A: Trial 1 (August 2014), B: Trial 2 (April 2015), and C: Trial 3 (May 2015) of biofilm growth on LPGs exposed to seawater. Temperature data also shown. Error bars denote standard deviation, n = 7,200. Bacterial growth phases are labeled and delineated by black lines.

polysaccharide coating (see 44 h of Figure 4.5), a coating that is typically produced by more mature biofilms (Pavlovsky et al., 2013). These larger, thicker clumps could be what drove wavelength shift upward. There is evidence that coating thickness does

impact wavelength shift in LPGs, when refractive index of the coating is held constant (James and Tatam, 2003).

4.5.4 Future Work

More work is now needed to conduct longer-term field tests whereby the long-term effect of biofilm growth on sensor signal is characterised. Measurement of biofilm thickness should also be attempted, though this may be challenging due to the likely variability in biofilm thickness along the LPG. More work is also needed to test LPG response to biofouling at other marine sites. This study site may have had slightly higher bacterial loads than other marine sites due to septic runoff, and nutrient load may have also been higher due to reverine runoff. Therefore the effects of biofouling may occur more slowly at most other marine locations.

4.6 Conclusion

Long period grating sensors have the potential to revolutionise environmental monitoring, especially in hard-to-access marine monitoring sites. These fibre optic sensors are capable of multi-parameter sensing (James and Tatam, 2003), and they can transmit signals over long distances with minimal loss. Biofouling may be a challenge for sensor developers because biofilm colonisation of LPGs has the potential to cause upward signal drift, especially in environments with high bacterial loads. The sensitivity of LPGs to biofouling is also an opportunity for an automated biofilm sensor to be developed.

This study was a follow-up to laboratory tests conducted where a single-species biofilm was grown on an LPG immersed in synthetic seawater (Chapter 5). In these field trials, biofilm was grown on LPGs immersed in seawater. These trials corroborate laboratory experiments conducted using single species biofilms. The results revealed colonisation of the fibre by multi-species films. The three field trials conducted showed a similar trend to laboratory tests, with bacterial growth driving upward wavelength

shift within the first 48 h of exposure. This result combined with the laboratory tests provides strong evidence that bacterial growth is likely to generate an upward wavelength shift. Wavelength shift in response to biofouling was lower and biofouling occurred more slowly *in situ* than in the laboratory setting. Scanning Electron Microscope images revealed bacterial colonisation of the fibre within the first 4 h of immersion. No direct link could be drawn between fractional coverage of the fibre and sensor signal, due in part to considerable variability in coverage over time. It is hypothesised that thickness of the bacterial clumps may play a more significant role in wavelength shift than fractional coverage.

Chapter 5

Speciation in Application Environments for Dissolved Carbon Dioxide Sensors

5.1 Preamble

Sonja Bhatia and David Risk

This chapter forms the basis for an article that was published in the April 2015 issue of the Journal of Water, Air, and Soil Pollution. I completed all of the modelling work for this chapter and was the principal author. I also received guidance and input from Drs. David Risk (supervisor and co-author), Shannon Sterling (supervisor), Helmuth Thomas, Ernie Perkins, and Bernhard Mayer. Springer and the original publisher, Water, Air and Soil Pollution, Volume 223, 154, 2015, Speciation in Application Environments for Dissolved Carbon Dioxide Sensors, Sonja Bhatia and David Risk, is reproduced with kind permission from Springer Science and Business Media.

5.2 Abstract

Measurement of the concentration of dissolved carbon dioxide in ground and surface aqueous environments is needed for a wide variety of scientific and industrial applications. These environments can be fresh, saline, or transitional in nature and can be hydrochemically complex. A next generation of sensors, like fibre optic sensors, offer real-time, direct, distributed sensing of dissolved carbon dioxide and are an improvement over current technology for many applications; however, these sensors may be susceptible to signal disturbance when deployed in hydrochemically complex, natural environments, particularly as development improves sensor sensitivity. This hydrochemical complexity can best be characterised using hydrochemical modeling techniques. The modeling software, *Phreeqc 2.18*, was used to conduct a comprehensive

review to gain perspective on published data of natural water samples. Freshwater, saltwater and transitional environments were characterised in terms of the distribution of carbonate and non-carbonate species present. Saline, transitional and deep freshwater environments had the broadest range of carbonate distribution and species that may interfere with sensor response. These data should be used to build complex laboratory test solutions that mimic the natural environment for use in sensor development. In some cases, specially engineered membranes may be required to mitigate the potentially interfering effect of these ions.

5.3 Introduction

Measurement of the concentration of dissolved CO_2 in surface and subsurface aqueous environments can be challenging due to the complex chemistry surrounding dissolved inorganic carbon (DIC), of which dissolved CO_2 is a component. Nonetheless, dissolved CO_2 measurement is needed for a wide variety of industrial and scientific applications. For example, direct sensing of dissolved CO_2 is required for measurement, monitoring and verification of carbon capture, utilisation and storage activities (the injection of supercritical CO_2 into a confined subsurface environment). To be effective tools for this purpose, sensors that target dissolved CO_2 must be deployed in shallow groundwater, deep groundwater and marine environments depending on the location and nature of the carbon capture, utilisation and storage operation (Benson and Surles, 2006; Themann et al., 2009). Dissolved CO_2 sensors may be used to quantify the amount of CO_2 stored post-injection (Themann et al., 2009), and to detect leakage into the natural environment at the seafloor.

From a purely scientific standpoint, collection of DIC data is also useful. Dissolved CO_2 in particular, is necessary for global ocean research efforts, like the Global Ocean Flux Study and World Ocean Circulation Experiment (Dickson et al., 2007). Measurement of dissolved CO_2 is also necessary to monitor for ocean acidification (Doney et al., 2009). In lake environments, dissolved CO_2 measurement is important to understand carbon cycling in the lake ecosystem (Almeida et al., 2001). Sensors that can measure dissolved CO_2 are therefore critical for industrial operations and scientific advancement. Hydrochemical modeling to characterise the environments in which these sensors are to be deployed can assist with sensor design and interpretation of

sensor output.

5.3.1 CO_2, Dissolved Inorganic Carbon (DIC) and Naming Conventions

DIC is the term typically used to describe all carbonate species present in a water sample. Its solution chemistry is complex due to the range of species that it can encompass. The general reaction path for carbonate speciation in aqueous environments is well understood (Appelo and Postma, 2005). In general terms, DIC can be expressed by the following equations (Equations 5.1a, 5.2, 5.3, 5.4, and 5.5):

$$DIC = [H_2CO_3^*] + [HCO_3^-] + [CO_3^{2-}] \tag{5.1a}$$

$$[H_2CO_3^*] = [CO_{2(aq)}] + [H_2CO_3] \tag{5.1b}$$

The dominant carbonate species and pH are strongly correlated. The dissolution and speciation of DIC is defined by the following equilibrium equations taken from Appelo and Postma (2005):

$$H_2O \leftrightarrow H^+ + OH^- K_W = [H^+][OH^-] = 10^{-14.0}\, mol^2\, kg^{-2} \tag{5.2}$$

$$CO_{2(g)} + H_2O \leftrightarrow H_2CO_3^* K_H = [H_2CO_3^*]/[pCO_2] = 10^{-1.5}\, M\, atm^{-1} \tag{5.3}$$

$$H_2CO_3^* \leftrightarrow H^+ + HCO_3^- K_1 = [H^+][HCO_3^-]/[H_2CO_3^*] = 10^{-6.3}\, mol\, kg^{-1} \tag{5.4}$$

$$HCO_3^- \leftrightarrow H^+ + CO_3^{2-} K_2 = [H^+][CO_3^{2-}]/[HCO_3^-] = 10^{-10.3}\, mol\, kg^{-1} \tag{5.5}$$

Where * indicates that H_2CO_3 is shifting between carbonic acid and CO_2, and K represents equilibrium constants. K_H predicts the dissolution of CO_2 in water. K_1 predicts that at pH 6.3, the effective concentrations of CO_2 and HCO_3^- will be equal. K_2 predicts that at pH 10.3, the effective concentrations of bicarbonate ion and carbonate ion will be equal. If one considers the carbonate system, there are six interconnected parameters: pH, total alkalinity (referred to here as buffering capacity), DIC, dissolved CO_2, HCO_3^-, and CO_3^{2-}. The six parameters of the carbonate system can all influence one another. The composition of DIC can change with changing pH, shifting the solution to a different dominant species of either CO_2, HCO_3^-, or CO_3^{2-}. If the solution shifts towards HCO_3^-, or CO_3^{2-} from dissolved CO_2, the

buffering capacity of solution increases due the ability of those species to react with H^+, thus limiting a shift in pH with the addition of an acid. Since CO_2 dissociates to HCO_3^-, or CO_3^{2-} in higher pH solutions, increased uptake of CO_2 in a more buffered solution may therefore initially increase the buffering capacity rather than decrease the pH, despite the fact that the dissolution of CO_2 in small part forms carbonic acid. The presence of certain key dissolved ions can also result in more complex carbonate species. For example, the presence of Mg^{2+} in a higher pH environment could result in the formation of $MgCO_3$. These species would also be included in the calculation of DIC. Dissolved ions, pH, and buffering capacity all help determine the dominant DIC species.

A myriad of measurement techniques (discussed below) to account for DIC or dissolved CO_2 do exist, but they are typically limited to measurement of CO_2, or DIC only (in general terms, rather than a detailed examination of speciation). Such general DIC studies that measure or estimate DIC are common in the marine and limnological literature (Takahashi et al., 1981, 1970; Goyet et al., 1992; Striegl et al.; Wium-Andersen and Andersen, 1971; Bradshaw et al., 1981), but detailed characterization can only be achieved computationally.

This complex hydrochemistry and range of measurement techniques have resulted in several naming conventions for dissolved CO_2. For example, when pCO_2 is measured via equilibrated air, either the fugacity of CO_2 (fCO_2) or pCO_2 is used (Schuster et al., 2009). These two terms are considered essentially interchangeable for CO_2 since the measured partial pressure of CO_2 is very similar to the ideal partial pressure (Schuster et al., 2009). Equilibrated air methods focus primarily on the dissolved CO_2 component of DIC. Newer methods that measure dissolved CO_2 directly are now under development. For these sensors it seems the term dissolved CO_2 is most appropriate. When sensors directly measure total dissolved inorganic carbon, the short-form DIC is typically used (Lueker et al., 2000). The focus of this manuscript is primarily on applications for sensors that can directly sense dissolved CO_2 and therefore this convention will be used throughout the paper, unless other terminology is required for accuracy.

5.3.2 Current Technology in Dissolved Inorganic Carbon (DIC) Measurement

Current technology can measure dissolved CO_2 or DIC in one of two ways: (1) DIC or dissolved CO_2 is measured directly in solution (Schuster et al., 2009); or (2) the quantity of dissolved CO_2 in a water body is calculated by measuring the equilibrated partial pressure of CO_2 (pCO_2). The mole fraction of CO_2 in air that is at equilibrium with the water sample multiplied by the total pressure (p) is equal to pCO_2 (Schuster et al., 2009; Equation 5.6). The dissolution of $CO_{(g)}$ in water is described by equation 1.3; the relationship between the pCO_2 in air and the mole fraction of pCO_2 in water. The equation reads:

$$pCO_2 = xCO_2 * p \tag{5.6}$$

To calculate DIC, pH may need to be lowered to shift all DIC species to CO_2. There are other indirect methods to calculate DIC via pH sensitive solutions or coatings and/or total buffering capacity, but they will not be discussed here.

5.3.2.1 Direct Measurement of CO_2

Direct measurement of dissolved CO_2 or DIC in a water sample can occur by coulometry, spectrophotometry, or non-dispersive infrared spectroscopy (NDIR). Coulometry refers to the acidification of a known quantity of CO_2 via reaction in solution where it reacts to form a strong acid. This acid can be titrated coulometrically, whereby a strong base is generated electrochemically (Johnson et al., 1998). Of the direct measurement techniques, coulometry can achieve the highest degree of accuracy and precision, if proper procedures are followed (Schuster et al., 2009).

There are, however, some challenges associated with the technique. Most notably, the analysis requires the use of hazardous chemicals that require replenishment and extensive chemical conditioning, preventing continuous measurement (Schuster et al., 2009); however, Non-dispersive infrared spectroscopy, on the other hand, employs acidification to release the CO_2 from the water sample (Friedrichs et al., 2010) and relies on CO_2 molecules' absorption of infrared radiation (Schuster et al., 2009).

Spectrophotometric instruments can be used to measure the pCO_2 and DIC. Spectrophotometric instruments require power at the sensing site, but are capable of high frequency, long-term measurement (Liu et al., 2013). Automated devices have been tested successfully *in situ* and show resistance to signal drift from biofouling and turbidity (Liu et al., 2013). Non-dispersive infrared spectroscopy can also be easily automated, deployed on buoys and moorings, though the large size of the instrumentation means that it is typically deployed on research vessels. With careful temperature control NDIR is subject to minimal signal drift (Pierrot et al., 2009). Non-dispersive infrared spectroscopy also has several major disadvantages, including, the large size of the instrument and susceptibility to biofouling (Schuster et al., 2009), though new miniature instruments are now becoming available commercially (Graziani et al., 2014).

Unfortunately, all of these direct measurement techniques can only provide general measurement of DIC or dissolved CO_2 and cannot provide a lot of insight into carbonate speciation without some type of concurrent pH or buffering capacity measurement. Without parallel measurement of both DIC and dissolved CO_2 or one of the two aforementioned parameters and buffering capacity or pH. Dissolved inorganic carbon cannot be ascertained from a pCO_2 measurement and vice versa. Further modeling is required to ascertain the dominant dissolved species, whether that be HCO_3^- or $NaHCO_3$, for example.

5.3.2.2 Measurement by Equilibration of Dissolved CO_2

Sensors that require equilibration of CO_2 with the water sample to calculate pCO_2 typically employ either gas chromatography (GC), NDIR, or spectrophotometry (Schuster et al., 2009). Different equilibration techniques are used depending on the sampling platform available and the sample type. These equilibration techniques determine the type of sensor used to take the measurement of pCO_2. Both GC and NDIR measure the mole fraction of CO_2 in air equilibrated with the water sample. GC requires that CO_2 is catalytically converted to CH_4, which is then measured via flame ionization detection (Weiss, 1981; Weiss et al., 1992; Dickson et al., 2007). Gas chromatography is advantageous because only a small air sample is required for accurate measurement and it is sensitive to a broad range of xCO_2 values (Schuster

et al., 2009). Non-dispersive infrared spectroscopy, described above can also be used in air-equilibration-type systems and can provide highly accurate and precise data; however, there is also a risk of sample contamination because samples need to be vented to maintain ambient pressure (Schuster et al., 2009). Unlike GC and NDIR, spectrophotometry typically uses a pH-sensitive indicator solution (Xie and Bakker, 2013). Carbon dioxide is equilibrated across a membrane with the water sample. The pH of the solution is dependent on the CO_2 content, and when coupled with alkalinity measurement, the dye is able to indicate the CO_2 content (Xie and Bakker, 2013). Long-term drift is a concern with indicator dye systems because the dye fades over-time though mitigation techniques do exist. Accuracy of indicator-type systems has been shown to be lower than for air-equilibration systems (Körtzinger et al., 1999).

5.3.3 Fibre Optic Sensors

A next generation of fibre optic sensors may provide a cost-effective, distributed option to sense dissolved CO_2. For example, a fibre optic sensor field tested by Goyet et al. (1992) makes use of fluorescent dyes to detect pCO_2. Orghici et al. (2008) also conducted laboratory testing on an evanescent field dCO_2 sensor whereby the fibre's cladding is removed, allowing for interaction between light and the surrounding medium, which can be seen in the form of an evanescent field (Orghici et al., 2008). The sensor makes use of the evanescent field that is produced along side the fibre, and the principal of spectroscopy. If the surrounding medium is absorbent for the wavelength of the evanescent field, then a change in the intensity of the transmitted wavelength is detected (Orghici et al., 2008). Conversely, if the surrounding medium is non-absorbent, no change in intensity is detected (Orghici et al., 2008). Different chemical species are likely to have different signature wavelengths, giving this sensor the potential to distinguish different carbonate species, though intensive calibration would be required, and may prove to be too challenging in hydrochemically complex environments.

A fibre optic sensor under development by Bao et al. (2013) also has the potential to detect DIC or simply dissolved CO_2 in real-time. The sensor could be deployed in distributed networks over areas greater than 1 km^2 and is thus an improvement over current technology for many applications. The sensor employs long period gratings

written into standard, single mode fibre. The signal of a Long Period Grating Fibre Optic Sensor (LPG) undergoes a wavelength shift in response to change in the refractive of the surrounding medium. For a complete description of the operating principle of LPGs, please refer to Section 1.1.6. In one experiment, Bao et al. (2013) diffused CO_2 into a brine solution up to the point of saturation to show the wavelength shift as brine became saturated by supercritical CO_2 due to the different refractive indices of the two substances (Bao et al., 2013). Although Bao et al. (2013)'s work focused on high pressure environments, a similar approach using LPGs could be deployed at atmospheric pressure (Bao et al., 2013), though the concentration of CO_2 dissolved in solution would be lower at this pressure, and may be below the detection limits for the sensor. Indeed, further development to allow for deployment in low pressure environments is ongoing. Though resolution is still coarse, the promise this technology shows for economical, distributed deployment warrants continued development.

Despite success in binary solution, Bao et al. (2013) have yet to test and LPG in more complex aqueous solutions that mimic the *in situ* environment (Bao et al., 2013). Sensor signal could be altered by potentially complex solution chemistry. Depending on pH, salinity, and buffering capacity, DIC encompasses a number of different carbonate species that may have different refractive indices and therefore induce different shifts in the attenuation bands in the transmitted spectrum. In their laboratory experiments, Bao et al. (2013), estimated that 99.87 % of DIC was in the form of CO_2, given the measured pH of 3.0 of the CO_2 saturated solution (Bao et al., 2013). As a result, the sensor signal would have been almost solely driven by CO_2. The authors calculated that the refractive index of the CO_2 saturated brine solution was 1.3163 (Bao et al., 2013).

In situ, however, differences in pH or buffering capacity could cause carbonate species with different refractive indices to be more dominant than dissolved CO_2. These differences in refractive index would cause wavelength shift of an LPG to be different from the laboratory test case. This could prove problematic for the interpretation of sensor response in some circumstances. For example, one potential application for fibre optic dissolved CO_2 sensors is MMV of geologic sequestration sites for dissolved CO_2. In a highly buffered environment, initial leakage of dissolved CO_2 will equilibrate rapidly with carbonate or bicarbonate ion. Since the wavelength

shift of the LPG may appear to be different from the laboratory test case in this scenario, it is possible that a small CO_2 leak could go unnoticed. Conversely, in environmental monitoring applications, where a distinction between background levels of dissolved CO_2 and other carbonate species is valuable, the potential of a fibre optic sensor to distinguish between different carbonate species could be considered to be a major technological advancement. Commercially available technology is not able to make this type of distinction; instrumentation is limited to measurement of dissolved CO_2 or DIC as a whole.

The presence of non-carbonate species or non-target carbonate species could also interfere with sensor response by mimicking a signal one might expect to see if dissolved CO_2 were present in high concentrations. For example, a single dominant non-carbonate species, non-target carbonate species, or combination of species could form a solution with a refractive index similar to the refractive index of brine saturated with dissolved CO_2 as suggested by the laboratory test solution used by Bao et al. (2013). Such a solution could therefore generate an attenuation spectrum that resembles the laboratory test solution, causing dissolved CO_2 to be detected by the sensor, although little or no dissolved CO_2 is present. Detailed characterization of the complex solution chemistry, broken out in terms of carbonate and non-carbonate species, is required to move beyond the binary solutions used thus far as part of laboratory testing by Bao et al. (2013). Identifying and characterizing responses to these species will allow for testing to develop methodologies and procedures to calibrate for variations in chemical composition *in situ*.

5.3.4 Objectives

There is a broad range of hydrochemical literature that generally provides pH, temperature, buffering capacity and key dissolved ions (e.g., SO_4, Mg^{2+}, Ca^{2+}, K^+, F^-, Cl^-, Na^+) (Table 5.1). The objectives of this study are to use data provided in these studies (Table 5.1) to undertake hydrochemical modeling using *Phreeqc 2.18*, a hydrochemical modeling software, to characterise a variety of ground and surface water (fresh, saline and transitional) environments in terms of their carbonate and non-carbonate hydrochemistry by doing the following: (1) undertaking a broad and

multi-dimensional literature review to define mean concentrations of DIC, pH and total buffering capacity across application environments to give context to the modeling work; (2) highlighting the mean molarity of dissolved CO_2 across possible application environments; (3) modeling the distribution of other carbonate species across application environments and (4) characterizing non-carbonate species likely to be present across these application environments.

5.4 Methods

The hydrochemical modeling software package, *Phreeqc 2.18* is commonly used to make speciation calculations (Bäckström et al., 2003). It is freely available from the United States Geological Survey (www.brr.cr.usgs.gov/projects/GWC/coupled/phreeqc/?). The software package was used to characterise freshwater, saltwater and transitional environments in the surface and subsurface in terms of carbonate speciation and species that may interfere with sensors response (Table 5.1). The accuracy of most commercially available sensors is $3.40X10^{-8}$ mol kg $^{-}$ CO_2. Given that this level of accuracy is presumed to be the target for fibre optic sensors under development, other species present in concentrations above this threshold were assumed to have the potential to interfere with sensor response.

Hydrochemical data containing basic information on how dissolved ions, pH, temperature and buffering capacity were compiled from the literature. Typically these studies did not investigate DIC in detail. The data from these studies were selected based on the following criteria: similarity of the measured environment to potential application setting for DIC sensors; completeness of the published data (pH, temperature, buffering capacity); and percentage charge balance error ([Σ cations - $|\Sigma$ anions$|$]\[Σ cations + $|\Sigma$ anions$|$]) below 10 %. This charge balance threshold is higher than the 5 % that is typical of hydrochemical studies; however, the purpose of this study is to estimate the hydrochemistry of a broad range of application environments. Setting a higher charge-balance cutoff allowed for a greater range of application environments and greater variety of samples within application environments.

Over 200 samples from nineteen different application environments were selected. Data from these environments were entered into *Phreeqc 2.18* as a single input file

Table 5.1: Modeled Application Environments (n represents sample size)

		Environment
Freshwater	Surface	Great Lakes (n=3; Cowell and Ford, 1980)
		Alpine lake (n=5; Mosello, 1984)
		Eutrophic lake (n=2; Papatheodorou et al., 2006)
		Glacial outflow (n=1; Puckett et al., 2002)
		Antarctic lake (sub-glacial) (n=2; Siegert et al., 2003)
		River (n= 8; Smart et al., 1998)
	Subsurface	Formation water (n=14; Birkle and Aragon, 2002)
		Hydrothermal vents (n=40; Dotsika et al., 2009)
		Fresh Quaternary zone (n=4; Hidalgo and Cruz-Sanjulián, 2001)
		Deep confined zone (n=5; Hidalgo and Cruz-Sanjulián, 2001)
		Shallow confined zone (n=3) Hidalgo and Cruz-Sanjulián, 2001)
		Shallow Unconfined zone (n=11; Hidalgo and Cruz-Sanjulián, 2001)
		Wetland Porewater (n=11; Puckett et al., 2002)
Trans		Freshwater intruded by Dead Sea saltwater (n=32; Abu-Jaber and Wafa, 1996)
		Freshwater intruded by seawater (n=14; Kim et al., 2003)
Salt	Surface	Estuary (n=9; Carol and Kruse, 2012)
		Saltmarsh (n=9; Carol and Kruse, 2012)
		The Dead Sea (n=11; Abu-Jaber and Wafa, 1996)
		Saltwater Lake Van (n=3; Reimer et al., 2008)
		Marine Average (n= 8; Bruland and Lohan, 2006)

(Table 5.1 lists sources of data used in *Phreeqc 2.18* calculations). The thermodynamic database, *Phreeqc.dat*, was considered to be the best suited database for this study; it provided sufficient data on the species of interest.

The software used the thermodynamic and input data to solve a series of non-linear mole-balance and mass-action equations that define an ion-association model (Parkhurst and Appelo, 1999; e.g., Equation 5.7). The software rewrote these mass-action equations in terms of predefined master species (for a complete list refer to Parkhurst and Appelo (1999)) whose concentrations were unknown, and iteratively solved these equations until the number of master unknowns was reduced to zero. Equation 5.7 provides an example of a mass-action equation used by the modelling software:

$$K_i = a_i \prod_{m}^{Maq} {a_m}^{-C_{m,i}} \tag{5.7}$$

"where K_i is a temperature-dependent equilibrium constant, $C_{m,i}$ is the stoichiometric coefficient of master species m in species i and M_{aq} is the total number of aqueous master species. The values of $C_{m,i}$ may be positive or negative" (Parkhurst and Appelo, 1996). The generated output provided total buffering capacity (the sum of all bases titratable by a strong acid; effectively a measure of the buffering capacity of solution), the molarity of all species calculated to be present and the percent charge balance error.

Carbonate speciation output data were compared across different application environments and categorised as follows: (1) low pH and very poorly buffered (pH and mean total buffering capacity less than 4.5 and 1.00X10^{-4} mol kg^{-1} respectively); (2) low-moderate pH and poorly buffered (pH from 5.5-7.5 and mean total buffering capacity from 1.00X10^{-4} to 9.99X10^{-4} mol kg^{-1}; (3a) low-moderate pH and low-moderate buffering capacity (pH from 5.5-8.4 and mean total buffering capacity from 1.00X10^{-3} to 4.99X10^{-3} mol kg^{-1}); (3b) low-moderate pH and moderate buffering capacity (pH from 5.0-8.4 and mean total buffering capacity from 5.00X10^{-3} to 9.99X10^{-3} mol kg^{-1}); and (4) high pH and highly buffered (pH greater than 9.5 and mean total buffering capacity greater than 1.00X10^{-1} mol kg^{-1}). The majority of application environments fell into Category (3) and so it was broken into (3a) and 3(b) for more detailed examination. The output data were categorised in this manner because pH and buffering capacity can act as predictors of carbonate speciation in many contexts. Regression analyses were also performed on modeling outputs to show how the model used predefined relationships between predictor variables, like pH, buffering capacity and temperature to define carbonate speciation across application environments. These same analyses were completed for non-carbonate species present in molarities greater than 3.40X10^{-8}, as well. Variables that may also contribute to speciation like salinity were not inputted directly, though key dissolved ions were included in the input file.

5.5 Results

5.5.1 Dissolved Inorganic Carbon (DIC), pH and Buffering

The general categories (described in detail in the methods) provided some insights into speciation discussed in the following sections, but estimated mean molarity of DIC could not always be predicted by pH or even buffering capacity. The application environments that fell into each category, as well as the DIC results for each environment are presented in this section to set the scene for more detailed examination of carbonate and non-carbonate speciation in later sections.

Only freshwater environments (both groundwater and surface water) fell into the first two categories (Figure 5.1). The only environment that fell into Category (1), low pH and very poorly buffered, was the alpine lake environment; a fresh, surface water environment. Despite having low pH and being very poorly buffered, mean DIC was categorised as moderate, with a mean value of $1.89\text{X}10^{-3} \pm 3.00\text{X}10^{-6}$ mol kg^{-1} (Figure 5.1). Only two environments fell into Category (2), low-moderate pH and poor buffering capacity: (1) the river; and (2) groundwater in the volcanics zone. Not all environments in this category had low DIC. The river environment had relatively low mean DIC, with a mean molarity of $4.38 \text{ X } 10^{-4} \pm 4.83\text{X}10^{-5}$ mol kg^{-1} (Figure 5.1). The volcanic groundwater environments had mean DIC, in the moderate to high range, $1.09\text{X}10^{-3} \pm 6.35\text{X}10^{-5}$ mol kg^{-1}.

Categories (3a and b) had a mix of saline, transitional and freshwater environments. These two categories had the broadest range of pH and the narrowest range of buffering capacity (Figure 5.1). The majority of environments fell into Category (3a), low-moderate pH and low-moderate buffering capacity: all freshwater aquifers, except the quaternary zone; the marine average; the salt marsh; and the remaining fresh, surface water environments (the eutrophic lake, sub-glacial Antarctic lake, glacial outflow, and the Great Lake) (Figure 5.1). The mean molarity of DIC was also low-moderate for all but two environments in this category, ranging from $1.96\text{X}10^{-3} \pm 2.76\text{X}10^{-5}$ to $4.67\text{X}10^{-3} \pm 1.55\text{X}10^{-4}$ mol kg^{-1} (Figure 5.1). The two exceptions were the deep confined freshwater aquifer and the Antarctic lake, which had mean DIC molarities of $3.82\text{X}10^{-3} \pm 1.66\text{X}10^{-4}$ and $1.79\text{X}10^{-2}$ mol kg^{-1}, respectively (Figure 5.1). Category (3b) contained the remaining transitional environments (thermal

Category 1	Category 2	Category 3a	Category 3b	Category 4
Alpine Lake (4.67)	Scotish Uplands River (6.89)	Subglacial Antarctic Lake (5.60)	Dead Sea (5.50)	Salt Water Lake Van (9.83)
	GW-Volcanics (7.26)	FW Aquifer Deep Confined Zone (7.42)	GW-Formation Water (5.90)	
		FW Aquifer Shallow Unconfined Zn (7.67)	GW-Thermal Fluids (6.91)	
		FW Aquifer Shallow Confined Zone (7.73)	GW-Wetland (7.25)	
		Eutrophic Lake (7.89)	FW Aquifer Quaternary Zn (7.45)	
		Glacial Outflow (7.90)	GW-Freshwater Intruded by Salt Water (7.73)	
		Salt Marsh (7.98)	Estuary (8.09)	
		Marine Average (8.00)		
		Great Lake (8.41)		

	DIC $<1.00X10^{-4}$
	$1.00X10^{-4}$<DIC<$4.99X10^{-3}$
	$5.00X10^{-3}$<DIC<$9.99X10^{-3}$
	DIC $>1.00X10^{-2}$

Figure 5.1: Categorisation of environments by buffering capacity and pH. Values for pH are provided in brackets.

subsurface fluids, freshwater groundwater intruded by saltwater and an estuary), the remaining fresh groundwater environments (the wetland, the deep formation water environment and quaternary aquifer), and one saline environment (the Dead Sea). All environments had moderate mean DIC (ranging from $6.44X10^{-3} \pm 1.28X10^{-4}$ to $9.86X10^{-3} \pm 6.14X10^{-4}$ mol kg^{-1}), with the exception of thermal fluids which had a mean DIC molarity of $1.14X10^{-2} \pm 1.86C10^{-3}$ mol kg^{-1} (Figure 5.1). Only the inland saltwater lake fell into Category (4), with a high pH and buffering capacity. Mean DIC was $9.11X10^{-2} \pm 6.80X10^{-4}$ mol kg^{-1} (Figure 5.1).

5.5.2 Dissolved CO_2

Some key general observations could be made from the modeling output with respect to the relative importance of dissolved CO_2. The only application environment in Category (1), the alpine lake environment, CO_2 dominant, with almost 100 % of DIC being dissolved CO_2 (Figure 5.2). The relative important of dissolved CO_2 decreased in Category (2), wherein dissolved CO_2 only made up between 18 and 29 % of DIC. In Category (3a) dissolved CO_2 was of decreasing importance, with only the subglacial lake (which had a pH of 5.6) still being CO_2 dominant at 89.72 % of DIC. In Category (3b) dissolved CO_2 was not dominant in any environment, though it was still present in significant quantities in thermal subsurface fluids (pH 6.9) and the wetland (pH 7.3), where it consisted of 41.36 and 17.78 % of DIC, respectively (Figure 5.2). Despite a low pH (5.5) the Dead Sea had 0 % of its DIC as dissolved CO_2. Dissolved CO_2 fell to 0.01 % in Category (4), where the mean pH was 9.8 ± 0.1 and buffering capacity was $1.57X10^{-1} \pm 2.52X10^{-3}$ mol kg^{-1}.

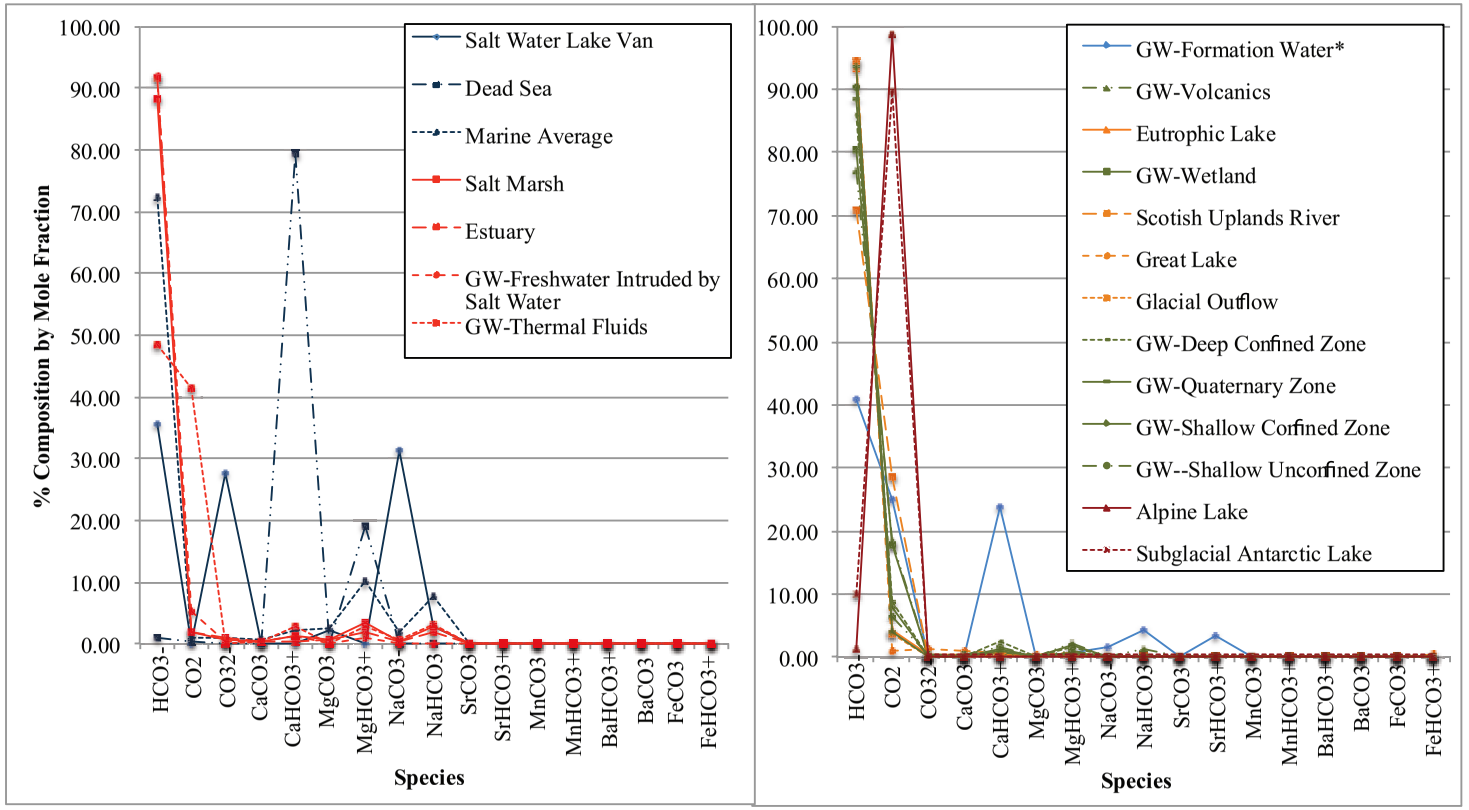

Figure 5.2: Percent distribution of carbonate species across freshwater (right), saltwater, and transitional environments (left).

Looking in more detail at mean molarities of dissolved CO_2, Category (1) had a mean molarity of dissolved CO_2 that was moderate compared to other categories, with a value of $1.86X10^{-3}$ ± 3.40 $X10^{-4}$ mol kg^{-1}. Relative to other environments in Category (2), mean molarity of dissolved CO_2 was highest in the formation water environment with a mean molarity of $1.77X10^{-3} \pm 3.61X10^{-3}$ mol kg^{-1}. This category could be characterised as moderate relative to environments in other categories. The river environment and volcanics environment had more similar values for dissolved CO_2, which ranged from 1.25 to 2.00 X $10^{-4} \pm 2.58$ to 3.42 X 10^{-4} mol kg^{-1} (Figure 5.3). These values could be categorised as low relative to other categories. With the exception of the subglacial lake and wetlands environment, Category (3a) also had relatively low mean molarities of dissolved CO_2, ranging from $2.00X10^{-5} \pm 2.91X10^{-4}$ to $3.33X10^{-4} \pm 7.00X10^{-6}$ to $2.22X10^{-4}$ mol kg^{-1} (Figure 5.3). The subglacial lake had a mean molarity of $1.61X10^{-2} \pm 1.88X10^{-2}$ and $5.17X10^{-3} \pm 1.05X10^{-3}$ mol kg^{-1} respectively. Category (3b) had relatively low values of dissolved CO_2 ranging from $2.80X10^{-5} \pm 1.00X10^{-5}$ to $4.71X10^{-3} \pm 9.31X10^{-3}$ mol kg^{-1} (Figure 5.3). In Category (4), the inland saltwater lake, dissolved CO_2 was very low, with a mean molarity of $8.00X10^{-6} \pm 3.00X10^{-6}$ mol kg^{-1} (Figure 5.3). Regression analysis on modeling output showed that the model considered pH had a statistically significant influence on dissolved CO_2.

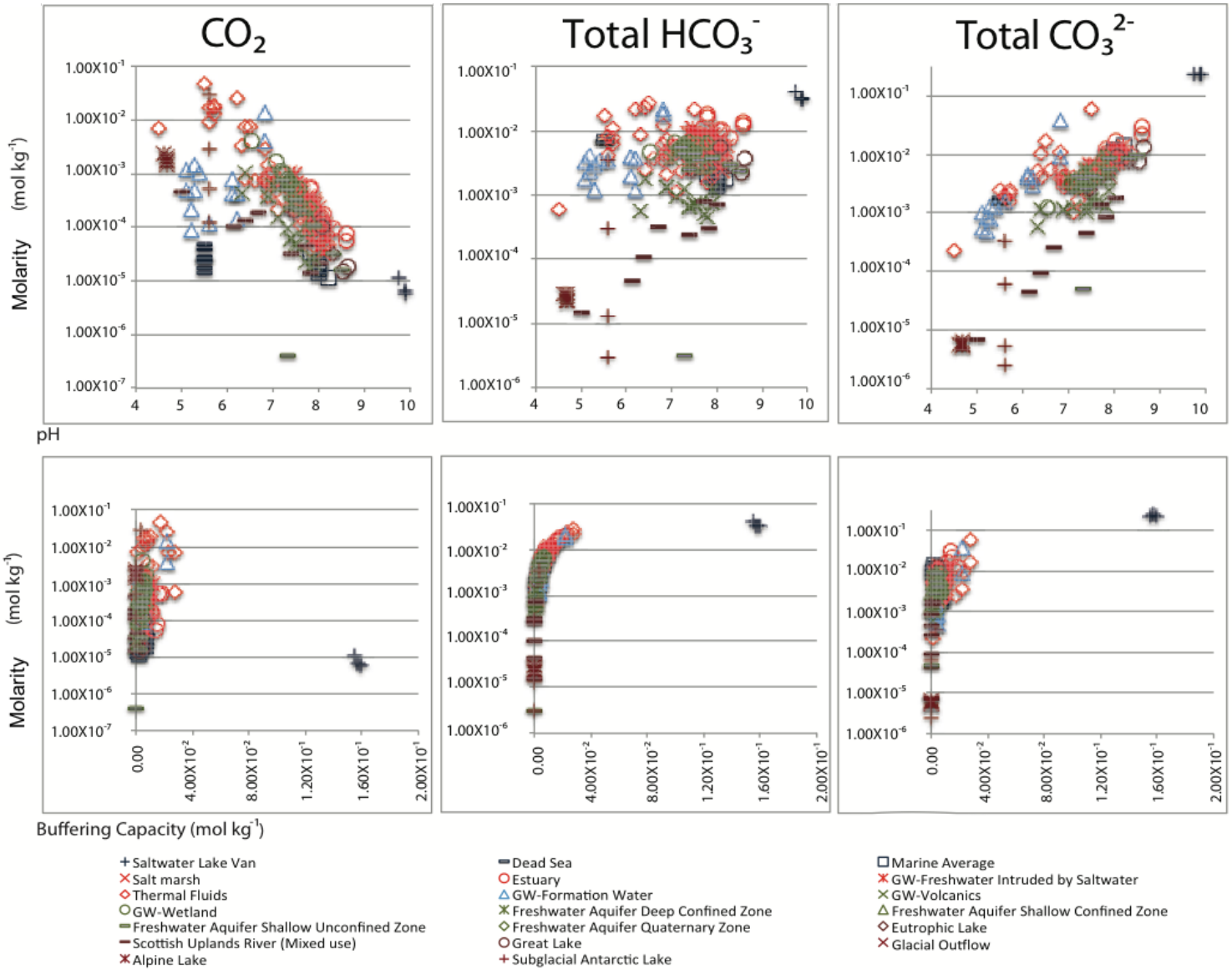

Figure 5.3: Distribution of CO_2, total HCO_3^-, and total CO_3^{2-} across Freshwater, Saltwater, and Transitional environments. Where buffering capacity denotes total alkalinity.

5.5.3 Distribution of Other DIC species

This section examines the relative distribution of total HCO_3^- and CO_3^{2-} (other DIC species) across application categories. Category (1) had close to 0 % other DIC species. Environments within Category (2) varied in their distribution of DIC species. The deep formation water environment had the highest distribution of DIC, with complex carbonate species present in quantities above 5 % of DIC (e.g., $CaHCO_3^+$; Figure 5.2). Nonetheless, all three environments had greater than 60 % total mean HCO_3^-, with less than 1 % CO_3^{2-}, as a percentage of DIC. Bicarbonate ion typically dominated Category (3a) environments, where concentrations of this species as a percentage of DIC were higher than in Category (2) environments, ranging from 72.5 % to 94.8 %, with the exception of the subglacial lake (Figure 5.2). Category (3a) environments generally had even higher concentration of HCO_3^- as percentage of DIC than Category (2) environments. Carbonate ion was still of little importance in this category, with no environment having above 1.3 % CO_3^{2-} (Figure 5.2). Only the marine average had a broad distribution of species, due to the prevalence of complex carbonate species present in percentages greater than 5 % (e.g., $MgHCO_3^+$; Figure 5.2). Category (3b) was also dominated by HCO_3^- species, with total HCO_3^- as a percentage of DIC ranging from 57.61 % to 99.59 % (Figure 5.2). Bicarbonate ion was below 5 % of DIC in all Category 3(b) environments (Figure 5.2). Several environments in this category had a greater distribution of complex carbonate species. The Dead Sea, for example had 79.3 % $CaHCO_3^+$. The only environment to fall into Category (4), the inland saltwater lake, had the most total carbonate as a percentage of DIC of any environment, 61.3 %. This environment also had a high distribution of complex carbonate species. For example, $NaCO_3^-$ was at 31.3 % of DIC.

Regression analysis on modeling output showed that the naturally occurring range of temperatures did not have a statistically significant influence on carbonate speciation in any environment. According to the regression analysis, both pH and buffering capacity had an influence on modeling outputs of carbonate speciation, though the natural variability in pH was much higher and therefore natural distribution of pH had stronger influence on modeled carbonate speciation than buffering capacity. Modeling outputs showed that pH had a statistically significant influence on HCO_3^-, CO_3^{2-}, $MgCO_3$, $NaCO_3^-$, $NaHCO_3$, but not on $CaCO_3$, $CaHCO_3$, or $MgHCO_3^+$. Figure 5.3

shows the mean concentration of total HCO_3^- and CO_3^{2-} by pH and buffering capacity.

5.5.4 Distribution of Non-Carbonate Species

Non-carbonate data were not categorised by pH and buffering capacity in the same way as carbonate species. Instead, freshwater, transitional, and saline environments were considered. The dominant non-carbonate species across application environments included: NaOH, KSO_4^-, Ca^{2+}, Mg^{2+}, SO_4^{2-}, $CaSO_4$,and $MgSO_4$ (Figure 5.4). The highest mean molarities of dissolved non-carbonate species occurred in saltwater environments (with the mean molarity of at least three species in each environment present in quantities greater than 1.00 mol kg^{-1}) (Figure 5.4). Transitional environments were more dilute, and though they showed a similar distribution of species, mean molarity of most species was not above 1.00 mol kg^{-1}, with the exception of thermal fluids. Deep groundwater showed a greater distribution of species at higher mean molarities than transitional environments. As expected, most other freshwater environments showed a similar distribution of species, though these species were typically present in mean molarities below $1.00X10^{-6}$. One notable exception to this general trend in freshwater environments was subglacial Lake Vostok, which had a similar distribution of species to other freshwater environments, but a higher mean concentration between $1.00X10^{-4}$ and $1.00X10^{-2}$ mol kg^{-1} of sulfate-rich, potassium-rich, and sodium-rich compounds (Figure 5.4).

5.6 Discussion

5.6.1 Dissolved CO_2

Dissolved CO_2 was dominant in the lowest two categories that were comprised only of fresh, surface water environments; an unsurprising result given the low pH and buffering capacity in these environments. Many fresh, surface water environments were poorly buffered since there would not be significant dissolution of rock or calcium carbonate reefs. Buffering capacity in some lakes has also been reduced as a result of acid rain (Schindler, 1988; Jeffries et al., 2003). The type of bedrock may have also contributed to buffering capacity. The contribution of anaerobic degradation

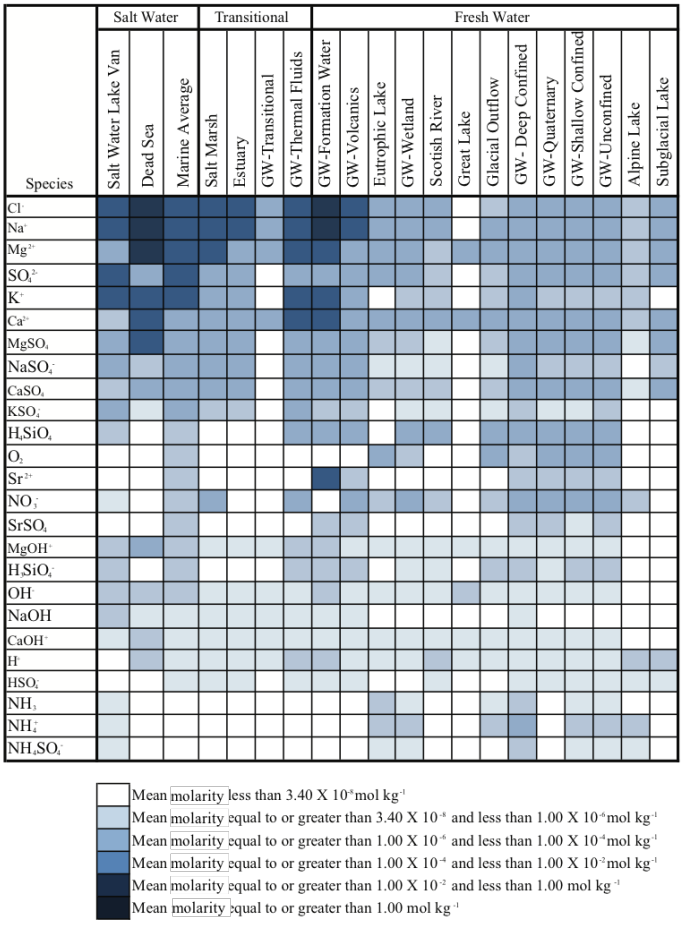

Figure 5.4: Range of mean distribution of non-carbonate species. Only species present in at least 30 percent and in molarities over 3.41 X 10^{-8} mol kg^{-1} of environments displayed. See legend for concentration ranges.

processes to buffering capacity may not be as common in these lakes as in other freshwater (Schindler, 1986), marine (Thomas et al., 2009), or terrestrial environments (Schindler, 1986), though weathering may still have an influence.

The decreasing dominance of dissolved CO_2 was also expected as pH and buffering capacity increased. Of note in Category (3b) was the thermal fluids environment, where dissolved CO_2 continued to be an important part of DIC. Expected seepage of CO_2 beneath the surface, supported by the moderately low pH (6.9) is the likely explanation for this observation (Dotsika et al., 2009). The wetland environment also had notable percent concentration of dissolved CO_2, though the mean pH was considerably higher and close to other values in this category. The continued presence of dissolved CO_2 could be due to a denitrification process occurring in the wetland described by Puckett et al. (2002) whereby CH_2O and $NO_2{}^-$ are reduced to CO_2 and N_2, respectively, through a microbially mediated process (Puckett et al., 2002).

Also interesting is the observation that despite a low pH of 5.5, the Dead Sea had less than 1 % dissolved CO_2 as a percentage of DIC. Buffering capacity of the Dead Sea was the highest, however, in that category, so perhaps a higher number of dissolved ions created complex carbonate species that were not as able to shift to dissolved CO_2 despite the low pH. The lack of relationship between pH and carbonate speciation in this case may be explained at least in part by Stumm and Morgan (1996), who describe a complex relationship where the presence of Mg^{2+} can interfere with the $CaCO_3$ reaction, thus limiting the influence of pH (Stumm and Morgan, 1996).

Understanding the relative abundance and mean concentrations of dissolved CO_2 across application environments will allows sensor developers to set target resolutions for their intended application, select test environments, and develop laboratory test solutions that mimic their intended application environment. For example, in the early phases, when resolution of a new technology may be low, sensor developers may wish to test their sensor in fresh, surface water environments that are poorly buffered, with a low pH, so any controlled release of CO_2 is likely to remain as CO_2 (Figure 5.5). As development matures, other test environments may become more important.

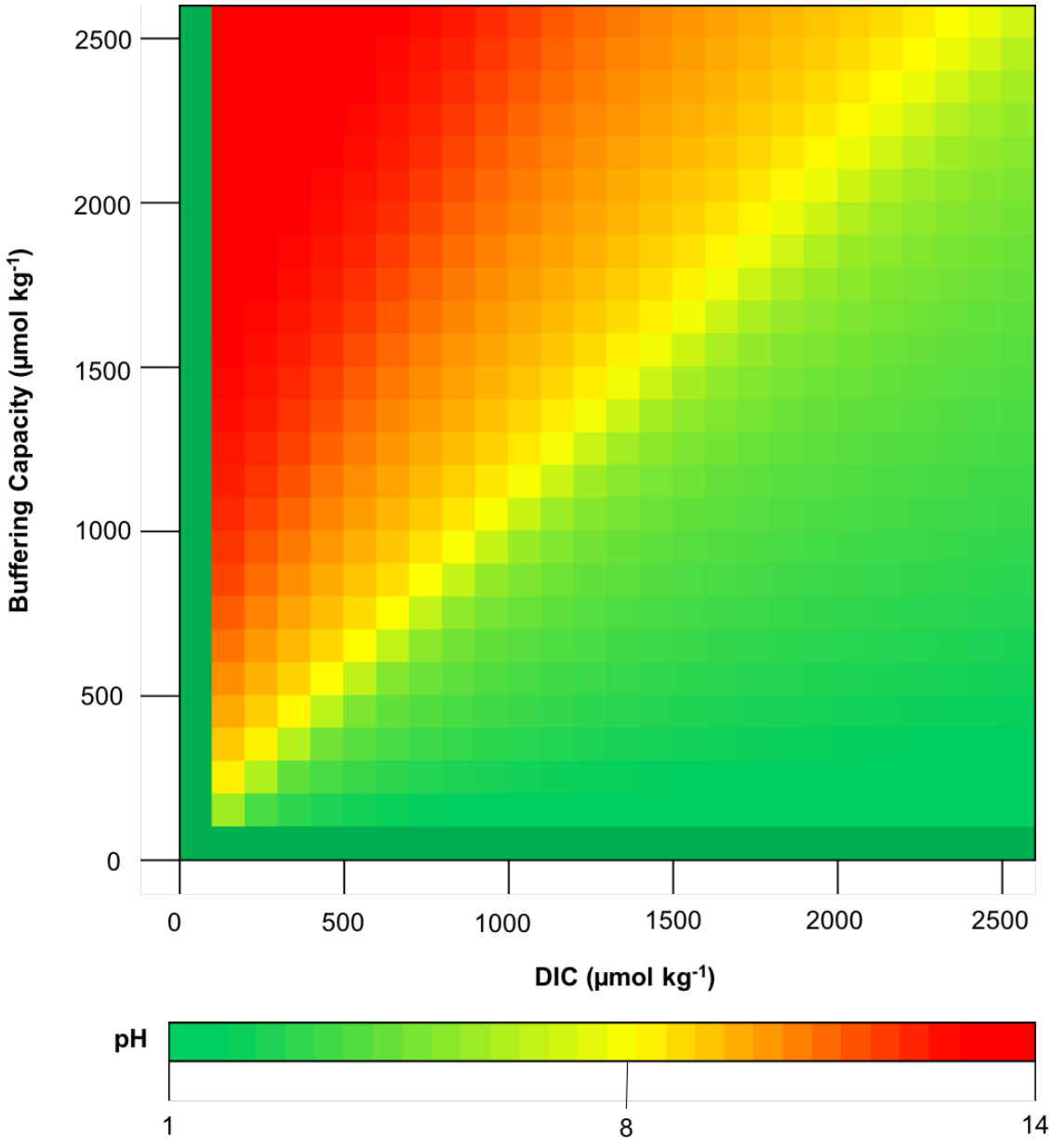

Figure 5.5: Interrelationship of DIC, pH and total alkalinity (buffering capacity).

5.6.2 Distribution of other DIC Species with the Potential to Interfere with Sensor Response

The increasing importance of other DIC species as one moves up the categories is unsurprising given the increase in pH that also occurs (Figure 6). Potentially of interest are the environments within the different categories that, despite similar pH and buffering conditions, were estimated to have a greater distribution of other DIC species than other environments in their category. These species may trigger a different sensor response than less complex DIC species. In the case of fibre optic sensors, for example, $MgHCO_3^+$ may have a different refractive index than HCO_3^-, so pH and buffering capacity alone may be insufficient to predict sensor response. In Category (3b), formation water had increased complexity of DIC species than the other environments in that category. Formation water by definition is water that was contained within the rock upon its formation. This environment was therefore characterised by long-term contact with the rock that may have led to more dissolved ions than other environments. Most saline environments had broad distributions of carbonate species also, and this was likely to be due to the broad range of dissolved ions present in these environments that contribute to their saline nature. Interestingly, most transitional environments had a low distribution of other carbonate species, mimicking fresh, surface water environments more than saline environments. Regardless of the cause of the distribution, or even the extent of the distribution of other DIC species, if these species are not the target of the sensor, membranes or other mechanisms to screen out these potentially cross-interfering carbonate species may be necessary. These options are discussed in the Implications for Sensor Development and Design Section.

5.6.3 Distribution of Non-Carbonate Species with the Potential to Interfere with Sensor Response

Similar to the other DIC species, it was not surprising that saltwater environments had the greatest number of non-carbonate species with the potential to interfere with sensor response. As with other DIC species, formation water probably showed more dissolved ions than transitional and surface freshwater ions, due to increased contact with the rock. Obviously, sensor developers wishing to target these environments need to pay special attention to species that may interfere, should their sensor design

be susceptible to this effect. Fibre optic sensors, of the type under development by Bao et al. (2013) may fall into this category (Bao et al., 2013). It is unlikely that a sensor is not sensitive to temperature, but should that be the case, developers must be careful to control for temperature nonetheless, given that it still has a small influence on the mean molarities of non-carbonate species.

5.6.4 Implications for Sensor Development and Design

Sensor design will vary according to the selected application environment(s). Once developers have achieved initial success in binary environments, they should begin increasing the complexity of the test solutions to move towards laboratory test solutions that are analogous to their intended application environments, beginning first by controlling pH to achieve the likely dissolved carbonate species. Depending on the design of the sensor, it may also be necessary to test for interferences. If multiple application environments are the intended target, developers should begin by introducing dissolved ions common to most application environments and that are expected to have similar properties to CO_2 in terms of the variables measured by the sensor. For example, for a fibre optic sensor like the one developed by Bao et al. (2013), testing species expected to have similar optical properties to CO_2 may be a good strategy.

Membranes may be needed to screen out some of the interfering species. Some sensors may require tailor-made solutions, like a combination of layered membranes to improve selectivity. Molecular sieves can be derived from a number of materials and have been shown to selectively screen out certain gases (Centeno and Fuertes, 2001). Organically modified sol-gels can be customised to be selective to specific gases by incorporating functional groups (e.g., amino groups) into their structure (Wolfbeis, 2000). Polymer membranes have been successfully imprinted to allow passage of certain certain molecular shapes (e.g., caffeine), though no success appears to have been achieved for dissolved gases as yet (Wolfbeis, 2000). Other substances swell or shrink in the presence of specific chemicals; e.g., tertiary amines swell in response to CO_2 (Lucklum et al., 1991), and silicone membranes have been shown to be highly selective to CO_2 (Goyet et al., 1992).

Membranes that allow CO_2 or other target species to pass through, but filter

out potential interferences, could be developed to enhance the signal. For example, Goyet et al. (1992) used a silicone membrane that was highly selective to CO_2 to conduct field experiments in a marine environment. Silicone membranes have also been used in oceanic mass spectrometry measurements (Tortell, 2005). Other customised membranes may also be useful, depending on the solution chemistry of the application environment and design of the sensor. Upper and lower constraints on the concentration of carbonate species across application environments is needed to allow sensor developers to set target resolutions to optimise sensor response for their intended applications and environments.

5.7 Conclusions and Next Steps

A comprehensive understanding of dissolved CO_2, along with other DIC and non-carbonate species that may interfere with sensor response in environments of interest will help inform sensor design, laboratory test solutions and the selection of *in situ* test sites. This review analyzed speciation of carbonate and non-carbonate species using *Phreeqc 2.18*, a hydrochemical modelling software. Modeling output showed that DIC was highest in deep aquifers, most transitional environments, saltwater Lake Van (though not the Dead Sea), and surprisingly, the Antarctic lake. Generally, carbonate speciation followed the expected trend, with HCO_3^- dominating in mid-pH environments, CO_2 in low pH environments, and CO_3^{2-} in high pH environments. More complex carbonate species emerged in environments with higher preponderance of dissolved ions. As expected, this included saline environments and groundwater (especially deep aquifers). Not surprisingly, these environments also had greater distribution and concentration of non-carbonate species that may interfere with sensor response. Of the quantified variables, *Phreeqc 2.18* assumed that pH had the most important influence on carbonate speciation.

These analyses should help with the development of dissolved CO_2 sensors intended for a range of application environments. Modeling various application environments using a well-established method to estimate speciation in a variety of application environments in which a dissolved CO_2 sensor could be deployed, provided important insights and analysis of the application environment from the point of view of a sensor developer. For example, someone wishing to monitor the seafloor

for CO_2 leakage from a carbon, capture, utilisation and storage operation now has data describing general marine hydrochemical conditions from a carbonate and non-carbonate point of view. Further analysis is required in deep environments, where high pressure and temperature could influence carbonate speciation. Furthermore, other confounds, like biofouling, exist *in situ*, so for a comprehensive synthesis of data that may be required to inform sensor development, a review of biofouling in various application environments is required.

5.8 Acknowledgements

Carbon Management Canada, the National Science and Engineering Research Council, Drs. Peter Wild, David Sinton, Don Lawton, Martin Jun, Ernie Perkins, Bernhard Mayer, Shannon Sterling and Geoff Burton, Luis Melo, Ben Davies, and Bo Bao.

Chapter 6

Speciation Experiments and Challenges with Working at Atmospheric Pressure

6.1 Preamble

This chapter discusses carbonate speciation experiments that were conducted to ascertain the sensor's sensitivity to carbonate speciation. I designed and conducted all experiments discussed in this chapter with input, financial support, and guidance from Dr. David Risk (supervisor). Dr. Shannon Sterling (Supervisor) provided conductivity, pH and temperature sensors.

6.2 Introduction

The dissolution and speciation of CO_2 is highly pH dependent (Weiss, 1974; Appelo and Postma, 2005). Small-scale seepage or leakage from a marine CO_2 geologic sequestration site that dissolves quickly in the overlying seawater is unlikely to alter pH. Above pH 10.3, dissolved inorganic carbon will be present predominantly as aCO_3, and at pH of 8, close to the pH of the marine environment, dissolved inorganic carbon will be present predominantly as $aHCO_3$, where a represents an alkali (earth) metal (Figure 6.1). Escaping CO_2 will therefore speciate quickly, taking the form of HCO_3^- rather than dissolved CO_2. The CO_2 plume could also form a more complex carbonate species, like $NaHCO_3$ (Bhatia and Risk, 2015).

Because the pH perturbation from a small-scale leak would be too small to be detected by a marine pH sensor (Blackford et al., 2009), other types of sensors are needed that can directly sense bicarbonate. Long Period Grating Fibre Optic sensors (LPGs) are able to detect a shift in the refractive index of the surrounding medium (James and Tatam, 2003) and could theoretically detect changes in bicarbonate concentration. Long period gratings are inscribed on the core of an optical fibre and

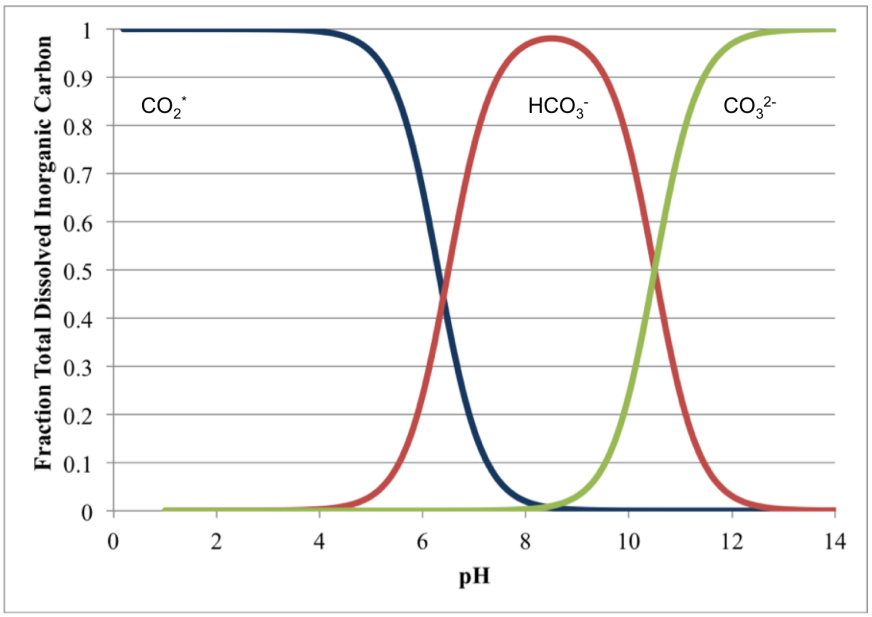

Figure 6.1: Relationship between pH and the distribution of carbonate species dissolved in solution at 25 ^{o}C. *A small portion of dissolved CO_2 forms $H_2CO_3^-$ the remainder is present as a dissolved gas. Calculated from equations published in Appelo and Postma (2005), based on pKa values published in Schwarzenbach and Meier (1958).

induce a permanent, localised, periodic modulation of the core of the fibre. The gratings cause coupling between the core mode and discrete cladding modes. Cladding modes attenuate more readily than the core mode, so certain discrete wavelengths are attenuated in the transmitted spectrum of an LPG. The central wavelength of these attenuation bands shifts ('wavelength shift') inversely with a change in the refractive index of the surrounding medium. Therefore, unlike pH sensors, LPGs could potentially detect a leak or seep whose dominant form was HCO_3^-, CO_3^{2-}, or a more complex carbonate species, provided the seep or leak sufficiently altered the refractive index of the surrounding medium. This ability to distinguish between different carbonate species could meet a marine sensing need to monitor for small-scale, or slow seepage or leakage at marine geologic sequestration sites. Though a slow seep or leak is unlikely to significantly alter pH and deleteriously impact the marine environment, a long-term seep or leak of this nature could undermine the climate mitigation potential of a CCUS project.

Conversely, background variability in carbonate speciation may also interfere with sensor response if the LPG is principally designed to target dissolved CO_2. Since a refractive index shift is not uniquely driven by CO_2, if carbonate speciation shifts refractive index sufficiently to alter sensor signal, this variability could contribute to sensor noise, or mimic a leak or seep if variability is sufficient in a given direction.

6.2.1 Objective

Long period grating sensors are able to detect a shift in refractive index of the surrounding medium (James and Tatam, 2003). Given that carbonate and bicarbonate solutions of the same percent mass have different refractive indices (Wolf, 1966), and LPGs are sensitive to changes in the refractive index of the surrounding medium, LPGs may be able to distinguish between carbonate and bicarbonate solutions, though there are no published studies that have tested this ability. This work attempts to develop a carbonate speciation sensor by undertaking laboratory experiments to demonstrate that the sensor could detect the shift in refractive index as a sodium carbonate solution was acidified with HCl, to answer the question: Can LPGs distinguish a 7.0 % Na_2CO_3 solution by mass from a 7.0 % $NaHCO_3$ solution by mass?

Based the theoretical refractive indices of $NaHCO_3$ and Na_2CO_3, LPGs should be able to detect the formation of $NaHCO_3$ as the Na_2CO_3 solution is acidified in solutions that have a concentration of 7 % by mass. The sensitivity of LPGs to changes in the refractive index varies, but in previous studies, the sensitivity (wavelength shift per refractive index unit change) of the LPG was calculated to be between -5.538 and -8.615 nm RIU^{-} (Chapter 5). Refractive index of Na_2CO_3 and $NaHCO_3$ solutions are available in the literature (measured at a wavelength of 597 nm): Five percent Na_2CO_3 solution by mass has a refractive index of approximately 1.3344 (Rodkey, 1966). The same percent concentration of $NaHCO_3$ solution by mass has a refractive index of 1.3396 (Rodkey, 1966). A shift from the carbonate dominated system to the bicarbonate dominated system should generate a refractive index shift of .0052 RIU at 5 % concentration by mass, and a wavelength shift of between 26 and 43 pm. At a solution concentration of 7 % by mass should produce a slightly higher shift in refractive index.

6.3 Methods

6.3.1 Titrations and Data Collection

A series of experiments were conducted where 550 mL of 7.0 % by mass Na_2CO_3 solution (pH 12) was titrated with 30.6 % HCl until pH reached 7. This high percent concentration of HCl was used to avoid diluting the carbonate solution. Experiments were also conducted at lower concentrations, where 550 mL of 1.4 % by mass of Na_2CO_3 was titrated with 0.4 % by mass HCl. With each titration, 7 mL of titrant was added to the Na_2CO_3 solution. The solution was allowed to equilibrate for 0.5 h before measurements were taken. With each titration, pH was measured (Figure 6.2H). Temperature and LPG data were measured at a rate of 2 Hz.

6.3.2 Equipment Setup

The LPG was housed inside a custom-fabricated housing open to the surrounding environment (Figure 6.2B). The LPG and the housing were placed inside a 600 mL container immersed in an insulated water bath. The LPG was connected to a Micron Optics SM125 Interrogator and wavelength shift was measured and recorded

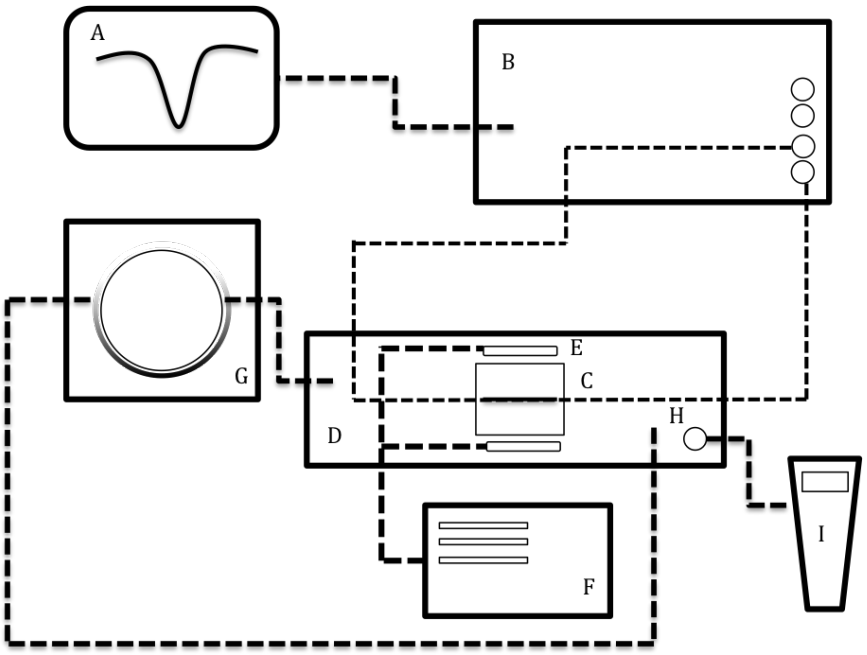

Figure 6.2: Experimental Setup. A computer (A) to analyze the signal from the interrogator (B). The long period grating fibre optic sensor was housed inside a flow cell (C) that was open to a container (D) that contained the Na_2CO_3 solution. The long period grating fibre optic sensor was connected to the interrogator via pigtails. Campbell Scientific Thermistors (E) were used to monitor temperature. Temperature data was logged on Campbell scientific logger (F). Solinst peristaltic pump (G) was used to mix the solution throughout the titration. A pH probe (H) connected to a pH metre (I) was used to monitor pH of solution. Thick dashed line denotes tubing and thinner dashed line represents the optical fibre.

using Micron Optics Enlight software. A Solinst 410 peristaltic pump was run continuously throughout the experiment to circulate the solution, ensuring even mixing (Figure 6.2F). Two Campbell Scientific Thermistor 107 temperature sensors were also immersed in the 600 mL container and placed in close proximity to the flow cell (Figure 6.2E). The thermistors were connected to a Campbell Scientific 1000 series data logger and temperature data was recorded using Loggernet Software. A Pro1020 pH metre was calibrated using standard buffer solutions, and inserted into the 600 mL container.

6.3.3 Temperature Control and Calibration

Prior to beginning the experiments, a temperature calibration was conducted to ascertain the temperature sensitivity of the LPG. The temperature of the water bath was raised to 40 ^{o}C and allowed to cool overnight to 12 ^{o}C. A regression analysis was conducted and the slope was calculated to be 0.0336 nm $^{o}C^{-1}$, with an R^2 square value of 0.99. This slope was used to remove any temperature effects from the sensor signal that could not be controlled by immersing the experimental setup in the insulated water bath (described in detail in Chapter 5).

6.4 Results and Discussion

The concentration of the test solutions was above the threshold calculated for the sensor to be sensitive to the refractive index change expected when the solution changed from Na_2CO_3-dominant to $NaHCO_3$-dominant. Despite the theoretical estimate that no dissolved CO_2 would form in solution since the pH remained above 8 for most of the experiment, localised acidification led to the formation of CO_2 bubbles at the titration site. An unknown amount of CO_2 was therefore lost to the environment, and mass was not conserved. As a result, it was not possible to demonstrate experimentally that the sensor was able detect a shift in speciation from Na_2CO_3 dominant solution to $NaHCO_3$, since the amount of mass lost was unknown and therefore could not be accounted for in the sensor signal.

To mitigate for the degassing that occurred with 30 % by mass HCl, more dilute solutions of HCl were considered as titrants, but only very dilute HCl solutions, like 0.4 % by mass HCl could be added without visible CO_2 bubbles degassing from solution. Working with these dilute concentrations was challenging because the titrant was not sufficiently concentrated to shift pH readily, and so the CO_3-dominant solution required greater than 150 mL of titrant to shift an HCO_3^--dominant solution. The 0.4 % M HCl significantly diluted the solution and also prolonged the experiment beyond acceptable run times for the pump. Pairing 0.4 % by HCl with more dilute carbonate solution, of 1.5 % by mass limited dilution of the carbonate solution. Initial calculations suggested that the refractive index shift as the solution moved from carbonate to bicarbonate-dominant should be sufficient to generate a wavelength

shift above background noise; however, this shift was not seen experimentally.

To titrate using 30 % by mass HCl solution and higher concentrations of carbonate solution, it may be useful to consider higher pressure environments. Titrations could be conducted in higher pressure laboratory conditions at pressures > 7 atm, because at these pressures, any CO_2 formed during the titration would remain as a liquid. No mass would therefore be lost during the titration. At atmospheric pressure, an open system can be used for the experimental apparatus, but at high pressure a closed system would be needed. At high pressure, each time a titrant was added, the increase in the volume of solution would cause a slight increase in the pressure of solution as well. Since LPGs are pressure-sensitive, a pressure calibration would be required and the effects of this pressure change would have to be removed.

Alternatively, working at atmospheric pressure could be successful if $NaHCO_3^-$ is dissolved rapidly in solution, causing the solution pH to remain close to 8, with $NaHCO_3^-$ being the dominant form. This solution could then be titrated using NaOH, to drive pH upward, ultimately shifting the solution from bicarbonate to carbonate-dominant.

Though initial experiments could not demonstrate that LPGs could be used as speciation sensors, it should be noted that even the dilute carbonate solutions used in these experiments were much higher than background concentrations of carbonate in the marine environment. In fact, in the marine environment, background concentrations of carbonate are well below detection limits for the LPG. For example, HCO_3^- is present in the marine environment below 0.06 ± 0.15 % concentration by mass (Bhatia and Risk, 2015), therefore, at the very least, interference due to background variability in carbonate concentration may not significantly contribute to noise if LPGs are being used to specifically target dissolved CO_2, and not other carbonate species.

6.5 Conclusion

Despite the theoretical possibility that the sensor could act as a speciation sensor, challenges with atmospheric pressure conditions and the localised acidification of the solution led to the degassing of CO_2 from solution. Since mass was not conserved

throughout the course of the experiment, it was not possible to demonstrate experimentally that the LPG could act as a speciation sensor in higher concentration solutions. Repeating these experiments at high pressure or starting with a bicarbonate-dominant solution and titrating with NaOH may garner different results, since under high pressure conditions more CO_2 may remain dissolved in solution, or if titrating $NaHCO_3$ with NaOH, CO_2 would not form. Results did demonstrate, however, that at concentrations higher than background concentrations likely to occur in the marine environment, carbonate speciation was unlikely to contribute to noise in LPGs specifically targeting dissolved CO_2, rather than other carbonate species.

Chapter 7

Consideration of Sediment Dynamics and Biogeochemical Cycling on Future Deployment of Seafloor Sensors: A North Sea Case Study

7.1 Preamble

Sonja Bhatia and Helmuth Thomas

This chapter presents a review, that when paired with modelling work, will form the basis for a manuscript intended for submission to the International Journal of Greenhouse Gas Control.

7.2 Introduction

Carbon dioxide capture and storage (CCUS) is being used as a mitigation tool to reduce greenhouse gas emissions from the burning of fossil fuels (Benson, 2015). Once CO_2 is injected in a confined geologic formation there is still a possibility that the CO_2 will escape to the surrounding environment, so ongoing monitoring programs are necessary (Aoki et al., 2013; Hvidevold et al., 2015). A combination of plume modelling, seismic surveys and flare imaging (Themann et al., 2009; Aoki et al., 2013) is currently used in most monitoring programs, but advances in sensing technology are opening the possibility of real-time seafloor monitoring of these sites. Both Long Period Grating fibre optic sensors (LPGs) and Miniature Non-Dispersive Infrared sensors (mNDIR) are monitoring tools that may be used to detect escaping pCO_2 near the seafloor, particularly as the technological development of these sensors for this application matures. To determine the efficacy of these two technologies as seafloor monitoring tools, detailed consideration of sedimentary and biogeochemical processes is required because these two factors (among others) have the potential to

interfere with sensor response in situ (Bhatia and Risk, 2015). Interference due to background variability is of particular concern in the detection of small-scale seeps or leaks (long term seepage or leakage at a rate below 6.93 x 103 mmol m-2 d-1 as defined by Blackford et al. (2009)).

As alarm sensors to detect highly concentrated leaks, like a burst pipeline, both LPGs and mNDIR are likely to be effective monitoring tools given their current state of development. Long period grating fibre optic sensors are sensing portions inscribed directly on an optical fibre. These sensing portions cause some of the light travelling through the core of the fibre to be transferred to the cladding (James and Tatam, 2003). Depending on the refractive index of the surrounding medium, certain cladding modes attenuate normal to the core-cladding interface. The central attenuated wavelength of these cladding modes varies inversely with the refractive index of the surrounding medium (James and Tatam, 2003). Sensitivity of LPGs is currently inadequate to detect natural variability in Total Alkalinity (A_T) or Dissolved Inorganic Carbon (DIC), but is sufficient to detect a large-scale seep or leak, particularly if the leak is in the form of gas bubbles.

Miniature non-dispersive infrared spectroscopy sensors are currently more sensitive than LPGs to small-scale shifts in pCO_2 (Chapter 8) and are already commercially available for seafloor pCO_2 detection. The former employ spectroscopy to quantify the amount of pCO_2 present in the sample (Graziani et al., 2014); however, in low-to-moderate leakage or seepage scenarios, these sensors may have a high noise component that may dwarf the seepage or leakage signal. Since mNDIR is specific to pCO_2, if small-scale seeps or leaks speciate rapidly to another component of DIC, like HCO_3^-, the sensors may not be able to detect the seep or leak (Chapter 8).

The importance of detecting small-scale escape events is as yet uncertain. Some authors argue that lower seepage and leakage conditions are unlikely to lead to pH perturbation beyond natural variability (Blackford et al., 2009); however, deeper investigation of the timing and length of these perturbations relative to background variability is needed to truly determine that these small-scale escape events are of minor importance; minor pH perturbations could alter conditions needed for processes that contribute to A_T production in the sediments and the resulting ability of a water body to absorb atmospheric CO_2.

If small-scale seeps or leaks are deemed to be of biogeochemical importance, LPGs and mNDIR both require further investigation of the geochemistry of a given monitoring location to determine the likely efficacy of these technologies to detect pCO_2 in low-to-moderate seepage and leakage scenarios. The signal-to-noise ratio of these sensors can be influenced by six interconnected parameters of the carbonate system: (1) Dissolved Inorganic Carbon (DIC), (2) Total Alkalinity (A_T), (3) pCO_2, (4) HCO_3^-, (5) CO_3^{2-}, and (6) pH. Only four components can be measured: DIC, A_T, pCO_2, and pH. If two of the components can be determined, the other four components can be calculated (Dickson et al., 2007). So, for example, in solutions of a known alkalinity and pCO_2 concentration, DIC and pH can be ascertained. Sensors specific to pCO_2 therefore require that a second parameter, typically A_T, be measured to determine the scale of a leak, since some of the escaping pCO_2 is likely to speciate to HCO_3^- in the marine environment, and the degree of speciation will be a function of pH, A_T, and DIC. Furthermore, background variability in these four parameters can interfere with sensor signal.

Both to further sensor development applications and to understand the likely effect of small pH perturbations on biogeochemical cycling, it is important to discuss the processes in near-shore environments, where the bulk of carbon dioxide geologic sequestration sites exist or are likely to exist (Chapter 8). One of the oldest carbon dioxide sub-seafloor geologic sequestration sites, Sleipner, is located in one such coastal environment, the North Sea (Arts et al., 2004), and the geochemistry of this region is widely studied (Burt et al., 2016; Thomas et al., 2009; Salt et al., 2013; Queste et al., 2016). The geochemistry and sedimentary processes of the North Sea will therefore be considered as a case study for sensor developers to understand the complexity of the biogeochemical controls on the carbonate system and the implications of background variability in these parameters to sensor development. Carbonate geochemistry and sedimentary process will also briefly be considered in the context of whether or not a small-scale, long-term seep or leak should be of ecological or biogeochemical concern.

7.3 The Carbonate System and Water Column Sensing

The four components of the carbonate system that can be measured may be described as follows (Dickson et al., 2007):
(1) Total DIC is described according to Equations 7.1a and 7.1b:

$$DIC = [H_2CO_3^*] + [HCO_3^-] + [CO_3^{2-}] \tag{7.1a}$$

$$[H_2CO_3^*] = [CO_{2(aq)}] + [H_2CO_3] \tag{7.1b}$$

H_2CO_3 is marked with a *, since

$$K = \frac{[H_2CO_3]}{[CO_{2(aq)}]} = 10^{-2.8}, \tag{7.2}$$

only a small fraction of H_2CO_2 remains as H_2CO_3; most dissociates to $CO_{2(aq)}$. DIC can be measured directly by converting all components to pCO$_2$, however, this does not tell us the species breakdown (Dickson et al., 2007).
(2) Total alkalinity (A_T) is defined by Dickson (1981) as the "...the number of moles of hydrogen ion equivalent to the excess of proton acceptors (bases formed from weak acids with a dissociation constant K=$10^{4.5}$ at 25^0C and zero ionic strength) over proton donors (acids with K > $10^{4.5}$) in 1 kilogram of sample." A_T can therefore be determined according to Equation 7.3 (Dickson et al., 2007):

$$\begin{aligned} A_T = [HCO_3^-)] + 2[CO_3^{2-}] + [B(OH)_4^-] + [OH^-] + [HPO_4^{2-}] + \\ 2[PO_3^{3-}] + [SiO(OH)3-] + [NH_3] + [HS^-]... - [H^+] - [HSO_4^-]... \end{aligned} \tag{7.3}$$

(3) Total hydrogen concentration is complicated to calculate because a lot of the [H+] is in the form of HSO_4^-, and so we also need to know the concentration of this species and the dissociation constant (K_S), but pH is measured according to Equation 7.4 (Dickson et al., 2007):

$$pH = -log[H^+] \tag{7.4}$$

(4) pCO$_2$ refers specifically to the component of DIC that is in the form of dissolved

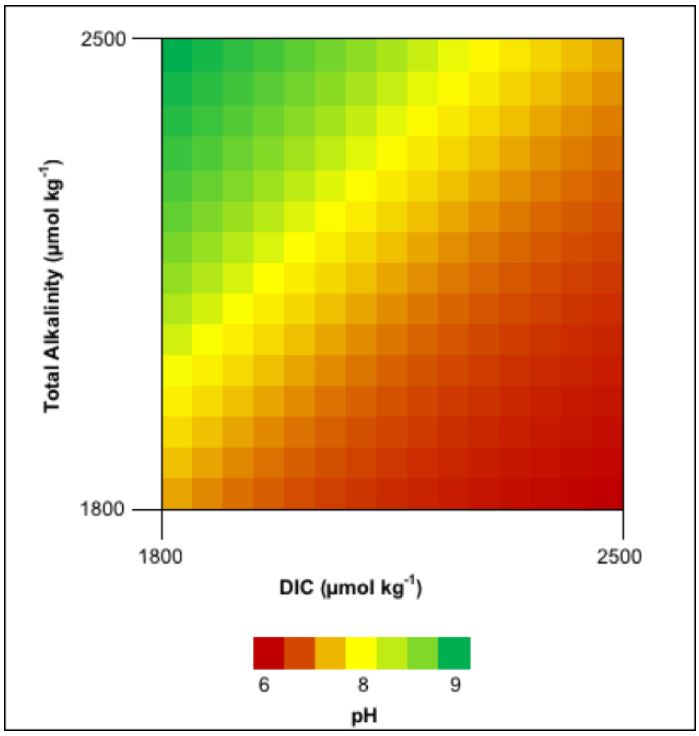

Figure 7.1: Theoretically predicted pH based on varying dissolved inorganic carbon and total alkalinity concentrations in ranges normally found in seawater. Graph made using the USGS CO2-SYS program (Pierrot et al., 2006).

CO_2.

These four parameters are strongly interrelated (Figure 7.1). Variations in anyone of these parameters can affect the others (Figure 7.1). The dominant species of DIC is influenced by pH, but there is a feedback mechanism: in higher pH environments, DIC shifts towards HCO_3^- and CO_3^{2-} (the components of DIC which contribute to A_T), which act to buffer the pH shift with the addition of an acid to solution (Appelo and Postma, 2005). Upon dissolution a small part of pCO_2 forms carbonic acid, so increased uptake of atmospheric CO_2 or CO_2 release from geologic sequestration sites may alter pH (Blackford and Gilbert, 2007), if the escaping CO_2 is sufficiently concentrated, but in higher pH environments, the dissolving pCO_2 may rapidly speciate to HCO_3^- or CO_3^{2-}, which would alter the composition of A_T, though no net change in the buffering capacity of A_T would occur.

This complex carbonate chemistry may negatively impact the efficacy of LPGs and mNDIR sensors to detect small-scale seeps or leaks. For both LPGs and mNDIR, in low leakage or seepage scenarios, the background variability in certain key components

of the carbonate system A_T, pCO_2, DIC, and pH may be greater than the perturbation generated by the escaping pCO_2. Furthermore, deep water release of CO_2 has demonstrated that escaping CO_2 will dissolve in the water column (Blackford et al., 2014). The geochemical conditions may be such that the escaping pCO_2 dissolves and dissociates to another component of DIC, like HCO_3^-. Conversely, if escaping pCO_2 contributes to a shift in pH, it may shift some of the other DIC species towards pCO_2. Both geochemical scenarios outlined above have implications for sensor design and deployment. In the former scenario, both sensors may be unable to detect the escaping plume since the HCO_3^- is not the intended measurand. In the latter scenario, the scale of escape may be magnified due to changes in the geochemistry and the scale of the escape event may therefore be over-estimated. These scenarios illustrate the importance that another parameter of the carbonate system, like A_T, be measured simultaneously to calculate the total amount of escaping DIC based on measurement of the pCO_2 component. It is possible that LPGs may be calibrated to detect other DIC species based on a unique refractive index signature, but particularly given the potential of escaping pCO_2 to shift carbonate speciation, it is likely that LPGs will also require this additional measurement parameter. Long period grating sensors also require that temperature be monitored, so temperature effects on refractive index can be removed (James and Tatam, 2003).

7.4 The Geographic and Oceanographic Context of the North Sea

The North Sea is located over the NW European Continental Shelf and connects directly to the North Atlantic (Thomas et al., 2009, Figure 7.1). The North Sea can be divided into two geochemically distinct regions along the 50 m depth boundary (Burt et al., 2014, Figure 7.2): the southern North Sea and the northern North Sea. The southern North Sea is made up of the Wadden Sea and Southern and German Bights (Burt et al., 2014). This southern region is shallower and is not stratified year round (Burt et al., 2014). The region is characterized by sandy sediments and mudflats that are often exposed to the atmosphere at low tide (Thomas et al., 2009). The southern region is influenced by sea-atmosphere interaction and resulting strong carbon cycling, as well as coastal and riverine carbon inputs (Burt et al., 2014). The deeper northern region is the part of the North Sea that exchanges water and therefore

A_T and DIC with the North Atlantic (Thomas et al., 2004).

7.5 Controls on pH, A_T and DIC in the North Sea

The North Sea basin acts as a strong continental shelf pump whereby CO_2 taken up in the shallow coastal regions moves through the deeper northern North Sea into the North Atlantic (Thomas et al., 2004, 2007; Bozec et al., 2006; Thomas et al., 2009). Uptake of CO_2 is biologically driven, where thermal stratification separates the productive, upper layer from the deeper, colder layers of the water column (Kühn et al., 2010). In the southern North Sea temperature-controlled release of CO_2 outweighs drawdown by primary productivity, but in the northern region, respiration and remineralization of dominate and contribute to net CO_2 uptake (Kühn et al., 2010). Overall undersaturation in the northern North Sea acts a CO_2 sink; the North Sea basin as a whole takes up $>$ 500 Gmol y^{-}1. This CO_2 uptake is transferred to deeper regions via a continental shelf pump (Thomas et al., 2009). Through this mechanism 93 % of the atmospheric CO_2 taken up by the North Sea is transferred to the North Atlantic (Thomas et al., 2004).

The intertidal portion of the Wadden Sea is the principal contributor to A_T in the southeastern portion of the North Sea (Thomas et al., 2009). Many continental rivers empty into this part of the Wadden Sea, carrying with them DIC and nutrients that drive biologic activity (Thomas et al. 2009). Air-sea exchange is also facilitated in the tidal mudflats area of the Wadden Sea because the sediments are often exposed to the atmosphere (Burt et al., 2014). Shallow seas facilitate uptake of CO_2 due to the net contribution to A_T from anaerobic degradation in shallow sediments (Thomas et al., 2009).

Seasonal and spatial variations in A_T are generally low in the North Sea, but some variability is noted due to the changing importance of different sources of A_T seasonally. In certain regions riverine concentrations of A_T can influence water column concentrations (Thomas et al., 2009), but seasonally driven biologic uptake and subsequent anaerobic degradation also play a role in A_T concentration (Thomas et al., 2009). Mean A_T concentrations in the southern North Sea water column average 2.3 mmol L^{-}, while pore water concentrations ranged from 2.6 to 3 mmol L^{-1} at 1 m depth (Burt et al., 2014). Values for the northern portion of the North Sea are not

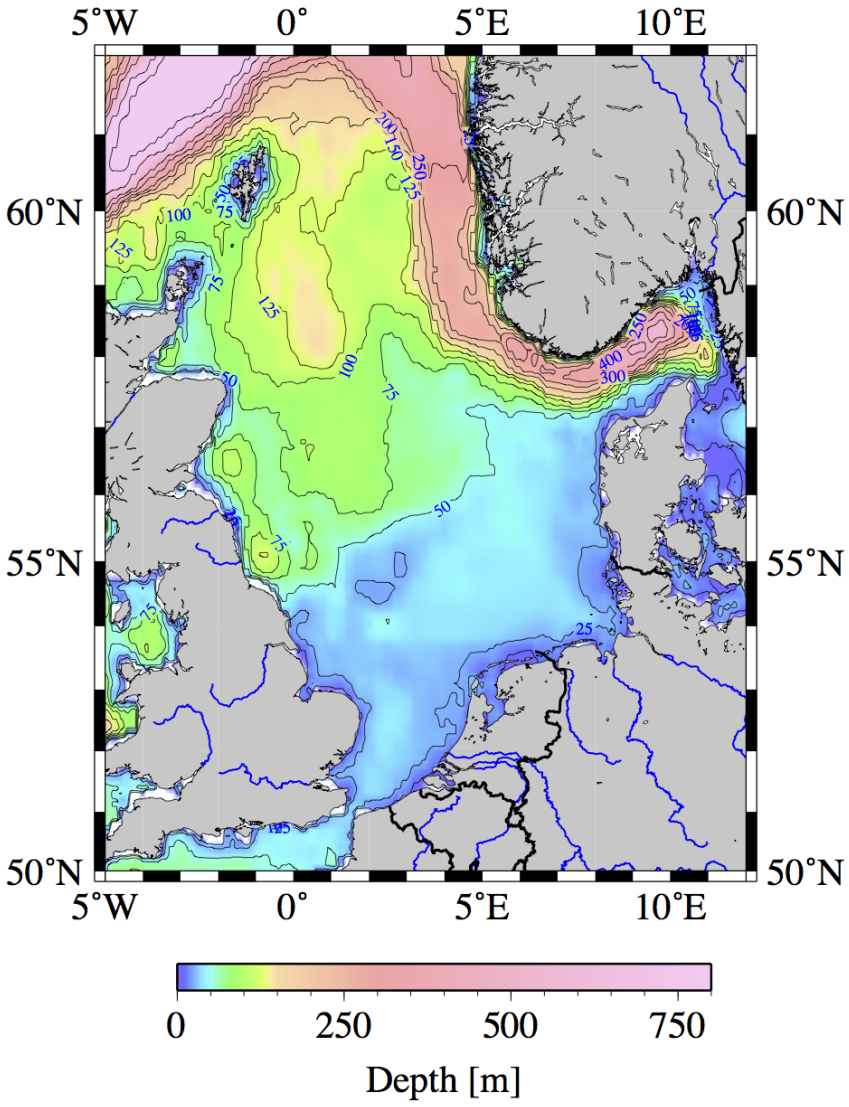

Figure 7.2: Depth profiles in the North Sea basin. Map reproduced with permission of Helmuth Thomas.

available in the literature, but are projected to be lower than in the southern portion since the former fluxes are lower (Burt et al., 2014).

Surface water DIC concentrations are strongly influenced by this air-sea exchange. Seasonal stratification creates a summertime boundary between the upper mixed layer and the thermally startified lower layer. Primary productivity in summer surface waters leads to increased DIC concentrations; subsequent sinking of the organic matter causes remineralization in the bottom water, releasing DIC to the water column. Stratification prevents mixing of DIC back into the surface waters. DIC concentrations in the surface waters are then replenished by uptake of atmospheric pCO_2 and the majority of the remaining CO_2 is transported into the Nort Atlantic via the previously described continental shelf pump (Clargo et al., 2015). Despite seasonal variability in surface water DIC, deep water DIC concentrations tend to be quite constant; Bozec et al. (2006) found no seasonal variability in DIC at depths of 300-500 m. In shallower regions and surface water, DIC variability was noted seasonally and spatially, ranging from 1,870 mol kg^{-1} near the Baltic Sea in summer and as high as 2,150 mol kg^{-1} in the southern region of the North Sea in winter (Bozec et al., 2006). Additional DIC inputs from terrestrial metabolic sources in the order of 4.87 x 10 11 mol C y^{-1} have also been observed (Burt et al., 2016). It is likely that these inputs are derived through land-based denitrification processes (Burt et al., 2016).

As a sink for atmospheric CO_2, mean basin-wide pH in the North Sea is slowly decreasing; pH is projected to decrease on average 0.1 pH units by 2050 (Blackford and Gilbert, 2007). At a basin-wide and annual scale it is expected that DIC concentrations will ultimately equilibrate with atmospheric pCO_2 concentrations (Burt et al., 2016). This pH decrease is likely due to increasing DIC levels in the water column, which is now contributing to a theoretically predicted decrease in A_T and increase in pCO_2 concentrations relative to DIC of the North Sea carbonate system (Thomas et al., 2007).

Seasonal variability in pH could be much greater than mean annual changes in the more biologically active regions. Seasonal variability was found to be as high as 1 pH unit, while in the less biologically active regions, pH was found to vary by < 0.2 (Blackford and Gilbert, 2007); however, the seasonal variability in pH in the biologically active regions has been decreasing in the past decade. Terrestrial

nutrient inputs, particularly riverine nitrate peaked in the late 1990s (Provoost et al., 2010). Burt et al. (2016) suggest that eutrophication in the southern portion of the North Sea may have contributed to increased seasonal production of A_T during peak primary productivity. Both pH and and riverine nitrate inputs are closely linked (Burt et al., 2016; Provoost et al., 2010; Pätsch and Lenhart, 2011). Data from the Dutch Coastal Zone show the highest nitrate delivery occurring in February/March, and the subsequent increase in pH occurring in May/June (Burt et al., 2016; Pätsch and Lenhart, 2011). In recent years nutrient runoff has been controlled more closely, thus reducing the production of A_T primarily through denitrifaction, thus contributing to the decrease in pH levels (Burt et al., 2016).

Even if the pH perturbation from a small seep or leak is below natural variability, small changes in pH may reduce nitrification, an important process needed for subsequent denitrification (Blackford et al., 2009). Denitrifcation contributes significantly to A_T production in the sediments (Thomas et al., 2009). Small changes in pH may also affect microbial composition and nutrient speciation; e.g. from NH_3 to NH_4^+ (Blackford and Gilbert, 2007).

7.6 Pore Water-Water Column Fluxes

Variability in A_T, DIC, and pCO_2 pose a problem for pCO_2 sensors. For seafloor sensors, in particular, sedimentary processes and pore-water column fluxes are of concern because they can contribute to production of A_T and DIC in the immediate vicinity of the sensor. These two variables can in turn affect speciation of DIC and the concentration of pCO_2 (Dickson et al., 2007). In the case of mNDIR sensors, A_T increase can lead to increased uptake of pCO_2 and DIC dissolved in the water column, thus increasing background variability. Furthermore, for LPGs, escaping pCO_2 is more likely to speciate in more highly buffered environments, so where A_T is relatively high, the refractive index of the signal may vary. For LPGs, changes in background concentrations of A_T and thus background variability in refractive index could mimic a small-scale seep or leak. These small changes in refractive index are likely to be of concern if LPG development matures to be able to detect these smaller refractive index shifts in the refractive index range of seawater. Sand or particles swept up by bottom currents could also impact LPG response. Consideration should

therefore be given to some of the sedimentary processes and fluxes of organic material and dissolved species between pore water and the overlying water column.

Sediment diagenesis–the remineralization of organic material primarily by marine organisms (Henrichs, 1992)–is the primary control of nutrient release to the water column from the sediments (Luff and Moll, 2004). Depending on depth and oxygen availability this nutrient release contributes to two classes of microbial processes that breakdown organic matter influence biogeochemical cycling: aerobic respiration and anaerobic degradation. A high volume of unstable organic matter is oxidized in the top few centimetres of sediment and decomposes aerobically, but much of this organic matter is transported deeper into the sediments, where it is degraded anaerobically (either by denitrification or sulfate reduction). Products of these anaerobic reactions are released back to the water column and are responsible for a net increase in A_T (Luff and Moll, 2004).

Since anaerobic degradation of organic matter is a primary net contributor to A_T production, there is some seasonal and spatial variability to the A_T flux since primary production varies seasonally and spatially as nutrient, terrestrial A_T, and sunlight inputs vary. Much of this A_T is generated in the shallow Wadden Sea (Burt et al., 2016), where A_T released from the sediments is released to the wider basin, and is likely to account for up to 25% of the atmospheric uptake of CO_2 in the North Sea Region. Burt et al. (2014) estimate excess A_T in pore waters of the North Sea to be approximately 0.7 mmol L^{-1} and Thomas et al. (2009) estimate A_T fluxes as high as 9.6 mmol m^{-2} d^{-1} in the Wadden Sea, with September, 2011 observations as high as 21.4 mmol m^{-2} d^{-1}. In the Norwegian Trench, the deepest portion of the North Sea, A_T flux has been found to be as high as 9.9 mmol m^{-2} d^{-1} and in the northern North Sea as high as 3 mol m^{-2} d^{-1} (Brenner et al., 2016). Aerobic respiration of organic matter produces nutrients and DIC in the pore waters with almost negligible decrease in A_T (Burt et al., 2013).

Diffusion, bioturbation, and advection are the physical process that can drive this exchange, but the importance of these mechanisms varies by sediment type and region. In sandy sediments, that are typically more permeable than fine-grained sediments, advection-driven pressure gradients (also called sediment irrigation) are the primary mechanism of pore water-water column exchange (Aller, 1980; Burt et al.,

2014; Janssen et al., 2005). Burt et al. (2014) present modeled data validated through pore water samples estimating the water flux between the sediments and the overlying water column. For sandy sediments water fluxes were highest from coarse silt sediments 33.7 ± 4.1 L m^{-2} d^{-1}, the Ra flux, which was a tracer used by Burt et al. (2014) to estimate exchange of chemicals, showed an inverse relationship to grain size and a positive relationship with porosity, where advective flows would be the primary driver of benthic fluxes.

While sedimentary processes can interfere with sensors deployed on the seafloor via variations in background concentration of A_T or physical interference with sand and particles being mobilized by movement of bottom water, these particularly high A_T fluxes in the Wadden Sea are not likely to impact sensors deployed for CCUS monitoring directly because the Wadden Sea is largely protected from industrial activity; however, the Wadden Sea's contribution to A_T in the broader North Sea basin could still have a significant impact on sensors deployed elsewhere in the North Sea Basin. As discussed, variability in A_T can influence speciation in DIC, ultimately contributing to sea-air exchange of pCO_2 of the pCO_2 signal at a leakage or seepage site. Still, sedimentary processes in the coarser grained sediments in the northern region of the North Sea are far more likely to impact sensors directly, since this is the region that is more likely to experience industrial activity, and thus require monitoring.

7.7 Characterizing the Effect of Small Seeps or Leaks

Small seeps or leaks are unlikely to change pH beyond background variability on average (Blackford and Gilbert, 2007); however, small pH perturbations have been shown to alter speciation for nutrients (Blackford and Gilbert, 2007) and other chemicals. Changes to benthic communities in the immediate location of an escape event have also been noted (Tait et al., 2015). These pH perturbations can therefore influence biogeochemical cycles at a local scale. Furthermore, depending on the duration, location and timing of release, it is conceivable that synergistic effects could amplify the impact of an escape event. Without considering the seasonal and spatial variability in the geochemistry in relation to the escape event it is not possible to definitively demonstrate that basin-wide impacts will not occur.

A number of investigations have furthered understanding of CO_2 plume dispersion

dynamics and potential ecosystem impacts. Many modelling studies (Blackford et al., 2009; Dewar et al., 2013) and laboratory investigations (e.g., Ardelan et al., 2009; Payán et al., 2012; Widdicombe et al., 2013) of the North Sea or biogeochemically similar regions have been conducted. Studies of natural analogue sites (e.g., Caramanna et al., 2011), and controlled release of CO_2 into the sediments (e.g., Taylor et al., 2015; Blackford et al., 2013) or water column (e.g., Barry et al., 2013) have also begun to characterize the ecosystem and biogeochemical effects of small-scale release. While these studies clearly contribute to a wide body of literature surrounding the impact of a small-scale CO_2 escape, none of these modelling studies have considered how the impact of an escape event of the same scale may change with seasonal variability in the biogeochemistry for the North Sea in particular. Characterizing this baseline variability is a key component to any monitoring program (Blackford et al., 2014). Natural analogue sites have inherent limitations in that the CO_2 seepage has been ongoing and therefore no baseline data is available. Controlled release experiments allow the response of the sediment processes to be tested more effectively (Taylor et al., 2015), but geographic and temporal representativeness is still limited.

One in situ example that is relevant to the present North Sea case study, is a short-term release, where one tonne of CO_2 was released at 10 m depth in soft sediments off the coast of Scotland (Taylor et al., 2015; Tait et al., 2015; Blackford et al., 2013). The study site was chosen for its similarity to the North Sea, an ecosystem that is likely to be affected by pH perturbations associated with CO_2 release (Taylor et al., 2015). Most of the released CO_2 (85 %) remained within the sediments (Tait et al., 2015). An assessment of the microbial communities pre and post released showed a rapid shift in community composition (Tait et al., 2015). Though Taylor et al. (2015) did not find that O_2, A_T, and DIC fluxes varied between the control and the test site.

Nonetheless small changes in pH have also been shown to alter nutrient speciation. For example, the phosphate flux is high relative to other pore water-water column fluxes in the North Sea, ranging from 30 to 40 mmol m^{-2} y^{-1} (Luff and Moll, 2004). To describe the annual cycle of this limiting nutrient using the C. CANDI model, transport and reactions for 20 different chemical species must be input, along with six primary redox reactions, and additional secondary reactions (Luff and Moll, 2004). These secondary reactions contribute to processes that produce A_T. Small changes

in pH near a pH of 8 (the marine average) have been shown to change the ratio of PO_4^{3-}:HPO_4^{2-} (Blackford and Gilbert, 2007). PO_4^{3-} is an important molecule in some primary redox reactions that occur in the sediments and also to the production of A_T (Luff and Moll, 2004). Changes to the PO_4^{3-}:HPO_4^{2-} can thus accelerate certain reactions, or delay others that are important to biologic production of A_T. In longer term leakage or seepage scenarios, it is therefore possible that A_T production could be affected despite the findings by Taylor et al. (2015).

Despite these findings, it is as yet uncertain what influence these pH changes will have on the wider ecosystem in a particular oceanographic region. Inter-regional or local response is likely to vary even for leaks of the same scale and duration (Blackford, 2014). In situ experiments may experience synergistic factors like coincident increase in solar radiation with controlled release of CO_2 (Tait et al., 2015). More research is needed given the spatial and temporal variability in the impact of small-scale leakage. Given the importance of sedimentation processes and the biogeochemical influence of pore water-water column fluxes to the production of A_T and therefore the ability of the basin to take up atmospheric CO_2, further study is warranted. Monitoring at least initially for small-scale seeps and leaks should be included in standard monitoring protocol until such time as the negative effect of these small perturbations in pH can be ruled out.

7.8 Conclusion

Given the limited data on the biogeochemical impacts of small-scales seeps or leaks, it is essential that monitoring protocol be developed to detect these small releases to the sediments. If development improves the sensitivity of LPGs to detect pCO_2 in seawater, and mNDIR are shown to be effective when coupled with alkalinity monitoring at detecting these small-scale events, they may be useful tools for this purpose; however, the complexity of the sedimentation processes and the rapid exchange of nutrients, organic matter and A_T from the sediments is likely to prove challenging for sensor developers to overcome. Further laboratory experimentation, followed by in situ testing is required to ascertain the effect these processes on sensor response and to develop technological solutions to these influences.

Chapter 8

Marine Carbon Dioxide Geologic Sequestration Sites: A Review of Fibre Optic Sensor MMV Potential

8.1 Preamble

Sonja Bhatia and David Risk

This chapter forms the basis of a review article submitted to the International Journal of Greenhouse Gas Control. I conducted all analysis for this chapter and was the principal author. I had input and guidance from my supervisor and co-author, Dr. David Risk.

8.2 Abstract

Sub-seafloor geologic sequestration of carbon dioxide has the potential to mitigate the effect of anthropogenic CO_2 on climate. The number of geologic sequestration projects is expected to increase over the next five years. Seepage and leakage of CO_2 can occur through pipelines, improperly capped wells, and fractures in the overlying cap rock. Monitoring, Mitigation, and Verification (MMV) of these sites is essential to protect the surrounding marine ecosystem, ensure that climate mitigation efforts are not negated, and to foster regulatory acceptance of the activity.

Fibre optic direct sensing has the potential to measure CO_2 and detect rapidly dispersing, diffuse plumes of CO_2 likely to occur in the marine environment. These sensors are likely to be capable of near-continuous, distributed seafloor monitoring, but are still in the research and development phase. This review sought to characterise challenges likely to be experienced *in situ* to estimate Signal-to-Noise Ratio (SNR) for a specific type of fibre optic sensor, a long period grating sensor (LPG) and compare this SNR to commercially available non-dispersive infrared spectroscopy (NDIR) technology. The review also assessed the state of technological development

for fibre optic direct sensors.

As refractive index based sensors, LPG signal is not uniquely driven by changing concentrations in dissolved CO_2; any substance that changes the refractive index of a solution can influence sensor signal. As a result, SNR is driven primarily by the likely change in refractive index caused by a given parameter. Leaks of the same scale, but of different phase, were found to alter SNR for LPGs. In liquid phase, escaping CO_2 was found to be undetectable, but in gas phase, the SNR was estimated to be 16 regardless of the scale of leakage, if CO_2 remained in gas bubble form and did not dissolve in the overlying water column.These SNR estimates suggest fibre optic sensors would be useful digital detection tools for seepage and leakage in shallow seafloor environments. For NDIR, SNR was directly proportional to the scale of leakage and ranged from 8.7 to nearly 3,000.

This work found that developers achieved laboratory validation for several evanescent field sensors in the down-hole context, but that more work is needed to achieve this validation for the marine environment, with the exception of the fibre tip sensor. All fibre optic sensors discussed in this work still required *in situ* calibration and field-testing to achieve *in situ* validation *in situ*.

8.3 Introduction

Anthropogenic emissions of CO_2 to the atmosphere are increasing (NOAA, 2016). Left unmitigated, these emissions are expected to drive climatic change, raising the global mean surface temperature (Pachouli and Meyer, 2014). Subsequent ocean uptake of the added atmospheric CO_2 is likely to also lead to ocean acidification (Bates et al., 2014; Zeebe et al., 2008; Zeebe, 2012). These changes to the Earth system are expected to have a predominantly deleterious effect on marine and terrestrial ecosystems, and the natural resources and ecosystem services they provide (Fabry et al., 2008; Guinotte and Fabry, 2008). In an effort to mitigate the effect of human-generated CO_2, geologic sequestration of captured CO_2 is being considered and implemented in some jurisdictions. Many models suggest CCS is required to limit atmospheric CO_2 to 450 ppm, the level above which warming will exceed 2 ^oC (Pachouli and Meyer, 2014). Sub-seafloor geologic sequestration sites are in operation either as demonstration facilities or now commercially purely for CCS–for example,

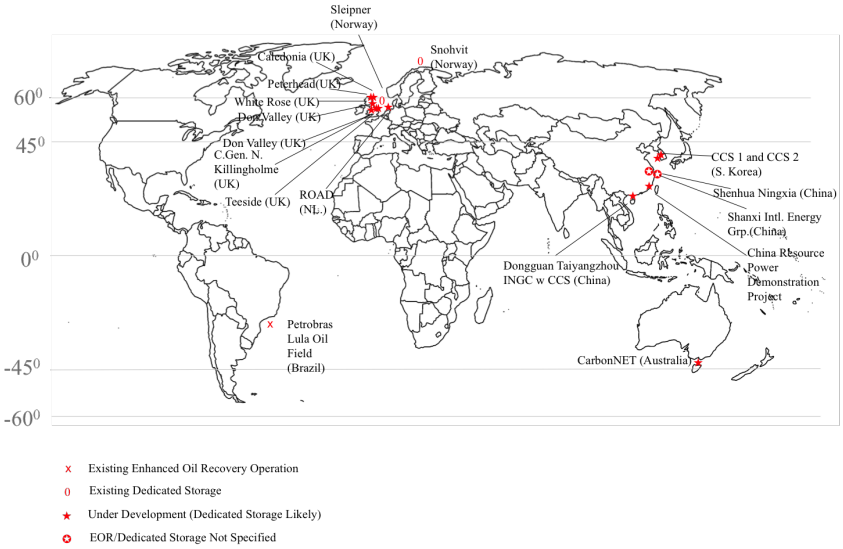

Figure 8.1: Map showing existing and planned CO_2 geologic sequestration sites.

Snøhvit (Oldenburg, 2010) or the Shell Quest project in Alberta, Canada (ABERCB, 2012). Most commercial facilities, however, inject CO_2 as part of enhanced oil or natural gas recovery activities, like that taking place at the Sleipner Natural Gas Field, operated by StatOil (Blackford et al., 2009; Korbøl and Kaddour, 1995; Kongsjorden et al., 1998; Chadwick et al., 2004; Figure 8.1). CO_2 is stored only as a byproduct of these enhanced recovery operations. Sub-seafloor injection of CO_2, in particular, is likely to increase, with several sites planned off the coast of the UK and Asia (Figure 8.1).

Seepage and leakage of previously sequestered CO_2 is a concern in the marine environment. Leakage can occur through well casings, fractures in the cap rock, or via a burst pipeline. Seepage can also take place through the pore network in more permeable cap rocks (Metz et al., 2005). Escaping CO_2 can acidify the local marine environment and it also poses a global climatic risk, should it be released back to the atmosphere. Given the potential risks associated with geologic sequestration, Monitoring, Mitigation, and Verification (MMV) of CO_2 geologic sequestration sites is essential to promote regulatory acceptance and minimise risk to the natural environment. A strong MMV program can monitor the geologic sequestration site to provide an early warning signal of a seep or leak, mitigate the deleterious effects of the leak, and verify the amount of CO_2 stored over a given time interval should credits be

sought for trading in international carbon markets (Metz et al., 2005).

Marine MMV is challenging because the CO_2 plume disperses rapidly in the marine environment and is likely to be diffuse. A new generation of distributed seafloor fibre optic sensors offers a robust monitoring option for seafloor CCUS sites; the sensors offer cost-effective deployment of multiple sensing nodes over a wide area, increasing the likelihood that a sensing node will be in close proximity to a leak or seep. Still in the early stages of development, these sensors require further testing to move toward *in situ* deployment. To guide laboratory experiments so that they reflect the *in situ* environment, the seafloor environment must be characterised in a context useful to fibre optic sensor developers. The signal-to-noise ratio (SNR) for the technology should also be assessed to ascertain the technology readiness level for this new generation of fibre optic sensors.

8.4 Objectives and Approach

The goal of this review is to identify the key challenges and assess the technological readiness for deployment of fibre optic sensor with target application of CO_2 monitoring for marine CCUS sites. To achieve this goal, this review integrates empirical data and modelling work from the literature to answer the following research questions:
(1) What are the likely the likely challenges for marine sensing?
(2) What factors (temperature, pressure, phase of leakage or seepage) will influence the phase and dispersion characteristics of escaping CO_2?
(3) What will be the dominant driver of signal and noise in the marine MMV context?
(4) What factors will be the dominant drivers of background variability for fibre optic CO_2 sensors?
(5) What is the estimated SNR for various leakage and seepage scenarios?
(6) What is the technology readiness levels of the fibre optic CO_2 sensing options?

8.4.1 Quantifying Scale of Seepage and Leakage Events

The scale of seepage and leakage events is difficult to quantify, but it is important to sensor developers, who must select a sensing avenue best-suited to detecting the most likely to occur leakage or seepage scenarios. It is probable that the scale of leakage

relative to background concentrations will be the most important component of the signal to noise ratio. Carbon dioxide concentration in close proximity to a leakage site is likely to be determined by the leakage rate and the plume dispersion characteristics discussed below. It is likely that all released CO_2 is dissolved and that with more rapid leakage, much of the CO_2 remains in the deep ocean for a period of time (Blackford et al., 2009). Diffusion processes and ocean-atmosphere fluxes are likely to occur at a slower rate than the initial input of CO_2 due to a seep or leak, causing CO_2 concentration to increase close to the leakage or seepage site until escaping CO_2 is stopped (Blackford et al., 2009). The following ranges of input concentrations, based on the various possible seepage and leakage scenarios have been modelled in the literature:

(1) Low, long-term seep (plausible): 3.85 mmol m^{-2} d^{-1} (Blackford et al., 2009).
(2) High, long-term seep, or low, short-term or long-term leak (plausible): 3.85 x 10^2 to 6.93 x 10^3 mmol m^{-2} d^{-1} (Blackford et al., 2009).
(3) High, short-term leak (plausible): 6.93 x 10^4 mmol m^{-2} d^{-1} (Blackford et al., 2009).
(4) Large-scale leakage scenarios (less likely): >50 tons day^{-1} (Dewar et al., 2013).

These seepage and leakage inputs differ from land-based leakage estimates published in the literature. For example, Nickerson and Risk (2013) suggest input concentrations of between 0.87 and 86.4 mmol m^{-2} d^{-11} for small-scale seepage. This review will make use of the seepage and leakage rates from Blackford et al. (2009) because the associated pH perturbation for each scenario is readily available in the literature (Blackford et al., 2009).

8.4.2 Estimating Environmental Impacts of Seepage and Leakage

Seepage or leakage of CO_2 poses both a global- and local-scale risk to the environment. Blackford et al. (2009) suggests that for a given leak or seep, some escaped CO_2 may remain in the marine environment, but it is likely that between 12-63 % of the escaped CO_2 will ultimately be released back into the atmosphere. Large-scale leaks may also have localised ecological impacts due to acidification of the seawater around

the leakage or seepage site. Studies of natural analog sites, along with *in situ* and laboratory experiments that tested the effect of ocean acidification on marine biota (e.g., Widdicombe et al., 2013), noted reduced biodiversity in more acidified environments, deleterious effects on calcifying organisms, decreased abundance in biota, and changes to behaviour and settlement patterns in some organisms (Widdicombe et al., 2009; Caramanna et al., 2011; De Vries et al., 2013; Kroeker et al., 2013; Murray et al., 2013). Blackford et al. (2009, p.272) identified four impact categories, depending on the scale of the expected pH perturbation, resulting from a given leakage or seepage scenario:

> "*Perturbation below 0.1 pH units*: no or minimal effect, likely perturbation less than natural variability.
> *Perturbation between 0.1-0.3 pH units*: perturbation of the order of natural variability, potentially small impacts of no systemic importance.
> *Perturbation between 0.3-0.4 pH units*: some species and processes experiencing significant impacts, possibly some systemic disruption.
> *Perturbation exceeding 0.4 pH units:* more wide ranging and significant-to-severe effects predicted."

8.5 Overview of Current Marine MMV Sensing Strategies

A robust MMV program requires a range of complementary strategies. Firstly, extensive modelling of the subsurface and surface is needed surrounding the injection site. Subsurface modelling combined with seismic imaging will allow for characterization of the storage reservoir and storage potential (Chadwick et al., 2004), identification of migration and leakage paths, and provision of a pre-injection baseline. Dispersion modelling is also needed to identify the likely dispersion patterns should a seep or leak occur from different plausible locations (Dewar et al., 2013; Blackford et al., 2008, 2009). During injection and post-injection, ongoing surface and subsurface surveillance is needed for monitoring purposes. Seismic monitoring can help with plume visualization during injection, and ongoing plume migration monitoring (Arts et al., 2004). For ongoing leakage scenarios, continuous, distributed seafloor monitoring is likely to be the most effective seepage and leakage detection system. Development is

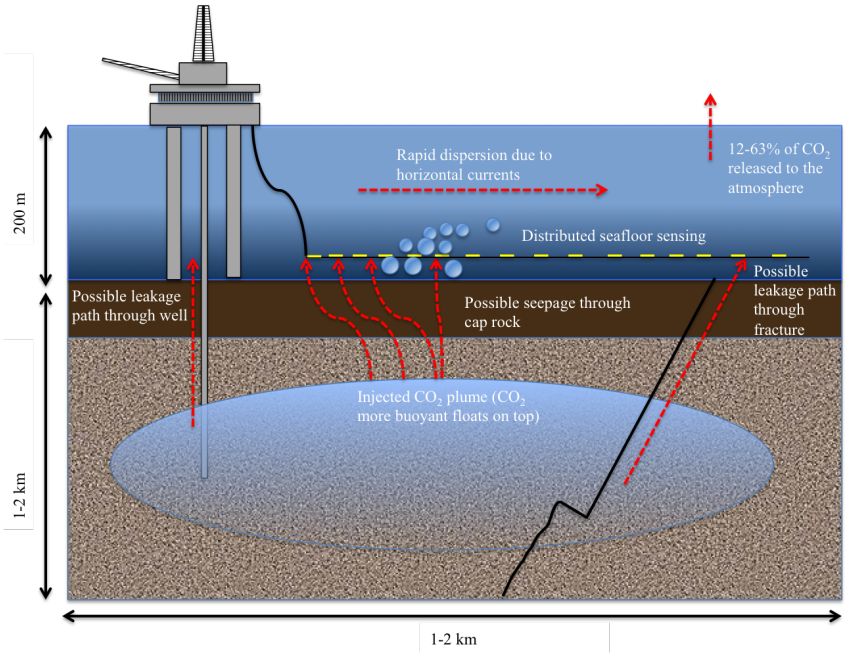

Figure 8.2: Conceptual figure illustrating possible leakage and seepage paths, plume migration in the subsurface, escaped plume dispersion, exchange with the atmosphere, and possible application for distributed sensing. Not to scale.

now moving towards sensors that can directly sense CO_2 in a distributed way. These sensors can be paired with the remote and indirect sensing techniques already in place to strategically monitor higher risk areas. Two direct sensing methods show the most promise with respect to seafloor monitoring: (1) non-dispersive infrared spectrometry (NDIR), discussed briefly in the following section, where pCO_2 is degassed and pumped through a membrane and then titrated against an acid of a known concentration (Graziani et al., 2014); and (2) CO_2 fibre optic sensing, which is able to detect a shift in the refractive index of the surrounding medium, caused by changes to the concentration of pCO_2 or $CO_{2(l)}$ (Orghici et al., 2008; Burton et al., 2014; Melo et al., 2014; Bhatia and Risk, 2015). Fibre optic CO_2 sensing has seen considerable advances of late and will be the focus of this review, and discussed in more detail in subsequent sections.

8.6 Miniature NDIR Sensors

Though not the focus of this review, NDIR sensing technology is worth considering briefly because recent developments allow for distributed sensing. Typically, large-scale NDIR and gas chromatography sensing methods are used to measure background concentrations of pCO_2 in the marine environment (Dickson et al., 2007), these sensors are not ideal for MMV because they require samples to be pumped onboard a ship or a moored platform, limiting distributed monitoring potential. Miniature NDIR sensors, however, are capable of high frequency, distributed monitoring and some are already commercially available (e.g., Pro-Oceanus Mini-Pro CO_2 based on Johnson and McNeil, 2008). Similar probes, called 'GasPro', also make use of miniature NDIR technology housed behind a gas-permeable membrane (Graziani et al., 2014). Field testing of GasPro sensors was recently conducted off the coast of Panera. Twenty probes were deployed for 2.5 days along a 6 m high transect near natural CO_2 seeps. Seafloor depths did not exceed 30 m (Graziani et al., 2014).

These miniature NDIR probes show promise with respect to distributed seafloor monitoring, offering a low-cost alternative to ship and mooring-based measurement techniques. In addition, miniature NDIR may be coupled with acoustic signal transmission (Graziani et al., 2014), which in some environments may be more practical than laying cable on the seafloor, especially in regions with high tidal flow. Graziani et al. (2014) point out that different calibration techniques may be required, depending on the expected background variability of pCO_2 and the expected scale of seepage or leakage. Proof-of-concept does not yet appear to have been established at depths greater than 30 m or in deeper cold water environments where escaping CO_2 may be in liquid phase, or gas/liquid phase, but with hydrate coatings. Furthermore, electronics are still required at the measurement site; Graziani et al. (2014) suggest that batteries will need to be replaced once per month.

8.7 Fibre Optic CO_2 Sensing

8.7.1 State of Development

Sensors manufactured directly on optical fibres have the potential to function well in atmospheric and high pressure environments; they are ideal for remote measurement

sites because they are capable of long-distance signal transmission. These sensors have an additional advantage in the marine context because there are no electronics required at the measurement site. Fibre optic sensors that are capable of distributed sensing, are already commercially available, and have been used successfully for monitoring in the oil and gas sector. These include distributed temperature (Kersey et al., 1997), strain (Kersey et al., 1997), acoustic (Hill and Kelly, 2012; Johannessen et al., 2012), and pH sensors that typically take the form of fluorescent dye-based sensors that respond to pCO_2-induced pH change (Goyet et al., 1992; Munkholm et al., 1988; Wolfbeis et al., 1988). These sensors, however, are only capable of detecting leakage or seepage via proxy measurement.

A new generation of fibre optic sensors is able to sense CO_2 either in dissolved gas phase, as gas bubbles, or in supercritical or liquid phase, and can be paired with more conventional, fibre optic sensing technology that detect leakage via temperature or pressure shifts. These new generation sensors use the fibres on which they are manufactured as waveguides to transmit the signal. The light is guided through the fibre because it is refracted inward from the lower refractive index cladding to the higher refractive index core. Several different types of fibre optic CO_2 sensors achieved proof-of-concept in the laboratory: fibre tip refractometers (Figure 8.3A; Burton et al., 2014, spectroscopy-based dissolved CO_2 fibre optic sensors (Figure 8.3B; Orghici et al., 2008, and coated (Melo et al., 2014) or uncoated (Bao et al., 2013) long period grating sensors (Figure 8.3C).

8.7.2 Fibre Tip Refractometer

Fibre tip refractometry has been used successfully to detect CO_2 in the laboratory at a pressure of 95 atm and 20 ^oC (Burton et al., 2014), a pressure at which CO_2 would be in liquid phase (Dewar et al., 2013). In these experiments, the fibre tip refractometer made use of Fresnal reflection to generate a reflection signal that detected CO_2 in a $CO_{2(l)}$-synthetic seawater mixture (Burton et al., 2014). The distal end of the fibre was immersed in the target solution, and a broadband light was shone down the fibre. The intensity of the light reflected back into the fibre was measured. The intensity of the reflected light is a function of the refractive indices of the fibre tip and the target medium (Burton et al., 2014). The sensor was able to detect both CO_2 droplets and

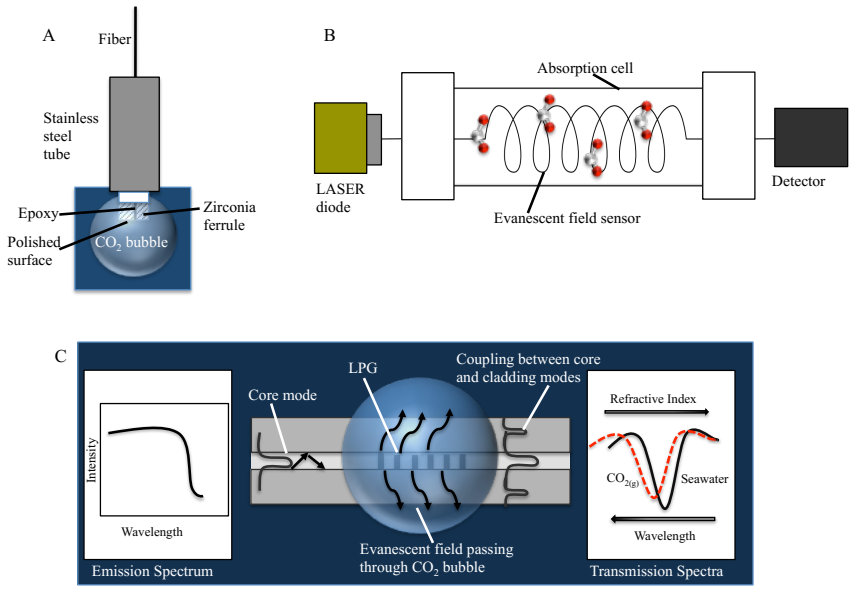

Figure 8.3: A: Fibre tip sensor (modified from Burton et al. (2014)). B: Spectroscopy-based evanescent field sensor (modified from Orghici et al. (2008). C: Long period grating fibre optic sensor (modified from Bhatia et al. (2014) and Chapter 5)

.

CH_4 bubbles, and also distinguish between these two substances. More testing is required to determine accuracy and sensitivity metrics. Furthermore, test conditions did not reflect the likely *in situ* conditions at marine geologic sequestration sites, where colder temperature may lead to hydrate coatings forming around bubbles and droplets at depths sufficient to generate 95 atm pressure; however, this initial proof-of-concept is a positive development in the world of dissolved gas sensing, especially given the demonstrated potential to distinguish between CH_4 and CO_2.

8.7.3 Spectroscopy-Based Evanescent Field fibre Optic Sensor

Evanescent field sensors are able to detect changes in the refractive index of the surrounding medium. As a result of the interaction of light at core-cladding interface, an evanescent wave exists parallel to the interface, and its electric field (evanescent field) decays exponentially in the cladding away from the core-cladding interface (Orghici et al., 2008). Evanescent field CO_2 sensors use modified portions of the fibre to cause the evanescent field to interact with the surrounding environment to detect CO_2-induced changes in the refractive index of the surrounding medium (Orghici et al.,

2008). Several spectroscopy-based evanescent field fibre optic sensors have been developed (Kumar et al., 2002; Orghici et al., 2008; Choudhury and Yoshino, 2004; Burck et al., 1992). Orghici et al. (2008) developed a spectroscopy-based evanescent field fibre optic sensor by removing the cladding a 4 m long section of large diameter core (200μm), multimode fibre (Figure 8.3B). If the surrounding medium is absorbing in the wavelength range of the sensor, the intensity of the evanescent wave is reduced due to attenuation (Orghici et al., 2008).

8.7.4 Long Period Grating Fibre Optic Sensors

Also an evanescent field sensor, an LPG is inscribed by ultraviolet irradiation causing a periodic, permanent localised change of the refractive index of the core of an optical fibre. Grating periods range from tens to hundreds of micrometres (James and Tatam, 2003). Light passing through the core of the fibre has a core mode and multiple cladding modes. These modes refer to a three dimensional distribution of the electromagnetic field propagating through the fibre. The presence of these unique core and cladding modes is a strong function of the diameters and refractive indices of both the core and the cladding. When an LPG is inscribed on a fibre, some of the forward propagating light from the core mode is transferred to the discrete cladding modes (Figure 8.3C). The cladding modes have higher attenuation (decay) compared to the core modes. As a result, the transmission spectrum of an LPG consists of a series of attenuation bands at discrete wavelengths (Figure 8.3C). The central wavelength of these attenuation bands shifts in response to the refractive index of the surrounding medium (James and Tatam, 2003), hereafter referred to as a 'wavelength shift'. The wavelength shift has an inverse relationship to the refractive index of the surrounding medium (James and Tatam, 2003)(Figure 8.3C). Bao et al. (2013) demonstrated that a CO_2-induced change in the refractive index of a binary solution at high pressure (at 95 atm) can generate a wavelength shift in the transmitted spectrum of the LPG. Melo et al. (2014) demonstrated a similar response in binary mixture at atmospheric pressure with a polystyrene-coated LPG.

In the range of refractive indices of brines or seawater-CO_2 solutions ($<$1.36), LPGs are less sensitive than in higher refractive index solutions (James and Tatam, 2003); LPGs achieve maximum sensitivity between refractive indices of 1.42 and 1.46.

Still, uncoated LPGs are able to detect CO_2 dissolved in solution in high pressure environments. Bao et al. (2013) demonstrated that LPGs were able to distinguish supercritical CO_2 from brine in a high pressure vessel at 95 atm and 40^{o}C. These conditions mimicked the downhole environment. Bao et al. (2013) alternated 3 M brine solution with 100 % supercritical CO_2, and then dissolved supercritical CO_2 in brine. A wavelength shift of 192 pm was detected between 3.0 M brine and CO_2-saturated brine (Bao et al., 2013). The LPG was found to have a sensitivity of 4.847 nm/refractive index unit. Bao et al. (2013), therefore, demonstrated proof-of-concept for deploying LPGs downhole for measurement of the injected CO_2 plume. Below 400 m depth, CO_2 and seawater are likely to be in a liquid-liquid mixture because deep seawater is usually cooler than 8^{o}C. Also, at the pressures tested, CO_2 droplets are likely to be coated in hydrates in cooler temperatures (Figure 8.4; Dewar et al., 2013). Since this could affect sensor signal, more work is needed to characterise the signal for these conditions.

At atmospheric pressure, less CO_2 is able to dissolve in solution than in higher pressure environments, and in the range of refractive index of brine-CO_2 solutions (<1.336), LPGs are less sensitive. Melo et al. (2014) therefore developed a polystyrene coated LPG (Melo et al., 2014). Coatings that have refractive indices higher than the cladding (refractive index > 1.44), can enhance the sensitivity of the LPG (Rees et al., 2002; Melo et al., 2014). With the polystyrene coating, Melo et al. (2014) demonstrated that the LPG was able to distinguish between N_2 and CO_2 gases. The refractive indices of these two gases are very close: 1.00027 and 1.00029, respectively (Melo et al., 2014), yet the wavelength shift was 138 $\pm$ 8 pm when 100 % CO_2 was replaced with 100 % N_2 (Melo et al., 2014). This method demonstrated that the sensitivity of LPGs could be enhanced in the lower refractive index range when coated with this specialised polystyrene coating. It seems likely that these coated sensors could be appropriate for marine seafloor sensing.

8.7.5 Impact of Marine Environment on Equipment

Marine environments can be hard on equipment. Laying seafloor cable in difficult to access monitoring sites can be a challenge, especially in areas with strong tidal dynamics. Inaccessibility of monitoring sites also means that equipment needs to

be robust and able to be deployed for extended periods without maintenance. Electronics at the measurement site may lead to requirements for battery replacement and other maintenance that may prove difficult in remote environments (Graziani et al., 2014). Also, in many aquatic environments, biofouling of sensing equipment can occur rapidly, with attachment occurring within 1 to 24 h (Chambers et al., 2006), interfering with sensor response and reducing sensor sensitivity. These challenges make distributed seafloor sensing difficult and may be why distributed sensing is more advanced at land-based monitoring sites than at marine sites.

8.8 Marine CO_2 Sensing Challenges

In both the terrestrial and marine contexts, injected CO_2 can migrate in the subsurface, causing leakage to occur away from the initial injection site (Figure 8.2, but marine sensing poses particular challenges because escaping CO_2 may disperse rapidly in the marine environment, and the residual plume may be diffuse (Figure 8.2). Furthermore, seafloor monitoring sites are relatively inaccessible compared to surface monitoring in the terrestrial environment. The phase of the escaping CO_2 plume may also vary depending on temperature and pressure of the leakage environment (Dewar et al., 2013, Figure 8.4). Spatial and temporal variation in background concentrations of temperature, DIC and pCO_2, combined with the diffuse nature of a marine CO_2 plume, pose challenges in distinguishing CO_2 seepage and leakage from background variability (Graziani et al., 2014). Characterising the phase and scale of expected seepage or leakage events is therefore needed to estimate the SNR for a given site and sensing method. Beyond sensing concerns, the marine environment is challenging due to the relative inaccessibility of measurement sites and the harshness of the marine environment on equipment.

8.8.1 Concentration of CO_2 at the Seepage and Leakage Site

Based on the modelled pH perturbations discussed in Section 8.4.2, and given the pH-dissolved CO_2 relationship in the highly buffered marine context, it is possible to reverse model dissolved CO_2 concentration at the leakage site. Estimates of dissolved CO_2 were derived using *Phreeqc 2.1* based on the modelled pH perturbation, marine average dissolved ions (Bruland and Lohan, 2006) and buffering capacity (Bruland

and Lohan, 2006), and an estimated marine pH of 8.1 (Table 8.8.3), and estimated temperature of 4^{o}C. In terms of localised acidification, the estimated pH change within the immediate leakage site can be as great as -1 (Blackford et al., 2008) to -2.5 (Dewar et al., 2013) pH units, for large leaks, with a concentration at leakage site >2.81x10^{-4} mmol kg^{-1} to shift pH -1 units downward and > 7.12x10^{-1} mmol kg^{-1} to shift pH downward by as much as -2.5 units. Smaller seeps see pH shifts < -0.12 pH units, below the range of natural variability (Blackford et al., 2009; Table 8.8.3).

8.8.2 CO_2 Dissolution Characteristics and Plume Dynamics

It is reasonable to assume that most CO_2 will dissolve in the water column before reaching the ocean-atmosphere interface (Dewar et al., 2013); however, the phase of the escaping CO_2 may vary at the leakage site. Temperature (determined mostly by latitude and season) and pressure (determined by depth) will influence the phase of dispersion at the leakage site (Dewar et al., 2013). Phase, leakage rate (discussed in the next section), and bubble size are likely to be the dominant drivers of plume dispersion characteristics (Dewar et al., 2013), though tidal dynamics and associated currents also influence horizontal mixing and dispersion (Blackford et al., 2008; Dewar et al., 2013).

In the range of likely pressures and temperatures expected in the marine environment, the phase of escaping CO_2 can take two forms: gas bubbles or liquid CO_2 droplets (Figure 8.4). In shallower environments (above 350 m), CO_2 is likely to take the form of gas bubbles (Dewar et al., 2013). Gas bubbles, being more buoyant than the seawater, will rise quickly in the water column, ultimately dissolving before reaching the ocean surface. Larger bubbles will rise more quickly; bubble size (estimated to range from 5-8 mm) is determined by several factors, including the circumference of the leakage channel, leakage depth, and ocean currents (Dewar et al., 2013). As the escaping CO_2 dissolves, this CO_2-rich seawater may eventually form a downward moving plume, as the solution becomes less buoyant (Dewar et al., 2013; Song et al., 2005; Metz et al., 2005). Liquid CO_2, is possible at depths below 350 m, depending on temperature (Dewar et al., 2013; Figure 8.4). Dewar et al. (2013) suggest that both liquid droplets and gas bubbles will be fully dissolved at 31 % of the height of the water column. Though liquid CO_2 is unlikely to dissolve in solution, merely

forming a mixture with seawater (Song et al., 2005), so pressures would need to drop sufficiently for CO_2 to be in gas phase before dissolution.

At depths below 180 m and temperatures below 4^oC, it is possible that CO_2 hydrate coatings may form instantaneously around the escaping CO_2 bubbles or droplets (Dewar et al., 2013; Tsouris et al., 2007; Figure 8.4). Mean ocean temperatures in mid to high latitude zones are below 4^oC year round (Figure 8.4; Locarnini et al., 2013). There are several sites in the North Sea that meet these temperature and pressure criteria: e.g., the Norwegian Channel (Dewar et al., 2013). These hydrate coatings affect dispersion dynamics and also have implications for sensing strategies. It is possible that these CO_2 hydrates will form crystalline structures on the seafloor, thus dispersing less readily than a dissolved or liquid CO_2 plume. Many traditional dissolved CO_2 sensors, referred to as pCO_2 sensors, rely on the dissolved CO_2 being degassed, and then titrated. The crystalline structures formed by CO_2 hydrates may not be easily degassed at depth without first increasing the temperature of solution. Fibre optic CO_2 sensors rely on shifts in refractive index of the surrounding medium to detect an increase in CO_2 concentration; the refractive index shift generated by a leak of the same scale, but one in gas phase, or liquid phase, or with hydrate coatings is something that needs to be characterised by sensor developers. It is important to note that even in the absence of hydrate formation, pressure can play a role in dispersion dynamics: higher pressure environments would impact buoyancy and ultimately plume dispersion.

Strong tidal and bottom currents are likely to contribute to horizontal mixing of the CO_2 plume (Blackford et al., 2008). Blackford et al. (2008) suggest that in an area with strong tidal currents like those found in the NorthWestern European Continental Shelf (Holt and James, 2001), it is reasonable to assume even mixing in a 49 km^2 area around the leakage site, within several days of the initial leak. Though modelling output suggests small, locally acidified parcels may be contained within the dispersed plume (Blackford et al., 2008). Even initially, these currents could impact values measured by CO_2 sensors. For example, in high-current environments, it is likely that CO_2 sensors will only be able to detect a portion of the escaping CO_2. Graziani et al. (2014) suggest that in horizontal currents of 10 cm s^{-1}, some values measured by their mini-pCO_2 sensors may be as low as 65 % of the actual concentration value

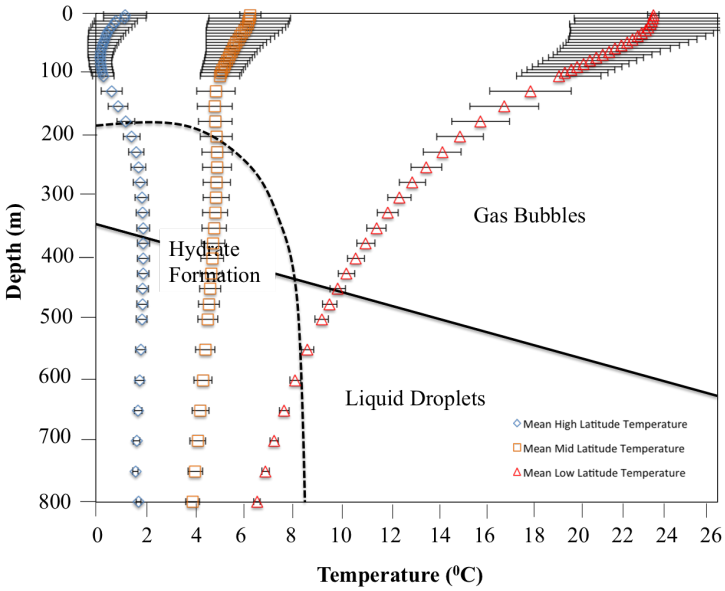

Figure 8.4: Conceptual components modified from Dewar et al. (2013): dashed line shows stability of hydrates. Solid line shows delineation between liquid and dissolved phase bubbles with pressure and temperature. Superimposed with temperature data from Locarnini et al. (2013): Blue diamonds indicate mean temperatures for high latitude ($>60^o$) marine environments by depth. Orange squares denote mid-latitude ($<60^o$ and $>45^o$) mean ocean temperatures by depth. Red triangles indicate low latitude ($>45^o$) mean ocean temperatures by depth. Error bars denote standard deviation, n<10 for each measurement site.

of escaping CO_2.Tidal and bottom currents also help determine maximum plume height (Dewar et al., 2013). In areas with weaker currents, dispersion is expected to be less, and high leakage scenarios in these regions are likely to lead to the highest concentrations of CO_2 and pH perturbations (Haugan and Drange, 1996; Cole et al., 1993).

8.8.3 Background Variability in Key Variables

Background variability in terms of temperature and pH and their influence on dissolved CO_2 concentration will be a challenge. Marine pH can range from 7.7 to 8.2 (Haugan and Drange, 1996). High latitude surface waters tend to have higher pH, especially in summer, while bottom water tends to be in the lower pH range (Haugan and Drange, 1996). Regional pH typically varies by between 0.2 and 0.3, but variability can be as high as 1.0 (Blackford et al., 2013).

Temperature varies both spatially and temporally. Deep water temperatures do vary significantly by latitude and depth (Figure 8.4; Locarnini et al., 2013). Local spatial variability in temperature is quite complex in shallower environments, though deeper temperatures tend to be quite stable. As an example, 14 years of moored data in collection for near-bottom water in the Bering Strait only varied from -1.8 ^{o}C to 2.3 ^{o}C, seasonally (Woodgate et al., 2005). In winter months, standard deviations did not exceed 0.03 ^{o}C in winter. In summer months standard deviations were as high as 1 ^{0}C For pCO_2 spatial and temporal variability are also a factor. In the North Sea, for example, dissolved CO_2 can range from 200 to 450 μatm (Blackford et al., 2013).

Boundary conditions, like riverine inputs and surrounding land use also influence dissolved inorganic carbon (of which dissolved CO_2 is a component) concentrations (Blackford et al., 2013). In the subtropical North Atlantic, Bates et al. (1996) found variability in pCO_2 to be ± 3.4 μmol L^{-1}. Organic processes also contribute to dissolved CO_2 concentrations, and these organic inputs vary spatially, seasonally, and diurnally (Blackford et al., 2013). Local variations in salinity are relatively stable. In the moored data collected in the Bering Strait, salinity only varied by 0.5-1 psu (Woodgate et al., 2005).

Table 8.1: Leakage and Seepage Scenarios and Expected pCO_2 Concentrations

Scenario	**Input Rate (mmol m^{-2} d^{-1})**	**pH Anomaly**	**dCO_2 Concentration (mmol kg^{-1})**
Low seepage	3.85 x 10^0*	Insignificant *	2.61x10^{-2}
High seepage	3.85 x 10^2 *	-0.12 *	3.34x10^{-2}
Short-term leak-low	6.93 x 10^3 *	-0.2 *	4.26x10^{-2}
Short-term leak-high	6.93 x 10^4 *	-0.5 *	8.72x10^{-2}
Long-term leak	6.93 x 10^3 *	-1 *	2.81x10^{-1}
Large-scale leakage	n/a	-2.51**	8.96x10^0

*Value came from Blackford et al. (2009)
**Value came from Dewar et al. (2013)

8.8.4 Characterising Signal and Noise, and Estimating Signal-to-Noise Ratio

8.8.4.1 Signal Component for Fibre Optic Sensors

Characterizing a seepage or leakage signal for refractive index-based sensors is challenging because the scale of the signal is a function of the change in refractive index of the surrounding medium. Because CO_2 may escape in many forms (gas, liquid, or gas bubbles or liquid droplets with hydrate coatings), the refractive index shift may be different depending on the *in situ* pressure and temperature conditions (which will drive the phase of escaping CO_2), even for leaks of the same scale. In terms of background variability, anything which modifies the refractive index of the surrounding medium could contribute to signal drift and noise. This includes biofilm growth on the sensing portion of the fibre and background variability in temperature.

Thinking first about the signal, in shallower environments (<180 m depth), a slower seep, where $CO_{2(g)}$ has a chance to dissolve before the sensor is able to detect the seeping CO_2, refractive index shift would depend on the amount of CO_2 dissolved in solution; however, at this scale of seepage, the concentration of dissolved CO_2 is likely to be below $< 8.72\text{x}10^{-2}$ mol kg^{-1} (Table 8.8.3). For refractive index-based sensors, even the coated LPG, may be unable to detect a refractive index shift. The refractive index is likely to be stable to at least the fifth decimal place. In these slow seep scenarios, miniature NDIR sensors show more promise than fibre optic sensors.

In shallow seepage or leakage scenarios, initially, CO_2 is expected to take the form

of gas bubbles (Figure 8.4, Dewar et al., 2013). If the sensor is close enough to the leakage or seepage site, it would be able to detect changes between gas phase CO_2 and seawater, the refractive index, and subsequent wavelength shift would be quite large. The scale of leakage is not important; if the sensor detects a bubble in gas phase, the refractive index change will cause a wavelength shift. A more sustained wavelength shift may suggest a larger scale leak, but regardless of the scale of the leak, the wavelength shift is likely to be the same. Taking the uncoated LPG discussed above as an example: the LPG has a sensitivity of 4.847 nm per refractive index unit, the refractive index of seawater from the literature is 1.3399 (at 0 ^{o}C and 30 psu), and the refractive index of $CO_{2(g)}$ is 1.0004, the wavelength shift may be as high as 1.6 nm. There is an added complexity in that if bubbles, which have complex refractive indices, brush the surface of the fibre without a clear change in phase around the LPG, wavelength shift could be different and less consistent than a clear change in phase around the fibre. This is in part a concern because bubble diameter may be smaller than the 2.5 cm length of the LPG (Dewar et al., 2013; Bao et al., 2013).

At depths, where escaping CO_2 would be in liquid phase, CO_2 and seawater are assumed to be in a mixture, since CO_2 is relatively immiscible in liquid phase. In this circumstance, refractive index may shift sufficiently to detect a leak. For liquid-liquid mixtures, a modified Lorentz-Lorenz equation can be used to calculate refractive index (Equation (8.1); Tasic et al., 1992), "with the implicit restriction that the molecules(or particles) may be considered as dipoles or assemblies of dipoles induced by an external field" (Heller, 1965):

$$(\frac{n_{12}^2-1}{n_{12}^2+2}) = \phi_1(\frac{n_1^2-1}{n_1^2+2}) + \phi_2(\frac{n_2^2-1}{n_2^2+2}) \tag{8.1}$$

where $\phi_i = \omega\rho_{12}/\rho_i, \omega = m_i/(m_1+m_2)$, and $i = 1$ and 2

From the Lorentz-Lorenz equation, it is apparent that ρ is an important driver of refractive index. Song et al. (2005) investigated the relationship between the concentration of $CO_{2(l)}$ mixed with seawater and the ρ of the mixture in pressures >49

atm (corresponding to depths of 500 m). The authors found an approximately linear relationship with concentration of CO_2 and density of solution. Different refractive index and wavelength shifts were calculated using the Song et al. (2005) data and the Lorentz-Lorenz equation for the leakage and seepage scenarios identified in Table 8.8.3. Song et al. (2005) found the ρ relationship of 0.273 g mL^{-1} per g increase in $CO_{2(l)}$ in seawater mixture. Using this ρ relationship and the Lorentz-Lorenz equation, the estimated wavelength shifts for and uncoated LPG in a mixture of $CO_{2(l)}$ even in the large leak scenario defined by Dewar et al. (2013), results in a relatively low CO_2 concentration and is therefore unlikely to generate a wavelength shift of more than 1 pm. Perhaps work with coated LPGs will be able to improve resolution in these scenarios once testing moves beyond the gas phase.

Despite the promise of improved resolution with added work on coated LPGs, the limited potential for uncoated LPGs to detect CO_2 leakage when CO_2 is in liquid phase is not of great concern because scenarios where escaping CO_2 is purely in liquid phase are likely to be relatively uncommon. At depths below 180 m, in temperatures below 8^oC (which is most deepwater CCS sites), it is likely that hydrate coating will form instantaneously between the CO_2 bubble- or droplet-seawater interface. These hydrates are likely to change the optical properties of the CO_2 plume, though the literature on the refractive index or other optical properties of CO_2 hydrates is sparse. It is likely that these crystalline structures will alter refractive index more than liquid CO_2; however, droplets with hard outer hydrate coatings could also damage equipment, and may pose increased challenges for sensor developers. It is clear that research into the optical properties of CO_2 hydrates and/or mechanisms to break apart the hydrate coating prior to interaction with the sensor is essential to development of MMV sensors, especially, given the fact that most marine geologic sequestration sites are under development for cold water environments (Figure 8.1).

8.8.4.2 Noise Component for Long Period Grating Sensors

Noise is likely to be influenced by both instrument error and background variability. Instrument error is likely to account for only $\tilde{5}$ pm of the noise, since that is typically the standard deviation measured when an LPG is immersed in triply deionized water, with temperature effects removed (Chapter 5). Environmental factors are likely to

play a larger role in signal drift and noise: biofouling of the sensors and temperature variability. Thus far, investigation has focused on the effect of biofilm growth on uncoated LPGs (Bhatia and Risk, 2015). In other evanescent field sensors, these variables could have a different effect on noise, beyond simply added influence due to enhanced sensitivity. The concentration of dissolved CO_2 is too low in the marine environment to detected by the sensor, and salinity is not likely to vary sufficiently to alter refractive index in the range of sensitivity of the LPG (even a 5 psu shift only corresponds to 1 change in RIU at 0^oC (Millard and Seaver, 1990).

Biofouling, though, can cause a refractive index shift in the sensor baseline. Previous biofouling work by (Chapter 5) showed that biofouling can shift the baseline wavelength higher by between 40 and 87 pm. Temperature may vary by several degrees, especially seasonally. For example, as mentioned above, seasonal temperature collected in the Bering Strait showed an annual range in temperature of 4.1^oC, though diurnal variability would probably be considerably less. Some studies have found temperature sensitivity as high as 100 pm shift per ^oC (Bhatia, 1999; James and Tatam, 2003); however, temperature dependence can be ascertained prior to deployment, and the sensor can be paired with a temperature sensor to ultimately back out most of the temperature signal from the data, limiting temperature-driven drift to within 5 -10 pm with changes of up to 5 ^oC in temperature based on field tests (Chapter 6). Total noise and drift is difficult to characterise because there is considerable variability in the biofouling signal, as well as inter-sensor variability in temperature response. Nonetheless, it is worthwhile to make a conservative estimate of the noise expected *in situ*. Taking the corrected temperature and biofouling effects together, it is possible that noise and drift could be as high as 100 pm.

8.8.4.3 Signal-to-Noise Ratio for Long Period Grating Sensors and Miniature NDIR

If we use this 100 pm value as the baseline 'noise' in LPGs, and we consider the scale of the signals discussed above, we can estimate SNR for LPGs under different leakage and seepage scenarios (Table 8.8.4.3), and for the different phases in which CO_2 might escape from a geologic sequestration site. As mentioned above, signal for uncoated LPGs is virtually 0 for liquid phase CO_2 at the concentrations for the various leakage

Table 8.2: Signal-to-Noise Ratios for Uncoated LPGs (Gas Phase) and Miniature NDIR Sensors under Different Leakage/Seepage Conditions

Scenario	**CO_2 Concentration (mmol kg^{-1})**	**LPG(Gas Phase)**			NDIR	
		Noise	*Signal (pm)*	*SNR*	*Noise (μmol L^{-1})*	*SNR*
Low seepage	$2.61x10^{-2}$	100	–*	–*	3.4	8.7
High seepage	$3.34x10^{-2}$	100	–*	–*	3.4	11.3
Short-term leak-low	$4.26x10^{-2}$	100	1600	16	3.4	14.2
Short-term leak-high	$8.72x10^{-2}$	100	1600	16	3.4	29
Long-term leak	$2.81x10^{-1}$	100	1600	16	3.4	93.6
Large-scale leakage	$8.96x10^{0}$	100	1600	16	3.4	2986

*pCO_2 likely to be in dissolved phase in concentrations below sensor detection limits.

or seepage scenarios considered, and for small leaks where escaping CO_2 is likely to be in aqueous or dissolved phase; however, the signal for gas bubbles is expected to be quite strong, with a conservative estimate of 1600 pm shift between seawater and $CO_{2(g)}$ (Table 8.8.4.3). These values suggest a SNR of 16 for leaks of sufficient scale for escaping CO_2 to be in gas phase. Though scale of leakage or seepage does not affect SNR in uncoated LPGs, duration of the signal shift generated by the leak or seep could give some indication as to the magnitude of the escaping CO_2 plume. Bubbles would dissolve quickly for seeps or leaks smaller than $3.34x10^{-2}$ mmol kg^{-1}, and thus escaping CO_2 would likely be undetectable by the sensor.

Though insufficient investigation has occurred to ascertain SNR for other types of fibre optic CO_2 sensors, a comparison to the only other distributed CO_2 sensor in the field testing stage, miniature NDIR sensors (Graziani et al., 2014), is useful (Table 8.8.4.3. Stability testing found a 3 σ value of ± 10 μmols(Graziani et al., 2014). Sensitivity analysis showed a detection limit of 0.68μmol L^{-1} (Graziani et al., 2014). At high temperatures, Graziani et al. (2014) estimated accuracy to be ± 2 % and at low temperatures within ± 10 %. Noise due to electromagnetic interference and also temperature variability were found to be minimal, therefore for these mini-NDIR sensors, the principal driver of noise is likely to be background variability in CO_2 concentration. Using the variability in the water column measurements for CO_2 from the Subtropical North Atlantic Gyre as an example, Bates et al. (1996) found water column variability for pCO_2 of ± 3.4 μmol L^{-1}. As with LPGs, the signal is likely to be driven by local CO_2 concentration at the leakage or seepage site. Therefore assuming a noise value of 3.4 μmol L^{-1}, the SNR for even the smallest leakage scenario would be 8.7 or greater (Table 8.8.4.3). In addition, unlike uncoated LPGs, signal-to-noise ratio for mini-NDIR sensors increases with increasing concentration of CO_2.

8.9 Challenges and Future Opportunities for Fibre Optic Direct Sensors in MMV Applications

8.9.1 Anti-Biofouling Techniques and Future Antifouling Work

Beyond contributing to signal drift and noise, biofouling can also reduce sensor sensitivity to changes in the refractive index of the surrounding environment. In a series of laboratory experiments, Bhatia et al. (2014) found that biofouling reduced the sensitivity of long period grating fibre optic sensors (LPGs) by between 37 and 65 % over 48 h of bacterial growth on an LPG immersed in nutrient-dense synthetic seawater. Mechanical cleaning of the sensor restored sensor sensitivity (Bhatia et al., 2014); however, in a marine environment, mechanical cleaning may be impossible or impractical depending on the location of the sensor network.

Historically, toxic products like lead, arsenic, and mercury-based products were used, but they were banned due to their adverse effects. Subsequently, tributylin-based products were used as highly effective anti-fouling agents, but they were banned in 2003 (Chambers et al., 2006) due to adverse effects on marine organisms, from shell deformation in oysters to immunological defects in certain fish species (Yebra et al., 2004), and bioaccumulation in seals and ducks (Chambers et al., 2006). Copper and zinc-based products are readily available (Chambers et al., 2006) and these products could be effectively paired with fibre optic sensors, serving the dual purpose of antifouling and if formed as part of a hard cylinder, a protective housing for the sensor as well; however, these products also tend to persist in sediments and are also inconsistent in the amount of biocide that they leach.

Moving away from metals, terrestrial pesticides have also been considered, but discounted due to their persistence in the environment and because the pesticides tend to be either too species specific, or too broad (Chambers et al., 2006). Foul release coatings, like silica-based polymer coatings have been shown to be quite effective (Chambers et al., 2006) and may act as interim replacements for trybutylin-based paints and coatings until new antifouling products are found. These coatings could be painted on housing surrounding a fibre optic sensor, preventing adhesion and fouling. This mechanism appears to be the most promising antifouling method available to-date and should be explored further, initially through laboratory experiments with

housed fibre optic sensors, where the housing is coated in a foul release coating and subject to fouling.

8.9.2 Solutions and Future Development Opportunities

Beyond fouling, several other challenges need to be overcome prior to commercialization for fibre optic CO_2 sensors. Taking LPGs as an example, consistency needs to be improved. Some off-the-shelf LPGs perform considerably better than others in terms of sensitivity and durability. Perhaps development of in-house fabrication techniques will improve quality control and reliability of sensor performance. Long period gratings on their own can be quite fragile. Protective encasements still need to be developed for *in situ* deployment. Temperature dependence of LPGs also is challenging. Rapid changes in temperature may make temperature compensation difficult since temperature sensors deployed with the LPGs may respond at a different rate to the temperature change than LPGs. Standard telecommunications LPGs (the LPGs used in this work) have temperature sensitivities that range from 30 to 100 pm $^oC^{-1}$. In Chapter 6, it was hypothesised that certain rapid shifts in sensor signal that could not be explained by biofouling may in fact have been due to inadequate temperature compensation. At depth, temperature is not expected to vary considerably (NOAA data suggests $<1^oC$ seasonally), but it is possible that in some instances, rapid temperature shifts could occur.

More work is needed to confirm that these rapid signal shifts were in fact due to temperature. Once this effect is confirmed, a solution to detect these shifts, or remove temperature effects more consistently is needed for successful deployment for CCUS monitoring because temperature effects could be large enough to mimic a seepage or leakage signal. In Chapters 5 and 6, Campbell Scientific 107 Thermistors were used to monitor temperature. Tests should be conducted with temperature sensors that respond more rapidly to temperature shifts than the Campbell Scientific 107 Thermistors. Sensors with more rapid response to temperature effects may be better able to remove temperature effects from the LPG signal. Alternatively, temperature compensated LPGs have been developed by shortening the period of the gratings, causing coupling to higher order cladding modes. The attenuation bands of theses modes have much lower responsiveness to temperature (1.8 pm ^oC; James and Tatam,

2003). Properties of these LPGs require further investigation because most discussion around these temperature insensitive LPGs pertains to strain applications, where refractive index sensitivity is not discussed (Bhatia, 1997; Wang et al., 2006); it is possible that their attenuation spectra are not suited for signals in the range of refractive indices of interest.

In terms of the plume itself, more work is needed to characterise the effect of hydrates on sensor response and function. Most laboratory work has focused on CO_2 either in gas, liquid, or supercritical phase, but given the temperature and pressure conditions of the marine environment, hydrate coatings are likely to form under many circumstances. Modelling is needed to characterise the refractive index of CO_2 hydrates, laboratory tests with the sensor should be conducted in pressure and temperature conditions where hydrates are allowed to form, both to characterise the impact on sensor response and to see if hard, hydrate coatings lead to sensor breakage. More work is also needed *in situ*, with controlled CO_2 release to test the sensors' ability to detect the CO_2 plume (whether in gas, liquid, or dissolved gas phase), understand how durable the sensors will be, and more rigorously test the impact of background variability on long-term signal drift and noise. Fibre optic sensors show promise because they are capable of continuous, direct sensing, they can be deployed in a distributed manner, they require no electronics at the measurement site, and they can transmit signals over long distances with minimal losses. Further *in situ* characterization is worth pursuing and necessary to improve MMV capabilities at sub-seafloor geologic carbon dioxide sequestration sites.

8.9.2.1 Technology Readiness Level

The basic operating principles are well established for all three fibre optic sensors discussed in this review. Experimental advances published in the literature were able to characterise the relationship of sensor response to the surrounding medium (e.g., James and Tatam, 2003; Xu et al., 2013). Fibre optic CO_2 sensors to be used in seafloor monitoring have strong potential as a tool in MMV at sub-seafloor geologic sequestration sites. Though the spectroscopy-based evanescent field sensor achieved initial proof-of-concept in 2003 (Choudhury and Yoshino, 2004), recent work demonstrated that long period grating sensors and fibre tip sensors were also able to detect

CO_2 in high pressure and atmospheric pressure environments (Burton et al., 2014; Melo et al., 2014; Bao et al., 2013). This recent work achieved laboratory proof-of-concept for down-hole applications for LPGs, and seafloor applications for the fibre tip sensor (Bao et al., 2013). Preliminary analysis of SNR revealed that even uncoated LPGs would be sensitive to CO_2 escaping in gas phase. Once more work is completed to ascertain the noise component of other fibre optic sensors discussed in this review, improvements to SNR may be seen for fibre optic CO_2 sensors.

To achieve laboratory proof-of-concept for LPGs in seafloor environments, more experimental work is needed in solutions that mimic the marine environment. All fibre optic sensors discussed in this paper need to be tested in the target environment to achieve *in situ* validation, though work completed in previous chapters already characterised individual application challenges, like biofouling and interference from non-target species for uncoated LPGs (Bhatia and Risk, 2015; Chapter 5). These factors should also be tested with the more sensitive coated LPGs. Future work to effectively deal with rapid temperature shifts, should they occur in the marine environment, to overcome the effect of biofouling with antifouling techniques, and to characterise the effect of hydrate coatings on LPGs and other fibre optic sensors is needed to move towards longer-term field trials, and ultimately commercialisation of fibre optic CO_2 sensing technology.

8.10 Conclusion

This review addressed some of the key challenge for sensor developers of refractive index-based fibre optic sensors for seafloor monitoring of CCUS sites. Under the range of seepage and leakage scenarios given, it appears that the phase of leakages or seepage is more important than the concentration of the escaping CO_2 plume to sensor signal; however, concentration of escaping CO_2 may determine the likelihood that a given sensing node would encounter a leak. The key drivers of noise for LPGs appear to be temperature and biofilm growth, with variation in salinity unlikely to affect an uncoated LPG. Distributed non-dispersive infrared spectroscopy may be more appropriate for small-scale seepage or leakage where CO_2 is in dissolved phase, but LPGs have a better SNR in gas phase.

Chapter 9

Conclusion

The aim of this thesis was to investigate the effects of the two most likely components of noise (biofouling and interference from non-target species) for Long Period Grating fibre optic sensors (LPGs) intended for seafloor monitoring of Carbon Capture, Utilisation, and Storage (CCUS) sites. These investigations assessed signal-to-noise ratios (SNR) for various leakage scenarios by integrating results from biofouling and interference work with an in-depth analysis of the likely signal response of uncoated LPGs to seepage and leakage scenarios of varying scales. The results from this integrated approach allowed for an assessment of the technology readiness level of LPGs as sensors for seafloor monitoring of CCUS sites.

For the first time in the literature, hydrochemical modelling, laboratory, and field trials assessed potential challenges associated with *in situ* deployment of LPGs to move development beyond the bench-testing stage. This built on previous work that served to either characterize LPG sensitivity (James and Tatam, 2003) or demonstrate the ability of LPGs to detect CO_2 in laboratory conditions(Bao et al., 2013; Melo et al., 2014), but did not yet consider the challenges associated with *in situ* deployment of these sensors. This work also considered solutions to overcome the challenges identified in the modelling, laboratory and field trials, ultimately advancing the technology readiness level of the LPGs, and bringing LPGs for detection of CO_2 closer to commercialisation. This advancement in development is important to foster regulatory acceptance of CCUS because robust monitoring provides insights into the safety and efficacy of the technology.

Uncertainties also emerged around potential field deployment of LPGs. For example, the effect of biofouling on sensors signal was shown to generate an upward wavelength shift; however, the scale and timing of this shift is as yet inconsistent. This inconsistency makes it challenging for calibrate out the signal if biofilm is not the target measured. On an optimistic note, however, one of the major themes to

emerge from this thesis is that challenges for a given target measurand may in fact also be a development opportunity in another field. Biofouling, for example, contributes to signal drift in dissolved CO_2 sensors, but also offers opportunities in biofilm sensing. Biofilm sensors could reduce maintenance costs for other equipment deployed in aquatic environments, but this work could also move beyond environmental monitoring, to monitor for water quality in industrial operations, and food quality, for example, measuring bacterial loads in milk. Future work should seek to overcome the challenges identified in this thesis: biofouling, temperature compensation, the effect of hydrate coatings on LPGs, but it should also look beyond the current target applications to other fields and applications.

Ongoing collaboration and interdisciplinary research are the keys to furthering sensor development and arriving at creative solutions to complex environmental problems. The applied nature of this research benefits from industry partnership and consultation so that research can target applications with commercial potential. This thesis would not have achieved the results it did without strong, interdisciplinary communication and support from experts in engineering, biofouling, chemistry, numerical modelling, and environmental science. Future research and development projects should consider a similar model for development.

Consideration of other fibre optic sensors for the target application should also be given. Research is already moving toward tapered optical fibres, but plastic optical fibres and other evanescent field sensors may be able to compliment LPGs in seafloor monitoring applications. Furthermore, advances made in LPG sensing could be applied to other evanescent field fibre optic sensors in earlier developmental stages. Future development should consider transferring some of the advances made in LPG development to these other sensors.

Fibre optics sensing is a rapidly developing field, and the deployment of these sensors are transforming telecommunications, structural health monitoring for bridges and equipment in the oil and gas sector. These sensors offer cheap, real-time sensing opportunities. Fibre optic sensors can transmit signals over long distances, but are also extremely compact and function well in high pressure environments. The oil and gas sector, and other industries are quickly adopting fibre optic sensing technology. For example, in the last three years, distributed acoustic fibre optic sensing moved

from the research and development stage to widespread commercialisation and adoption by the oil and gas sector. The advances made in fibre optics demonstrate the potential of this fast evolving field to transform sensing capabilities across sectors.

Bibliography

ABERCB, 2012. Shell Canada Limited: Application for the Quest Carbon Capture and Storage Project. Technical Report. Energy Resources Conservation Board. Calgary, Alberta.

Abu-Jaber, N.S., Wafa, N.A., 1996. Hydrochemistry of aquifers in the southern Dead Sea area, southern Jordan. Environmental Geology 28, 213–222.

Aller, R.C., 1980. Quantifying solute distributions in the bioturbated zone of marine sediments by defining an average microenvironment. Geochimica et Cosmochimica Acta 44, 1955–1965.

Almeida, F., Guimaraes, J., Jardim, W., 2001. Measuring the CO_2 flux at the air/water interface in lakes using flow injection analysis. Journal of Environmental Monitoring 3, 317–321.

Amin, S.A., Parker, M.S., Armbrust, E.V., 2012. Interactions between diatoms and bacteria. Microbiology and Molecular Biology Reviews 76, 667–684.

Aoki, N., Takahashi, A., Xue, Z., 2013. Development of a permanent OBC system for CCS monitoring in shallow marine environments. Energy Procedia 37, 4174–4181.

Appelo, C.A.J., Postma, D., 2005. Geochemistry, Groundwater and Pollution. CRC Press, Amsterdam, ND. 2 edition.

Ardelan, M.V., Steinnes, E., Lierhagen, S., Linde, S.O., 2009. Effects of experimental CO_2 leakage on solubility and transport of seven trace metals in seawater and sediment. Science of the Total Environment 407, 6255–6266.

Arts, R., Chadwick, A., Eiken, O., 2004. Recent time-lapse seismic data show no indication of leakage at the sleipner CO_2-injection site, in: Proceedings of the 7th International Conference on Greenhouse Gas Technologies (GHGT-7), pp. 653–662.

Austin, R., Halikas, G., 1976. The index of refraction of seawater. Technical Report. Scripps Institution of Oceanography. La Jolla, CA.

Bäckström, M., Nilsson, U., Hå kansson, K., Allard, B., Karlsson, S., 2003. Speciation of Heavy Metals in Road Runoff and Roadside Total Deposition. Water, Air, and Soil Pollution 147, 343–366.

Bao, B., Melo, L., Davies, B., Fadaei, H., Sinton, D., Wild, P., 2013. Detecting supercritical CO_2 in brine at sequestration pressure with an optical fiber sensor. Environmental Science & Technology 47, 306–13.

Barry, J., Buck, K., Lovera, C., Brewer, P., Seibel, B., Drazen, J., Tamburri, M., Whaling, P., Kuhnz, L., Pane, E., 2013. The response of abyssal organisms to low pH conditions during a series of CO_2-release experiments simulating deep-sea carbon sequestration. Deep Sea Research Part II: Topical Studies in Oceanography 92, 249–260.

Bates, N., Astor, Y., Church, M., Currie, K., Dore, J., Gonaález-Dávila, M., Lorenzoni, L., Muller-Karger, F., Olafsson, J., Santa-Casiano, M., 2014. A time-series view of changing ocean chemistry due to ocean uptake of anthropogenic CO_2 and ocean acidification. Oceanography 27, 126–141.

Bates, N.R., Michaels, A.F., Knap, A.H., 1996. Seasonal and interannual variability of oceanic carbon dioxide species at the us jgofs bermuda atlantic time-series study (bats) site. Deep Sea Research Part II: Topical Studies in Oceanography 43, 347–383.

Bellard, C., Bertelsmeier, C., Leadley, P., Thuiller, W., Courchamp, F., 2012. Impacts of climate change on the future of biodiversity. Ecology letters 15, 365–377.

Benson, S.M., Surles, T., 2006. Carbon Capture and Storage : An Overview With Emphasis on Capture and Storage in Deep Geological Formations, in: Proceedings of the IEEE, pp. 1795–1805.

Bhatia, S., Risk, D., 2015. Speciation in application environments for dissolved carbon dioxide sensors. Water, Air, & Soil Pollution 226, 1–16.

Bhatia, S., Risk, D., Pustam, A., Smith-Palmer, T., Burton, G., Melo, L., Wild, P., 2014. Biofouling of an All-Optical Sensor for Seafloor Monitoring of Marine Carbon Capture and Storage Sites. Energy Procedia 63, 3848–3852.

Bhatia, V., 1997. Temperature-insensitive and strain-insensitive long-period grating sensors for smart structures. Optical Engineering 36, 1872–1876.

Bhatia, V., 1999. Applications of long-period gratings to single and multi-parameter sensing. Optics Express 4, 457–466.

Birkle, P., Aragon, J., 2002. Evolution and origin of deep reservoir water at the Activo Luna oil field, Gulf of Mexico, Mexico. AAPG Bulletin 3, 457–484.

Blackford, J., Gilbert, F., 2007. pH variability and CO_2 induced acidification in the North Sea. Journal of Marine Systems 64, 229–241.

Blackford, J., Jones, N., Proctor, R., Holt, J., Widdicombe, S., Lowe, D., Rees, a., 2009. An initial assessment of the potential environmental impact of CO_2 escape from marine carbon capture and storage systems. Proceedings of the Institution of Mechanical Engineers, Part A: Journal of Power and Energy 223, 269–280.

Blackford, J., Stahl, H., Bull, J.M., Bergès, B.J., Cevatoglu, M., Lichtschlag, A., Connelly, D., James, R.H., Kita, J., Long, D., et al., 2014. Detection and impacts of leakage from sub-seafloor deep geological carbon dioxide storage. Nature Climate Change 4, 1011–1016.

Blackford, J.C., Jones, N., Proctor, R., Holt, J., 2008. Regional scale impacts of distinct CO_2 additions in the North Sea. Marine Pollution Bulletin 56, 1461–1468.

Blackford, J.C., Torres, R., Cazanave, P., Artioli, Y., 2013. Modelling dispersion of CO_2 plumes in sea water as an aid to monitoring and understanding ecological impact. Energy Procedia 37, 3379–3386.

Bourne, S., 2010. Measurement , Monitoring and Verification Plan. Technical Report November. Shell Canada Ltd.

Bozec, Y., Thomas, H., Schiettecatte, L.S., Borges, A.V., Elkalay, K., De Baar, H.J., 2006. Assessment of the processes controlling the seasonal variations of dissolved inorganic carbon in the north sea. Limnology and Oceanography 51, 2746–2762.

Bradshaw, A.L., Brewer, P.G., Shafer, D.K., Williams, R.T., 1981. Measurements of total carbon dioxide and alkalinity by potentiometric titration in the GEOSECS program. Earth and Planetary Science Letters 55, 99–115.

Brenner, H., Braeckman, U., Le Guitton, M., Meysman, F.J., 2016. The impact of sedimentary alkalinity release on the water column CO_2 system in the North Sea. Biogeosciences 13, 841–863.

Bruland, K., Lohan, M., 2006. Controls of trace metals in seawater, in: Elderfield, H., Holland, H., K., K., T. (Eds.), The oceans and marine geochemistry. Elsevier, pp. 23–47.

Burck, J., Conzen, J.P., Ache, H.J., 1992. A fiber optic evanescent field absorption sensor for monitoring organic contaminants in water. Fresenius' Journal of Analytical Chemistry 342, 394–400.

Burt, W., Thomas, H., Fennel, K., Horne, E., 2013. Sediment-water column fluxes of carbon, oxygen and nutrients in Bedford Basin, Nova Scotia, inferred from 224 Ra measurements. Biogeosciences 10, 53–66.

Burt, W., Thomas, H., Hagens, M., Pätsch, J., Clargo, N., Salt, L., Winde, V., Böttcher, M., 2016. Carbon sources in the North Sea evaluated by means of radium and stable carbon isotope tracers. Limnology and Oceanography .

Burt, W.J., Thomas, H., Ptsch, J., Omar, A.M., Schrum, C., Daewel, U., Brennar, H., Baar, H.J.W., 2014. Radium isotopes as a tracer of sediment-water column exchange in the North Sea. Global Biogeochemical Cycles 28, 786–804.

Burton, G., Melo, L., Warwick, S., Jun, M., Bao, B., Sinton, D., Wild, P., 2014. Fiber refractometer to detect and distinguish carbon dioxide and methane leakage in the deep ocean. International Journal of Greenhouse Gas Control 31, 41–47.

Campbell Scientific Inc., 2013. Sensor with antifouling control. Patent US 8429952 B1.

Campbell Scientific Inc., 2014. Model 107 temperature probe. Manual.

Caramanna, G., Voltattorni, N., Maroto-Valer, M.M., 2011. Is Panarea Island (Italy) a valid and cost-effective natural laboratory for the development of detection and monitoring techniques for submarine CO_2 seepage? Greenhouse Gases: Science and Technology 1, 200–210.

Carol, E.S., Kruse, E.E., 2012. Hydrochemical characterization of the water resources in the coastal environments of the outer Río de la Plata estuary, Argentina. Journal of South American Earth Sciences 37, 113–121.

Centeno, T.A., Fuertes, A.B., 2001. Carbon molecular sieve membranes derived from a phenolic resin supported on porous ceramic tubes. Separation and Purification Technology 25, 379–384.

Chadwick, R.A., Zweigel, P., Gregersen, U., Kirby, G.A., Holloway, S., Johannessen, P.N., 2004. Geological reservoir characterization of a CO_2 storage site: The Utsira Sand, Sleipner, northern North Sea. Energy 29, 1371–1381.

Chambers, L.D., Stokes, K.R., Walsh, F.C., Wood, R.J.K., 2006. Modern approaches to marine antifouling coatings. Surface and Coatings Technology 201, 3642–3652.

Chavez, F.P., Wright, D., Herlien, R., Kelley, M., Shane, F., Strutton, P.G., 2000. A device for protecting moored spectroradiometers from biofouling. Journal of Atmospheric and Oceanic Technology 17, 215–219.

Choudhury, P.K., Yoshino, T., 2004. On the fiber-optic chlorine sensor with enhanced sensitivity based on the study of evanescent field absorption spectroscopy. Optik 115, 329–333.

Chow, J., Watson, J., Herzon, A., Benson, S., Hidy, G., Gunter, W., Penkala, S., and White, C., 2003. Separation and Capture of CO_2 from Large Stationary Sources and Sequestration in Geological Formations. EM: Air and Waste Management Association's Magazine for Environmental Managers 53, 1172–1182.

Clargo, N.M., Salt, L.A., Thomas, H., de Baar, H.J., 2015. Rapid increase of observed DIC and pCO_2 in the surface waters of the North Sea in the 2001-2011 decade ascribed to climate change superimposed by biological processes. Marine Chemistry 177, 566–581.

Cole, K.H., Stegen, G.R., Spencer, D., 1993. The capacity of the deep oceans to absorb carbon dioxide. Energy Conversion and Management 34, 991–998.

Costerton, J.W., Stewart, P.S., Greenberg, E., 1999. Bacterial biofilms: a common cause of persistent infections. Science 284, 1318–1322.

Cowell, D., Ford, D., 1980. Hydrochemistry of a dolomite karst: the Bruce Peninsula of Ontario. Canadian Journal of Earth Sciences 17, 520–526.

Davis, R., Moore, C., Zaneveld, J., Napp, J., 1997. Reducing the effects of fouling on chlorophyll estimates derived from long-term deployments of optical instruments. Journal of Geophysical Research: Oceans (1978–2012) 102, 5851–5855.

De Vries, P., Tamis, J.E., Foekema, E.M., Klok, C., Murk, A.J., 2013. Towards quantitative ecological risk assessment of elevated carbon dioxide levels in the marine environment. Marine Pollution Bulletin 73, 516–523.

Dewar, M., Wei, W., McNeil, D., Chen, B., 2013. Small-scale modelling of the physiochemical impacts of CO_2 leaked from sub-seabed reservoirs or pipelines within the North Sea and surrounding waters. Marine Pollution Bulletin 73, 504–515.

Dickson, A., 1981. An exact definition of total alkalinity and a procedure for the estimation of alkalinity and total inorganic carbon from titration data. Deep-Sea Research 28A, 609?623.

Dickson, A.G., Sabine, C.L., Christian, J.R., 2007. Guide to best practices for ocean CO_2 measurements. Technical Report 8. PICES.

Doney, S.C., Fabry, V.J., Feely, R.a., Kleypas, J.a., 2009. Ocean acidification: the other CO_2 problem. Annual Review of Marine Science 1, 169–192.

Dotsika, E., Poutoukis, D., Michelot, J., Raco, B., 2009. Natural tracers for identifying the origin of the thermal fluids emerging along the Aegean Volcanic arc (Greece): Evidence of Arc-Type Magmatic Water (ATMW) participation. Journal of Volcanology and Geothermal Research 179, 19–32.

Fabry, V.J., Seibel, B.A., Feely, R.A., Orr, J.C., 2008. Impacts of ocean acidification on marine fauna and ecosystem processes. ICES Journal of Marine Science: Journal du Conseil 65, 414–432.

Falciai, R., Mignani, A., Vannini, A., 2001. Long period gratings as solution concentration sensors. Sensors and Actuators B: Chemical 74, 74–77.

Fletcher, M., 1977. The effects of culture concentration and age, time, and temperature on bacterial attachment to polystyrene. Canadian Journal of Microbiology 23, 1–6.

Friedrichs, G., Bock, J., Temps, F., Fietzek, P., Körtzinger, A., Wallace, D.W., 2010. Toward continuous monitoring of seawater $^{13}CO_2/^{12}CO_2$ isotope ratio and pCO_2: Performance of cavity ringdown spectroscopy and gas matrix effects. Limnology Oceanography: Methods 8, 539–551.

Friis, K., Krtzinger, A., Wallace, D.W.R., 2003. The salinity normalization of marine inorganic carbon chemistry data. Geophysical Research Letters 30, 1–3.

Gaston, A., Lozano, I., Perez, F., Auza, F., Sevilla, J., 2003. Evanescent wave optical-fiber sensing (temperature, relative humidity, and ph sensors). Sensors Journal, IEEE 3, 806–811.

Government of Alberta, 2012. Carbon Capture & Storage: Summary Report of the Regualtory Framework Assessment. Technical Report. Alberta Energy. Edmonton, Alberta.

Goyet, C., Walt, D.R., Brewer, P.G., 1992. Development of a fiber optic sensor for measurement of pCO_2 in sea water: design criteria and sea trials. Deep Sea Research Part A. Oceanographic Research Papers 39, 1015–1026.

Graziani, S., Beaubien, S.E., Bigi, S., Lombardi, S., La, R., Moro, P.A., 2014. Spatial and Temporal pCO_2 Marine Monitoring Near Panarea Island (Italy) Using Multiple Low-Cost GasPro Sensors. Environmental Science & Technology 48, 2126–12133.

Guinotte, J.M., Fabry, V.J., 2008. Ocean acidification and its potential effects on marine ecosystems. Annals of the New York Academy of Sciences 1134, 320–342.

Haugan, P., Drange, H., 1996. Effects of CO_2 on the environment. Energy Conversion Management 37, 1019–1022.

Heller, W., 1965. Remarks on refractive index mixture rules. The Journal of Physical Chemistry 69, 1123–1129.

Henrichs, S.M., 1992. Early diagenesis of organic matter in marine sediments: progress and perplexity. Marine Chemistry 39, 119–149.

Heupel, M., Reiss, K., Yeiser, B., Simpfendorfer, C., 2008. Effects of biofouling on performance of moored data logging acoustic receivers. Limnology and Oceanography: Methods 6, 327–335.

Hidalgo, M., Cruz-Sanjulián, J., 2001. Groundwater composition, hydrochemical evolution and mass transfer in a regional detrital aquifer (Baza basin, southern Spain). Applied Geochemistry 16, 745–758.

Hill, D.J., Kelly, C.J., 2012. Distributed Acoustic Sensing. Technical Report. US Patent App. 13/984,426.

Holt, J.T., James, I.D., 2001. An s coordinate density evolving model of the north-west European continental shelf 1, Model description and density structure against both on and off the shelf, the whole of the North Sea Project sources. Journal of Geophysical Research 106, 15–34.

Hutchinson, N., Nagarkar, S., Aitchison, J.C., Williams, G.A., 2006. Microspatial variation in marine biofilm abundance on intertidal rock surfaces. Aquatic Microbial Ecology 42, 87–197.

Hvidevold, H.K., Alendal, G., Johannessen, T., Ali, A., Mannseth, T., Avlesen, H., 2015. Layout of CCS monitoring infrastructure with highest probability of detecting a footprint of a CO_2 leak in a varying marine environment. International Journal of Greenhouse Gas Control 37, 274–279.

James, S.W., Tatam, R.P., 2003. Optical fibre long-period grating sensors: characteristics and application. Measurement Science and Technology 14, R49–R61.

Janssen, F., Huettel, M., Witte, U., 2005. Pore-water advection and solute fluxes in permeable marine sediments (ii): Benthic respiration at three sandy sites with different permeabilities (german bight, north sea). Limnology and Oceanography 50, 779–792.

Jeffries, D.S., Clair, T.A., Couture, S., Dillon, P.J., Dupont, J., Keller, W., McNicol, D.K., Turner, M.A., Vet, R., Weeber, R., 2003. Assessing the recovery of lakes in southeastern Canada from the effects of acidic deposition. AMBIO: A Journal of the Human Environment 32, 176–182.

Johannessen, K., Drakeley, B.K., Farhadiroushan, M., et al., 2012. Distributed acoustic sensing-a new way of listening to your well/reservoir, in: SPE Intelligent Energy International, Society of Petroleum Engineers. pp. 1–9.

Johnson, B., McNeil, C., 2008. System for the transfer and sensing of gas dissolved in liquid under pressure. US Patent 7,434,446.

Johnson, K.M., Dickson, A.G., Eischeid, G., Goyet, C., Guenther, P., Key, R.M., Millero, F.J., Purkerson, D., Sabine, C.L., Schottle, R.G., et al., 1998. Coulometric total carbon dioxide analysis for marine studies: assessment of the quality of total inorganic carbon measurements made during the US Indian Ocean CO_2 survey 1994–1996. Marine Chemistry 63, 21–37.

Kersey, A., Davis, M., Patrick, H., LeBlanc, M., Koo, K., Askins, C., Putnam, M., Friebele, E., 1997. Fiber grating sensors. Journal of Lightwave Technology 15, 1442–1463.

Kim, Y., Lee, K.S., Koh, D.C., Lee, D.H., Lee, S.G., Park, W.B., Koh, G.W., Woo, N.C., 2003. Hydrogeochemical and isotopic evidence of groundwater salinization in a coastal aquifer: a case study in Jeju volcanic island, Korea. Journal of Hydrology 270, 282–294.

Kongsjorden, H., Karstad, O., Torp, T.a., 1998. Saline aquifer storage of carbon dioxide in the Sleipner project. Waste Management 17, 303–308.

Korbøl, R., Kaddour, A., 1995. Sleipner vest CO_2 disposal - injection of removed CO_2 into the utsira formation. Energy Conversion and Management 36, 509–512.

Körtzinger, A., Mintrop, L., Duinker, J.C., 1999. The international intercomparison exercise of underway fco_2 systems during the r/v meteor cruise 36/1 in the north atlantic ocean. Carbon Dioxide Information Analysis Center, Oak Ridge National Laboratory , T.N. USA.

Kroeker, K.J., Kordas, R.L., Crim, R., Hendriks, I.E., Ramajo, L., Singh, G.S., Duarte, C.M., Gattuso, J.P., 2013. Impacts of ocean acidification on marine organisms: Quantifying sensitivities and interaction with warming. Global Change Biology 19, 1884–1896.

Kühn, W., Pätsch, J., Thomas, H., Borges, A.V., Schiettecatte, L.S., Bozec, Y., Prowe, A.F., 2010. Nitrogen and carbon cycling in the North Sea and exchange with the North Atlantic: A model study, Part II: Carbon budget and fluxes. Continental Shelf Research 30, 1701–1716.

Kumar, P.S., Vallabhan, C.P.G., Nampoori, V.P.N., Pillai, V.N.S., Radhakrishnan, P., 2002. A fibre optic evanescent wave sensor used for the detection of trace nitrites in water. Journal of Optics A: Pure and Applied Optics 4, 247–250.

Kurz, W.A., Dymond, C., Stinson, G., Rampley, G., Neilson, E., Carroll, A., Ebata, T., Safranyik, L., 2008. Mountain pine beetle and forest carbon feedback to climate change. Nature 452, 987–990.

Lee, J.W., Nam, J.H., Kim, Y.H., Lee, K.H., Lee, D.H., 2008. Bacterial communities in the initial stage of marine biofilm formation on artificial surfaces. Journal of Microbiology 46, 174–182.

Liu, X., Byrne, R.H., Adornato, L., Yates, K.K., Kaltenbacher, E., Ding, X., Yang, B., 2013. *In situ* spectrophotometric measurement of dissolved inorganic carbon in seawater. Environmental Science & Technology 47, 11106–14.

Locarnini, R., Mishonov, A., Antonov, J., Boyer, T., Garcia, H., Baranova, O., Zweng, M., Paver, C., Reagan, J., Johnson, D., Hamilton, M., Seidov, D., 2013. NOAA WORLD OCEAN ATLAS Volume 1: Temperature. Technical Report September. NOAA.

Lucklum, R., Henning, B., Hauptmann, P., Schierbaum, K.D., Vaihinger, S., Gopel, W., 1991. Quartz microbalance sensors for gas detection. Sensors and Actuators 27, 705–710.

Lueker, T.J., Dickson, A.G., Keeling, C.D., 2000. Ocean pCO_2 calculated from dissolved inorganic carbon, alkalinity, and equations for K1 and K2: validation based on laboratory measurements of CO_2 in gas and seawater at equilibrium. Marine Chemistry 70, 105–119.

Luff, R., Moll, A., 2004. Seasonal dynamics of the North Sea sediments using a three-dimensional coupled sediment–water model system. Continental Shelf Research 24, 1099–1127.

Manov, D.V., Chang, G.C., Dickey, T.D., 2004. Methods for reducing biofouling of moored optical sensors. Journal of Atmospheric and Oceanic Technology 21, 958–968.

Markusson, N., Kern, F., Watson, J., Arapostathis, S., Chalmers, H., Ghaleigh, N., Heptonstall, P., Pearson, P., Rossati, D., Russell, S., 2012. A socio-technical framework for assessing the viability of carbon capture and storage technology. Technological Forecasting and Social Change 79, 903–918.

Melo, L., Burton, G., Davies, B., Risk, D., Wild, P., 2014. Highly sensitive coated long period grating sensor for CO_2 detection at atmospheric pressure. Sensors and Actuators B: Chemical 202, 294–300.

Metz, B., Davidson, O., de Coninck, H., Loos, M., Meyer, L., et al., 2005. IPCC Special Report on Carbon Dioxide Capture and Storage. Technical Report. Intergovernmental Panel on Climate Change.

Millard, R., Seaver, G., 1990. An index of refraction algorithm for seawater over temperature, pressure, salinity, density, and wavelength. Deep Sea Research Part A. Oceanographic Research Papers 37, 1909–1926.

Monod, J., 1949. The growth of bacterial cultures. Annual Review of Microbiology 3, 371–394.

Mosello, R., 1984. Hydrochemistry of high altitude alpine lakes. Schweizerische Zeitschrift für Hydrologie 46, 86–99.

Munkholm, C., Walt, D.R., Milanovich, F.P., 1988. A fiber-optic sensor for CO_2 measurement. Talanta 35, 109–112.

Murray, F., Widdicombe, S., McNeill, C.L., Solan, M., 2013. Consequences of a simulated rapid ocean acidification event for benthic ecosystem processes and functions. Marine Pollution Bulletin 73, 435–442.

Nickerson, N., Risk, D., 2013. IUsing subsurface CO_2 concentrations and isotopologues to identify CO_2 seepage from CCS/CO_2 at EOR sites: A signal-to-noise based analysis. International Journal of Greenhouse Gas Control 14, 239–246.

Niklès, M., Vogel, B.H., Briffod, F., Grosswig, S., Sauser, F., Luebbecke, S., Bals, A., Pfeiffer, T., 2004. Leakage detection using fiber optics distributed temperature monitoring, in: Smart Structures and Materials, International Society for Optics and Photonics. pp. 18–25.

NOAA, 2016. Recent, Monthly Mean CO_2 at Mauna Loa. Technical Report.

Oldenburg, C., 2010. Comparative Assessment of Status and Opportunities for CO_2 Capture and Storage and Radioactive Waste Disposal in North America. Technical Report.

Orghici, R., Willer, U., Gierszewska, M., Waldvogel, S., Schade, W., 2008. Fiber optic evanescent field sensor for detection of explosives and CO_2 dissolved in water. Applied Physics B 90, 355–360.

Orr, J.C., Fabry, V.J., Aumont, O., Bopp, L., Doney, S.C., Feely, R.A., Gnanadesikan, A., Gruber, N., Ishida, A., Joos, F., et al., 2005. Anthropogenic ocean acidification over the twenty-first century and its impact on calcifying organisms. Nature 437, 681–686.

Pachouli, R., Meyer, L., 2014. IPCC, 2014: Climate Change 2014: Synthesis Report. Contribution of Working Groups I, II and III to the Fifth Assessment Report of the Intergovernmental Panel on Climate Change. Technical Report. IPCC, Geneva, Switzerland.

Papatheodorou, G., Demopoulou, G., Lambrakis, N., 2006. A long-term study of temporal hydrochemical data in a shallow lake using multivariate statistical techniques. Ecological Modelling 193, 759–776.

Parkhurst, D.L., Appelo, C., 1999. User's guide to *PHREEQC* (Version 2): A computer program for speciation, batch-reaction, one-dimensional transport, and inverse geochemical calculations. Technical Report. United States Geological Survey, Denver, CO.

Parmesan, C., Yohe, G., 2003. A globally coherent fingerprint of climate change impacts across natural systems. Nature 421, 37–42.

Patrick, H., Kersey, A., Bucholtz, F., 1998. Analysis of the response of long period fiber gratings to external index of refraction. Journal of Lightwave Technology 16, 1606–1612.

Pätsch, J., Lenhart, H., 2011. Daily nutrient loads of nutrients, total alkalinity, dissolved inorganic carbon and dissolved organic carbon of the European continental rivers for the years 1977–2009. Berichte aus dem Zentrum fur Meeres-und Klimaforschung. Reihe B: Ozeanographie 50.

Pavlovsky, L., Younger, J.G., Solomon, M.J., 2013. In situ rheology of staphylococcus epidermidis bacterial biofilms. Soft Matter 9, 122–131.

Payán, M.C., Verbinnen, B., Galan, B., Coz, A., Vandecasteele, C., Viguri, J.R., 2012. Potential influence of CO_2 release from a carbon capture storage site on release of trace metals from marine sediment. Environmental pollution 162, 29–39.

Philip-Chandy, R., Scully, P.J., Eldridge, P., Kadim, H., Grapin, M.G., Jonca, M.G., D'Ambrosio, M.G., Colin, F., 2000. An optical fiber sensor for biofilm measurement using intensity modulation and image analysis. IEEE Journal of Selected Topics in Quantum Electronics 6, 764–772.

Pierrot, D., Lewis, E., Wallace, D.W.R., 2006. MS Excel Program Developed for CO_2 System Calculations, ORNL/CDIAC-105a. Technical Report.

Pierrot, D., Neill, C., Sullivan, K., Castle, R., Wanninkhof, R., Lüger, H., Johannessen, T., Olsen, A., Feely, R.A., Cosca, C.E., 2009. Recommendations for autonomous underwater pCO_2 measuring systems and data-reduction routines. Deep Sea Research Part II: Topical Studies in Oceanography 56, 512–522.

Possetti, G., Kamikawachi, R., Prevedello, C., Muller, M., Fabris, J., 2009. Salinity measurement in water environment with a long period grating based interferometer. Measurement Science and Technology 20, 034003.

Provoost, P., Heuven, S.v., Soetaert, K., Laane, R., Middelburg, J., et al., 2010. Seasonal and long-term changes in pH in the Dutch coastal zone. Biogeosciences 7, 3869–3878.

Puckett, L., Cowdery, T., McMahon, P., Tornes, L., Stoner, J., 2002. Using chemical, hydrologic, and age dating analysis to delineate redox processes and flow paths in the riparian zone of a glacial outwash aquifer-stream system. Water Resources Research 38, 9–29.

Qian, P.Y., Lau, S.C.K., Dahms, H.U., Dobretsov, S., Harder, T., 2007. Marine biofilms as mediators of colonization by marine macroorganisms: implications for antifouling and aquaculture. Marine biotechnology (New York, N.Y.) 9, 399–410.

Queste, B.Y., Fernand, L., Jickells, T.D., Heywood, K.J., Hind, A.J., 2016. Drivers of summer oxygen depletion in the central North Sea. Biogeosciences 13, 1209–1222.

Rees, N.D., James, S.W., Tatam, R.P., Ashwell, G.J., 2002. Optical fiber long-period gratings with langmuir–blodgett thin-film overlays. Opt. Lett. 27, 686–688.

Reimer, A., Landmann, G., Kempe, S., 2008. Lake Van, Eastern Anatolia, hydrochemistry and history. Aquatic Geochemistry 15, 195–222.

Riding, J.B., Rochelle, C., 2005. The IEA Weyburn CO_2 Monitoring and Storage Project - Integrated results from Europe. Technical Report. International Energy Agency Greenhouse Gas Research and Development Programme.

Rodkey, F.L., 1966. Aqueous solutions and body fluids. their concentrative properties and conversion tables. Clinical Chemistry 12, 517–518.

Salt, L.A., Thomas, H., Prowe, A., Borges, A.V., Bozec, Y., Baar, H.J., 2013. Variability of North Sea pH and CO_2 in response to North Atlantic Oscillation forcing. Journal of Geophysical Research: Biogeosciences 118, 1584–1592.

Sandt, C., Smith-Palmer, T., Comeau, J., Pink, D., 2009. Quantification of water and biomass in small colony variant pao1 biofilms by confocal raman microspectroscopy. Applied Microbiology and Biotechnology 83, 1171–1182.

Schindler, D., 1986. The significance of in-lake production of alkalinity. Water, Air, and Soil Pollution 30, 931–944.

Schindler, D.W., 1988. Effects of acid rain on freshwater ecosystems. Science 239, 149–157.

Schuster, U., Hannides, a., Mintrop, L., Körtzinger, a., 2009. Sensors and instruments for oceanic dissolved carbon measurements. Ocean Science Discussions 6, 491–524.

Schwarzenbach, G., Meier, J., 1958. Formation and investigation of unstable protonation and deprotonation products of complexes in aqueous solution. Journal of inorganic and nuclear chemistry 8, 302–312.

Siegert, M.J., Tranter, M., Ellis-Evans, J.C., Priscu, J.C., Berry Lyons, W., 2003. The hydrochemistry of Lake Vostok and the potential for life in Antarctic subglacial lakes. Hydrological Processes 17, 795–814.

Smart, R., Soulsby, C., Neal, C., Wade, A., Cresser, M., Billett, M., Langan, S., Edwards, a., Jarvie, H., Owen, R., 1998. Factors regulating the spatial and temporal distribution of solute concentrations in a major river system in NE Scotland. The Science of The Total Environment 221, 93–110.

Song, Y., Chen, B., Nishio, M., Akai, M., 2005. The study on density change of carbon dioxide-seawater solution at high pressure and low temperature. Energy 30, 2298–2307.

Stoodley, P., Sauer, K., Davies, D.G., Costerton, J.W., 2002. Biofilms as complex differentiated communities. Annual Review of Microbiology 56, 187–209.

Striegl, R.G., Kortelainen, P., Chanton, J.P., Wickland, K.P., Bugna, G.C., Rantakari, M., . Carbon dioxide partial pressure and ^{13}C content of north temperate and Boreal lakes at spring ice melt. Limnology and Oceanography , 941–945.

Stumm, W., Morgan, J., 1996. Aquatic Chemistry; Chemical Equilibria and Rates in Natural Waters. Wiley Interscience, New York, NY, USA. 3rd edition.

Tait, K., Stahl, H., Taylor, P., Widdicombe, S., 2015. Rapid response of the active microbial community to CO_2 exposure from a controlled sub-seabed CO_2 leak in Ardmucknish Bay (Oban, Scotland). International Journal of Greenhouse Gas Control 38, 171–181.

Takahashi, T., Broecker, W., Bainbridge, A., 1981. The alkalinity and total carbon dioxide concentration in the world oceans. Carbon Cycle Modelling, SCOPE 16, 271–286.

Takahashi, T., Weiss, R.F., Culberson, C., Edmond, J., Hammond, D., Wong, C., Li, Y., Bainbridge, A., 1970. The alkalinity and total carbon dioxide concentration in the world oceans. Journal of Geophysical Research 75, 7648–7666.

Tasic, A.Z., Djordjevic, B.D., Grozdanic, D.K., Radojkovic, N., 1992. Use of mixing rules in predicting refractive indexes and specific refractivities for some binary liquid mixtures. Journal of Chemical & Engineering Data 37, 310–313.

Taylor, P., Stahl, H., Vardy, M.E., Bull, J.M., Akhurst, M., Hauton, C., James, R.H., Lichtschlag, A., Long, D., Aleynik, D., et al., 2015. A novel sub-seabed CO_2 release experiment informing monitoring and impact assessment for geological carbon storage. International Journal of Greenhouse Gas Control 38, 3–17.

Themann, S., Schmidt, H.M., Esser, D., Systems, C., 2009. SPE 129127 Measurement, Monitoring, and Verification of CO_2 Storage: An Integrated Approach, in: Proceedings of SPE International Conference on CO_2 Capture, Storage, and Utilization, pp. 2–5.

Thomas, H., Bozec, Y., Elkalay, K., De Baar, H.J., 2004. Enhanced open ocean storage of CO_2 from shelf sea pumping. Science 304.

Thomas, H., Friederike Prowe, A.E., van Heuven, S., Bozec, Y., de Baar, H.J., Schiettecatte, L.S., Suykens, K., Koné, M., Borges, A., Lima, I. Doney, S.C., 2007. Rapid decline of the CO_2 buffering capacity in the North Sea and implications for the North Atlantic Ocean. Global Biogeochemical Cycles 21, 1–15.

Thomas, H., Schiettecatte, L.S., Suykens, K., Koné, Y., Shadwick, E., Prowe, A.F., Bozec, Y., de Baar, H.J., Borges, A., 2009. Enhanced ocean carbon storage from anaerobic alkalinity generation in coastal sediments. Biogeosciences 6, 1–8.

Tortell, P.D., 2005. Dissolved gas measurements in oceanic waters made by membrane inlet mass spectrometry. Limnology and Oceanography: Methods 3, 24–37.

Tsouris, C., Szymcek, P., Taboada-Serrano, P., McCallum, S., Brewer, P., Peltzer, E., Walz, P., Adams, E., Chow, a., Johnson, W., Others, 2007. Scaled-up ocean injection of CO_2 hydrate composite particles. Energy & Fuels 21, 3300–3309.

US EPA, 2013. Geologic Sequestration of Carbon Dioxide: Draft Underground Injection Control (UIC) Program Class VI Well Plugging, Post-Injection Site Care, and Site Closure. Technical Report May. US EPA.

Vojinović, V., Cabral, J., Fonseca, L., 2006. Real-time bioprocess monitoring: Part I: In situ sensors. Sensors and Actuators B: Chemical 114, 1083–1091.

Vurek, G.G., Feustel, P., Severinghaus, J., 1984. A fibre optic pCO_2 sensor. Annals of Biomedical Engineering 11, 499–510.

Wang, Y.P., Xiao, L., Wang, D.N., Jin, W., 2006. Highly sensitive long-period fiber-grating strain sensor with low temperature sensitivity. Optics letters 31, 3414–3416.

Wang, Z., Heflin, J., Stolen, R., Ramachandran, S., 2005. Analysis of optical response of long period fiber gratings to nm-thick thin-film coating. Optics express 13, 2808–2813.

Watson, A.J., Schuster, U., Bakker, D.C., Bates, N.R., Corbière, A., González-Dávila, M., Friedrich, T., Hauck, J., Heinze, C., Johannessen, T., et al., 2009. Tracking the variable North Atlantic sink for atmospheric CO_2. Science 326, 1391–1393.

Weiss, R., 1974. Carbon dioxide in water and seawater: the solubility of a non-ideal gas. Marine chemistry 2, 203–215.

Weiss, R.F., 1981. Determinations of carbon dioxide and methane by dual catalyst flame ionization chromatography and nitrous oxide by electron capture chromatography. Journal of Chromatographic Science 19, 611–616.

Weiss, R.F., Van Woy, F., Salameh, P., Sepanski, R., 1992. Surface water and atmospheric carbon dioxide and nitrous oxide observations by shipboard automated gas chromatography: Results from expeditions between 1977 and 1990. Technical Report. Oak Ridge National Lab., TN (United States). Carbon Dioxide Information Analysis Center.

Whelan, A., Regan, F., 2006. Antifouling strategies for marine and riverine sensors. Journal of Environmental Monitoring 8, 880–886.

White, C.M., Strazisar, B.R., Granite, E.J., Hoffman, J.S., Pennline, W., 2003. Separation and capture of CO_2 from large stationary sources and sequestration in geological formations–coalbeds and deep saline aquifers. Journal of the Air & Waste Management Association 53, 645–715.

Widdicombe, S., Blackford, J.C., Spicer, J.I., 2013. Assessing the environmental consequences of CO_2 leakage from geological CCS: Generating evidence to support environmental risk assessment. Marine Pollution Bulletin 73, 399–401.

Widdicombe, S., Dashfield, S.L., McNeill, C.L., Needham, H.R., Beesley, A., McEvoy, S., Øxnevad, S., Clarke, K.R., Berge, J.a., 2009. Effects of CO_2 induced seawater acidification on infaunal diversity and sediment nutrient fluxes. Marine Ecology Progress Series 379, 59–75.

Wium-Andersen, S., Andersen, J.M., 1971. Carbon dioxide content of the interstitial water in the sediment of Grane Langso, a Danish Lobelia lake. American Society of Limnology and Oceanography 17, 943–947.

Wolf, A., 1966. Aqueous Solutions and Body Fluids. Hoeber.

Wolfbeis, O.S., 2000. Fiber-optic chemical sensors and biosensors. Analytical Chemistry 72, 81–89.

Wolfbeis, O.S., Weis, L.J., Leiner, M.J.P., Ziegler, W.E., 1988. Fiber-optic fluorosensor for oxygen and carbon dioxide. Analytical Chemistry 60, 2028–2030.

Wong, Y., Scully, P., Bartlett, R., 2003. Plastic optical fibre sensors for environmental monitoring: biofouling and strain applications. Strain 39, 115–119.

Woodgate, R.A., Aagaard, K., Weingartner, T.J., 2005. Monthly temperature, salinity, and transport variability of the Bering Strait through flow. Geophysical Research Letters 32, 1–4.

Woods Hole Oceanographic Institute, 2014. Marine environment antifouling system and methods. Patent US WO 2014014779 A1.

Xie, X., Bakker, E., 2013. Non-Severinghaus potentiometric dissolved CO_2 sensor with improved characteristics. Analytical chemistry 85, 1332–1336.

Xu, W., Huang, X.G., Pan, J.S., 2013. Simple fiber-optic refractive index sensor based on fresnel reflection and optical switch. IEEE Sensors Journal 13, 1571–1574.

Yakimov, M.M., Golyshin, P.N., Lang, S., Moore, E.R., Abraham, W.R., Lünsdorf, H., Timmis, K.N., 1998. Alcanivorax borkumensis gen. nov., sp. nov., a new, hydrocarbon-degrading and surfactant-producing marine bacterium. International Journal of Systematic Bacteriology 48, 339–348.

Yebra, D.M., Kiil, S.r., Dam-Johansen, K., 2004. Antifouling technology - Past, present and future steps towards efficient and environmentally friendly antifouling coatings. Progress in Organic Coatings 50, 75–104.

Zapp, P., Schreiber, A., Marx, J., Haines, M., Hake, J.F., Gale, J., 2012. Overall environmental impacts of CCS technologies-A life cycle approach. International Journal of Greenhouse Gas Control 8, 12–21.

Zeebe, R.E., 2012. History of seawater carbonate chemistry, atmospheric CO_2, and ocean acidification. Annual Review of Earth and Planetary Sciences 40, 141–165.

Zeebe, R.E., Zachos, J.C., Caldeira, K., Tyrrell, T., 2008. Carbon emissions and acidification. Science 321, 51.

Zibaii, M.I., Kazemi, A., Latifi, H., Azar, M.K., Hosseini, S.M., Ghezelaiagh, M.H., 2010. Measuring bacterial growth by refractive index tapered fiber optic biosensor. Journal of Photochemistry and Photobiology B: Biology 101, 313–320.

Zwietering, M., Jongenburger, I., Rombouts, F., Van't Riet, K., 1990. Modeling of the bacterial growth curve. Applied and Environmental Microbiology 56, 1875–1881.

Appendix A: Copyright Permission Letters

SPRINGER LICENSE
TERMS AND CONDITIONS
Sep 28, 2015

This is a License Agreement between Sonja Bhatia ("You") and Springer ("Springer") provided by Copyright Clearance Center ("CCC"). The license consists of your order details, the terms and conditions provided by Springer, and the payment terms and conditions.
All payments must be made in full to CCC. For payment instructions, please see information listed at the bottom of this form.
License Number: 3717750293333
License date: Sep 28, 2015
Licensed content publisher: Springer
Licensed content publication: Water, Air, and Soil Pollution
Licensed content title: Speciation in Application Environments for Dissolved Carbon Dioxide Sensors
Licensed content author: Sonja Bhatia
Licensed content date: Jan 1, 2014
Volume number: 226
Issue number: 5
Type of Use: Thesis/Dissertation
Portion: Full text
Number of copies: 1
Author of this Springer article: Yes and you are the sole author of the new work
Order reference number: None
Title of your thesis / dissertation: FIBRE OPTIC APPLICATIONS FOR DISSOLVED CARBON DIOXIDE MONITORING OF MARINE GEOLOGIC SEQUESTRATION SITES

Expected completion date: Oct 2015

Estimated size(pages): 130

Total: 0.00 CAD

Terms and Conditions

Introduction

The publisher for this copyrighted material is Springer Science + Business Media. By clicking "accept" in connection with completing this licensing transaction, you agree that the following terms and conditions apply to this transaction (along with the Billing and Payment terms and conditions established by Copyright Clearance Center, Inc. ("CCC"), at the time that you opened your Rightslink account and that are available at any time at http://myaccount.copyright.com).

Limited License

With reference to your request to reprint in your thesis material on which Springer Science and Business Media control the copyright, permission is granted, free of charge, for the use indicated in your enquiry. Licenses are for one-time use only with a maximum distribution equal to the number that you identified in the licensing process. This License includes use in an electronic form, provided its password protected or on the university?s intranet or repository, including UMI (according to the definition at the Sherpa website: http://www.sherpa.ac.uk/romeo/). For any other electronic use, please contact Springer at (permissions.dordrecht@springer.com or permissions.heidelberg@springer.com). The material can only be used for the purpose of defending your thesis limited to university-use only. If the thesis is going to be published, permission needs to be re-obtained (selecting "book/textbook" as the type of use). Although Springer holds copyright to the material and is entitled to negotiate on rights, this license is only valid, subject to a courtesy information to the author (address is given with the article/chapter) and provided it concerns original material which does not carry references to other sources (if material in question appears with credit to another source, authorization from that source is required as well). Permission free of charge on this occasion does not prejudice any rights we might have to charge for reproduction of our copyrighted material in the future.

Altering/Modifying Material: Not Permitted